A first Step of a Methodology for the Physical Modelling of Wind Turbines Wakes

Dissertation with the aim of achieving a doctoral degree

at the Faculty of Mathematics, Informatics and Natural Sciences

Department of Earth Sciences

of Universität Hamburg

submitted by Francesco Cuzzola

2013 in Hamburg

- corrected version -

Day of oral defense: 15.11.2013
The following evaluators recommend the admission of the dissertation:
Prof. Dr. Michael Schatzmann
Prof. Dr. Bernd Leitl

Declaration according to §7.4 of the Doctoral Degree Regulations of the MIN Faculty;

I hereby declare, on oath, that I have written the present dissertation by my own and that I have not used other than the acknowledged resources and aids.

Hamburg, 06/06/2013 _____

Abstract

Wind energy is a very important renewable resource. The optimization of a wind farm layout depends strongly on the aerodynamic characteristics of the wind turbines. Within the scope of the WAUDIT project, this work covers in particular the topic of the wind turbine wakes.

In particular, I designed a wind turbine model developing a iterative procedure based on the blade element momentum theory. Also, I carried out a large experimental campaign which describes the wake of a wind turbine in different flow conditions, assessing the impact on the wake of a second wind turbine model placed directly behind the first one. A vast amount of data has been collected providing chances for many further investigations. Also, given the variety of operational conditions of the turbine and the difficulties in achieving conditions of full similitude, I describe a strategy for a comprehensive physical modelling of the wakes.

This thesis consists of three parts. The necessary overview about the scientific problem is first given, followed by the development of the research project, and finally conclusions and suggestions for further developments are provided.

Deutsche Fassung

Die Windkraft ist eine bedeutende regenerative Energiequelle. Die Optimierung der Anordnung von Windkraftanlagen in einem Windpark wird von den aerodynamischen Eigenschaften der Windkraftanlagen bestimmt. Im Rahmen des WAUDIT-Projektes untersucht die vorliegende Arbeit insbesondere den Nachlauf von Windkraftanlagen.

Basierend auf der "blade element momentum theory" wurde in einem iterativen Prozess ein Modell einer Windkraftanlage entwickelt. Dieses Modell wurde in einer umfassenden Windkanalstudie verwendet, um den Einfluss unterschiedlicher Grenzschichten auf den Nachlauf der Windkraftanlage zu untersuchen. Des Weiteren wurde bei diesen Untersuchungen der Einfluss auf den Nachlauf einer zweiten Windkraftanlage analysiert, die im Nachlaufbereich der ersten Anlage platziert wurde. Im Rahmen der Windkanalstudie wurde ein umfassender Datensatz erstellt, der die Moeglichkeit fr weitere Untersuchungen bietet. Die vorliegende Arbeit zeigt zudem Strategien zur physikalischen Modellierung von Nachlaeufen von Windkraftanlagen auf.

Die Arbeit gliedert sich in drei Abschnitte. Eine Uebersicht ueber das behandelte wissenschaftliche Problem wird im ersten Teil der Arbeit gegeben. Im Anschluss wird auf die Entwicklung des Forschungsprojektes eingegangen, insbesondere wird die entwickelte Methodik zur physikalischen Modellierung von Windkraftanlagen vorgestellt. Im letzten Abschnitt werden die Ergebnisse und Schlussfolgerungen der Arbeit zusammengefasst und es werden Vorschlaege fuer weitere Untersuchungen gegeben.

Acknowledgements

During the three years spent for this research, I received the support of many persons. Besides the FP7-People program which funded the WAUDIT project and my research, I would like to thank:

First and foremost Prof. M. Schatzmann and Prof. B. Leitl, who gave me the chance to be part of this project and of EWTL, with their supervision and support I become a better and more a self-assured scientist.

Prof. A. Cuerva and Prof. S. Aubrun, their availability to work side by side gave me the opportunity to understand better the basics, to improve my results and to experience different work environments in Europe.

Prof. G. Schepers, Dr. M. Hölling also supported me with their experience and provided good advices.

Dr. Heather Holmes, Dr. Frank Harms, Dr. Graciana Petersen, Martin Dörenkämper and all other members of the EWTL group in Hamburg, as well as Cristobal Gallego in Madrid, gave me particular support in my work. They provided advice, scientific discussions and, most important, friendship. A special thank goes to all of you guys!

Herr Knut, Herr Mahlcke and all the workshop.

I ringraziamenti più importanti vanno a Simone, a tutta la mia famiglia e agli *amici miei*. Ascoltarmi, supportarmi e sopportarmi tutto questo tempo non dev'esser stato facile.

Finally, I would like to thank G. Marconi, O.Wright and W.Wright. They made my life better.

List of Abbreviations and symbols

List of Abbreviations

ABL	Atmospheric Boundary Layer
ADC	Actuator Disc Concept
BEM	Blade Element Momentum theory
CFD	Computational Fluid Dynamics
CWT	Continuous Wavelet Transform
EWTL	Environmental Wind Tunnel Laboratory
EWTL	Environmental Wind Tunnel Laboratory
FFT	Fast Fourier Transform
HWA	Hot Wire Anemometry
LC	Linear Cord blade
LDA	Laser Doppler Anemometry
OB	Optimum Blade
PIV	Particle Image Velocimetry
RMS	Root Mean Square
TKE	Turbulent Kinetic Energy
TSR	Tip Speed Ratio

List of Symbols

A_d	Area of the actuator disc
a	Axial induction factor
a'	Tangential induction factor
B	Number of the blades
c	Chord
C_D	Drag coefficient
C_L	Lift coefficient
C_P	Power coefficient
C_T	Thrust coefficient
D	Rotor diameter
E	Kinetic energy
g	gravitational acceleration
m	mass
P	Power
Q	Torque
r	Radius
R	Rotor radius
T	Thrust
U_∞	Velocity of the unperturbed inflow
U_d	Velocity at the disc
U_{ref}	Velocity at the reference point
u_t	Tangential component of the velocity
u_{t_∞}	Tangential component of the unperturbed inflow
U_W	Velocity in the far wake
V_b	Velocity at the blade
α	angle of attack
β	pitch angle
λ	tip speed ratio
ν	kinematic viscosity
ϕ	angle between the local velocity at the blade and the axis of rotation
φ	twist angle
ρ	density
Ω	rotational velocity
Fr	Froude number
Re	Reynolds number
Ro	Rossby number

Contents

Part I.

Introduction

1. Overview

This chapter gives an overview about the importance of the subject of this research and about the physical challenges involved. Also, a description of the object of the project is given as well as an outline of the structure of this Ph.D. thesis.

Importance of studying the wind turbine wake

Wind turbine wake aerodynamics is currently a very active research field, particularly because of the scientific challenge presented by this complex physical phenomenon. Also, wind turbine design and wind farm planning are influenced by new insights on the wake flow. Therefore, this branch of research has a significant impact on the wind energy industry.

There are three approaches that can be utilized for investigations of wind turbine wakes:

- numerical modelling;
- field studies;
- physical modelling.

As the computational capabilities of modern computers increase, there is an increasing number of attempts to model complex flows such as the atmospheric boundary layer in complex terrain, wind turbine wakes and wind farm wakes. In particular, the wind turbine is often modelled as a device that introduces a momentum loss in the flow field. Then, the momentum loss is related to the thrust coefficient of the wind turbine modelled. Behind the wind turbine, the wake develops as a velocity deficit area.

Numerical models need to be validated and the community is constantly seeking case studies to be modelled and reliable datasets. Although full scale data measured in real wind farms is indispensable, the variability of the weather conditions and the high costs of measurement campaigns make field investigations of the wake extremely challenging. Hence, a definition of the wake of a wind turbine through field studies or a *standard wake* to refer to, simply does not exist. The capability of wind tunnel data to provide high quality, statistically meaningful datasets in controlled conditions might answer to this need.

Physics of the problem

The wake of a wind turbine is a complex flow. It is the result of the interactions among the Atmospheric Boundary Layer (ABL) flow, the wind turbine and the terrain. Nowadays, the largest blade of a wind turbine is the $75\mathrm{m}$ long blade of the Siemens SWT-6.0 150 wind turbine. Typically,

chord lengths at the tip are in the range of $0.5\mathrm{m}$. The aerodynamic performances of each blade section strongly depend on the characteristics of the incoming flow. In particular they depend on the velocity, direction and turbulence. Thus, the complexity of this particular flow lays also in the interactions of all the scales of turbulence present in the atmospheric boundary layer.

The use of the experiments in fluid mechanics research is based on the theory of similitude. Within the limits of its application (see *Heller* (2011)), results can be extrapolated to full scale. In the case of the wind turbine wake flow, the achievement of similarity condition in the laboratory requires the matching of the similarity parameters related to both the inflow (ABL), the terrain and the interacting structure (wind turbine).

Details about similarity requirements for the physical modelling of the ABL flow can be found in *Snyder* (1972). In particular, the non-dimensional form of the momentum balance equation is here quoted:

$$\frac{\partial U_i'}{\partial t'} + U_j' \frac{\partial U_i'}{\partial x_j'} + \frac{2}{Ro} \epsilon_{ijk} U_k' \Omega_j' = -\frac{1}{\rho'} \frac{\partial \delta P'}{\partial x_i'} + \frac{1}{Fr^2} \delta T' \delta_{3i} + \frac{1}{Re} \frac{\partial^2 U_i'}{\partial x_j' \partial x_j'} \tag{1.1}$$

where:

- U_i', x_i', t', ρ' are the non-dimensional form of velocity, spatial position, time and density respectively;
- $\partial P'$, $\partial T'$ are the non-dimensional form of the pressure and the temperature deviation from the neutral atmosphere;
- the Earth is taken as reference frame and Ω' is the non-dimensional form of its angular velocity
- ϵ_{ijk} and δ_{ij} are the alternating tensor and the Kronecker's delta;

Particularly relevant for the scope of this research are the three non-dimensional parameters included in the equation 1.1:

- Rossby number $Ro = \frac{U_R}{L\Omega_R}$;
- Froude number $Fr = \frac{U_R}{\sqrt{gL\delta\frac{T_R}{T_0}}}$;
- Reynolds number $Re = \frac{U_R L}{\nu}$.

Where L, U_R, Ω_R, δT_R are reference values of length, velocity, angular velocity and temperature deviation respectively; T_0 is the temperature of a neutral atmosphere, ν is the kinematic viscosity and g is the gravitational acceleration. An ABL flow simulation in the wind tunnel achieves condition of complete similitude only if these three similarity parameters are identical to the full scale case.

Froude number describes the influence of buoyancy with respect to the inertial forces. If neutral stability conditions are modelled (isothermal conditions), $Fr \to \infty$ and the buoyancy term is no more relevant. Isothermal conditions can easily be established in a wind tunnel.

Rossby number is the ratio between inertial forces and Coriolis forces. Since the deviation effects are generally not modelled in the wind tunnel, formally full similarity is typically not achieved. However, restricting the model to the atmospheric surface layer, the impact of the Coriolis effect may be neglected if the horizontal domain extends less than $5\mathrm{Km}$, *Snyder* (1972).

The value of the Reynolds number depends mainly on the reference length. Typically, models for wind tunnel simulations may be between hundred and several thousand times smaller than the real scale. Therefore, Reynolds number in the wind tunnel can be several orders of magnitude smaller. Following the approach of *Townsend* (1956), it can be shown that in a turbulent flow most statistical quantities depend on the Reynolds number up to a certain value Re_{crit}, beyond this critical value they are Re-independent. Thus, provided that the Reynolds number of the simulation is larger than Re_{crit}, the Reynolds number similarity criterion for ABL modelling can be relaxed. *Petersen* (2013) carried out a thorough Reynolds number independence test for the ABL flow which was used for the experimental campaign described in Ch.7. Another example, for the case of transport and dispersion around buildings, can be found in *Neff and Meroney* (1995). However, it must be noted that the effect of the lower Reynolds number in a wind tunnel simulation results in a larger size of the dissipative eddies when compared to those present in the natural ABL flow, see *Snyder* (1972) and *Hertwig* (2009).

According to *Neff et al.* (1990), a dimensional analysis of the wake of a wind turbine model leads to the definition of four non-dimensional parameters that characterize the wind turbine wake flow:

- Thrust coefficient $C_T = \dfrac{T}{\frac{1}{2}\rho S U_\infty^2}$;
- Power coefficient $C_P = \dfrac{P}{\frac{1}{2}\rho S U_\infty^3}$;
- Tip Speed Ratio (TSR) $\lambda = \dfrac{R\Omega}{U_\infty}$;
- Reynolds number $Re = \dfrac{U_\infty L_R}{\nu}$.

where U_∞ is the wind speed, T is the thrust acting on the rotor, P is the power extracted by the turbine, S is the reference value of the surface (typically the rotor disc area), R is the rotor radius and Ω is the rotational velocity of the rotor. In the wind energy community, the reference value L_R is typically the blade chord length.

C_T and C_P describe the amount of momentum harvested in the flow field and the part of this momentum actually transformed into power, see *Ainslie* (1988) for details. These two parameters are directly related to the lift and drag coefficients of the blade, C_L and C_D respectively. TSR describes the operative conditions of the wind turbine and is an indicator of the distance between two subsequent tip vortices. In addition, Reynolds number has an influence on the overall characteristics of the flow.

Similarly to the case of the ABL flow modelling, the condition of full similitude is unlikely to be achieved in the laboratory at usual model scales. The main reason being the Reynolds number, which can be several orders of magnitude lower for the model, due to the large difference of the blade chord (up to $3\mathrm{m}$ for full scale wind turbines). Also, C_L and C_D are significantly lower at low Re and the matching of C_T and C_P, using a scaled model, can be difficult. Thus, geometric similarity to a specific wind turbine model might not be the best strategy to model wind turbines in the wind tunnel.

It must be pointed out that an attempt to match a similarity parameter requires a specific design of the model such as a different shape of the blades. In addition, different blades would perform differently at the same ambient conditions (λ may vary). Any comparison between different rotors has to be made using particular care.

While the physical meaning of these parameters is known, the influence that each of them has on the wake is still unclear. *Neff et al.* (1990) suggest C_T as the main parameter driving the behaviour of the wind turbine wake. However, they do not provide details that clearly define this concept.

Definition of the research interest

A literature review, summarized in Ch.3, pointed out the lack of a standardized method for the physical modelling of wind turbine wakes. Different approaches and many experiments can be found. Often, previous projects focus on pressure measurements along the blade and on the near wake, otherwise the main objective of the investigations is the far wake only. Therefore, features such as the rotation of the wake are often not modeled. In addition, the large scale experiments were carried out in conventional wind tunnels with homogeneous free stream conditions. Thus, a description of the whole wake (i.e, near and far wake) of a wind turbine in the atmospheric boundary layer is an important contribution to the scientific community provided by this study.

The Environmental Wind Tunnel Laboratory (EWTL) of the Meteorology Institute - University of Hamburg - operates the largest available atmospheric boundary layer wind tunnel in Europe (see App.A for details).The dimensions of this facility allow wind turbine models in scale of about $1:250$ to be used. Also, it provides enough space behind the model for the wake flow to develop.

As stated above, the dependencies of the wake characteristics on the similarity parameters are not fully understood. Therefore, a strategy for identifying the relative dependencies of the wake on the similarity parameters is strongly needed. Hence, a series of experiments with systematic variation of the parameters has to be planned.

This experimental methodology requires:

1. a basic wind turbine model equipped with a motor/generator that allows the electric output to be monitored and recorded;
2. different blades specifically designed for the matching (if possible) of each design parameter;
3. a preliminary sensitivity analysis of the performances of each rotor;

4. an experimental campaign in the boundary layer wind tunnel where the velocity field in the wake flow can be measured;

5. a description of the differences found in the flow field with respect to the variation of each similarity parameter.

It is necessary to point out that this methodology is highly interdisciplinary and each of these steps presents many challenges. In order to achieve partial similarity for one single similarity parameter, a specific design of the rotor has to be made. The three years available for the presented work do not allow the whole procedure to be accomplished for each similarity parameter. Therefore, this research project focuses on investigating on condition of partial similarity, designing a rotor for C_T matching.

The design of the model is performed first, then the equipment of the model is defined and the manufacture procedure are supervised. A sensitivity analysis is carried out and finally measurements in the wake of a rotor wind turbine model in ABL flow are performed. In addition, in order to give a reference and allow comparisons to be made, similar measurements are carried out in the case of free stream flow. Furthermore, the wake of a second wind turbine model placed directly behind the first one is characterized.

This methodology, besides delivering datasets valuable for validation purposes, allows the documentation of the wind turbine performances as well as of the wake behaviour (in terms of velocity field with respect to the particular set up and operative conditions). Once complete, this methodology will address the following scientific questions:

- Can the wake be modelled just by a change of momentum?
- Does the width of the wind turbine depend on the tip speed ratio?
- How far from the turbine is the wake still rotating?

Development of the thesis

This research topic is highly interdisciplinary, it combines many engineering fields (aerodynamic design, mechanical design, electrical design) as well as physics and meteorology (fluid mechanics, atmospheric boundary layer modelling). Approaching the challenging field of the wind energy from a technical point of view, this study aims to give a contribution in bridging the gap between engineering and meteorology.

The complexity of this field is reflected in the thesis. Therefore, the Introduction aims to be a guideline through the thesis more than a general overview about the importance of wind energy, which is well known. Besides this overview, the "Introduction" consists of a description of the European project WAUDIT (this research project is part of it) and a literature review. The "Development" section describes the design of the model, the preliminary tests, the sensitivity analysis and the experimental campaign in the boundary layer wind tunnel. Also, comparisons between measurements are shown. The concluding section of this thesis summarizes the content and suggests further developments of this research project.

2. The WAUDIT project

WAUDIT (**W**ind resource assessment **AUDIT** and standardization) is an Initial Training Network (ITN), a Marie-Curie action funded under the FP7-People program. The project's motivation is based on TPWind 3% vision which aims to reduce uncertainties in wind resource assessment and forecasting below 3% by 2030, regardless of site conditions.

The project comprises six work packages which cover all the relevant aspects of the wind resource assessment. This particular fields of interest are:

- WP1: Advanced measurement techniques.
  - Decrease measurement uncertainties of LIDARs in complex terrain through characterization of measurement errors.
  - Assess LIDAR uncertainty on complex terrain based on CFD simulations.
  - Create a database of measurements that can be used for validation of CFD models in complex terrain.
- WP2: Micro-scale numerical modelling.
  - Improve numerical models for wind resource assessment on complex terrain, forested areas and offshore based on CFD (with respect to linearized models, only suitable in non-complex terrain).
  - Simulate stochastic winds and improve turbulence models for atmospheric flows and wind turbine wakes under various atmospheric and topographic conditions.
  - Carry out a comprehensive characterization of extreme winds at different atmospheric scales.
  - Benchmark different modelling strategies regarding cost versus uncertainty analysis.
- WP3: Micro-scale physical modelling.
  - Determine the potential of using wind tunnel modelling as a complementary tool to field testing, for site calibration and validation of numerical models.
  - Create a database of measurements that can be used for validation of CFD models.
- WP4: Multi-scale wind conditions assessment.
  - Improve regional wind mapping with the aid of meteorological models of different spatial/temporal scales.
  - Assess the competitiveness of meteorological models versus micro-scale models and ways to complement each other.

- WP5: Offshore Meteorology.
  - In-depth analysis of offshore winds from offshore measurements.
  - Explore parameterizations for meteorological models.
- WP6: Quality assurance of wind resource assessment models.
  - Determine quality-check procedures for wind resource assessment models.
  - Reach consensus among modellers for the standardization of wind resource assessment methodologies.

In particular the University of Hamburg was in charge of the Work Package 6. The development of a quality assurance procedure for wind assessment models, carried out by an experienced researcher, has to be based on an ensemble of data coming from experiments both in controlled conditions and in the field. It was decided to create part of these data in-house, in particular the present work, carried out by an early stage researcher, deals with the micro-scale problem of the wake flow of wind turbines.

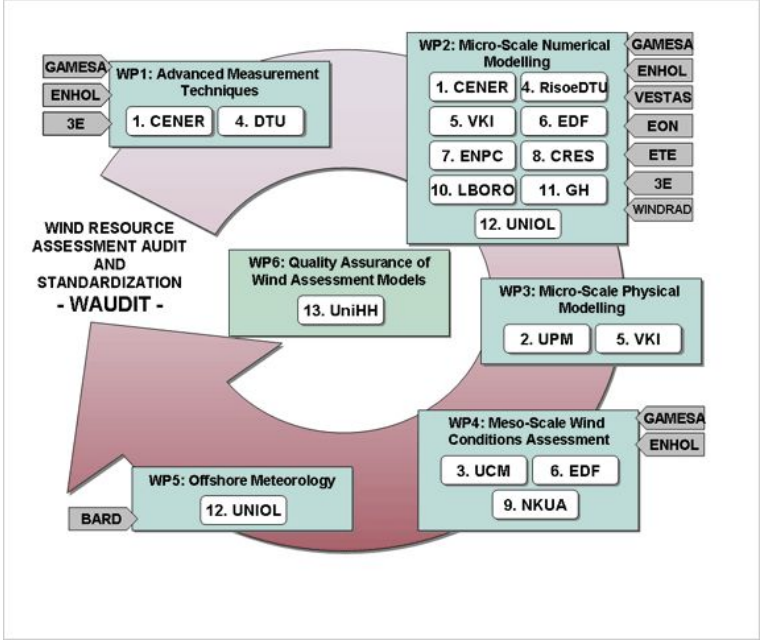

Figure 2.1.: The work structure of the WAUDIT project

3. Literature

Wind energy research through wind tunnel testing of wind turbine models started in the late seventies in Europe. Most of the models are designed by geometrically scaling a specific wind turbine, attempting to achieve dynamic similarity within certain ranges. In the next sections, previous contribution have been reviewed and classified with respect to the concept used in the scaling procedure. The aim of this literature review is to give a general overview to the research field, an extensive review of the literature available can be found in *Vermeer et al.* (2003).

3.1. Actuator Disc Concept based models

An experimental approach, based on the actuator disc concept (ADC - see Ch.4 for details), was first used by *Vermeulen* (1978) from the Energy research Centre of the Netherlands (ECN). The research was carried out in the wind tunnel of the Netherlands Organization for Applied Scientific Research (TNO) in Apeldoorn, with a model $14.6\mathrm{cm}$ in diameter. Experimental results were compared with data from a wind turbine $36\mathrm{cm}$ in diameter tested in the same wind tunnel at the same inflow conditions. From this comparison the author claims that the mean wake structure of the simulator (ADC model) resembles the one of the wind turbine enough to allow the use of ADC models for research purposes. Further developments in this direction came from *Vermeulen and Builtjes* (1982) and from *Builtjes and Millborrow* (1980) at TNO in Apeldoorn. In particular, *Vermeulen and Builtjes* (1982) investigated the turbulence structure within clusters of wind-turbines using wind tunnel tests. The authors claim that, several diameters downstream of the model, the velocity structure of the wake was correctly simulated. Also the turbulence structure compared fairly well with the one produced by a rotor model. Fig.3.1 shows the simulator used at TNO.

Nowadays, this approach is in use at the Polytechnic University of Orleans, see *Aubrun et al.* (2007) and *Aubrun* (2007). For these studies, porous discs of $100\mathrm{mm}$, $200\mathrm{mm}$ and $300\mathrm{mm}$ in diameter, built from metallic mesh, were used. *Aubrun* (2007) tested these simulators in the Malavard wind tunnel at the Prisme Laboratory in Orleans, using homogeneous freestream conditions and simulating offshore atmospheric boundary layer at a scale of $1:400$. In order to make a parametric study of the influence of size, porosity and mesh features of the disc used, mean velocity and turbulence intensity were measured . As expected by the author, changing the porosity level of the mesh, any velocity deficit can be reproduced. Also, varying the homogeneity of the porous material, it is possible to reproduce a non-uniform velocity deficit as well. *Aubrun et al.* (2007) investigated the behaviour of a model wind farm composed of 9 porous discs, proving the feasibility of this concept once more, by reproducing the desired velocity deficit profiles (U component only). Fig.3.2 shows the simulated wind farm.

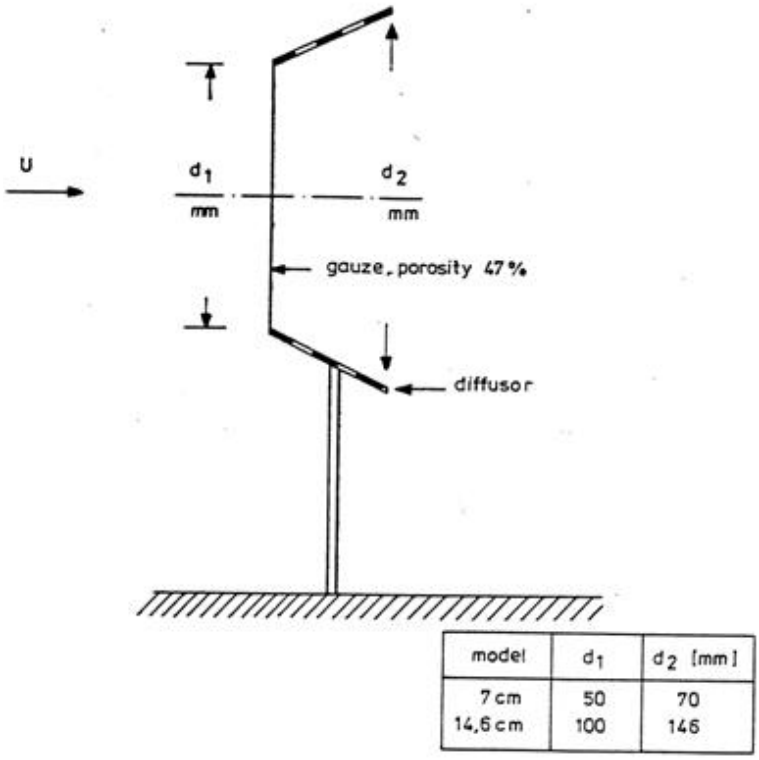

Figure 3.1.: TNO wind turbine simulator, from *Vermeulen and Builtjes* (1982)

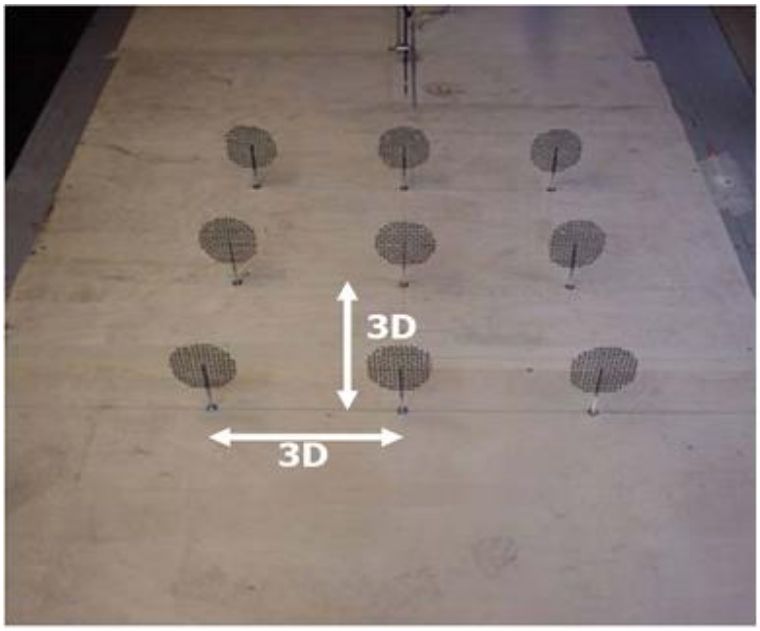

Figure 3.2.: Wind farm simulated through ADC models, from *Aubrun et al.* (2007)

The simple geometry of mesh models prevents from uncertainties in the manufacturing process. Furthermore, many numerical models are based on the ADC allowing direct comparisons to be made. On the other hand, ADC approach to the physical modelling has the drawback that wake characteristic of the model can not be assessed in advance. A number of preliminary tests must be carried out until the desired wake characteristics are reproduced. In addition, effects of rotation on the wake flow can not be investigated.

3.2. Rotor models

Many researchers tried to investigate the behaviour of rotating wind turbines reproducing them at small scale in wind tunnels. One of the first experiments was carried out by *Alfredsson and Dahlberg* (1979) who tested two different sets of two-bladed models. The first set showed low C_p values. The latter, re-designed with larger chord in order to increase the Reynolds number, showed better performances as shown by Fig.3.3.

The atmospheric boundary layer was simulated and a transverse hot-wire anemometer was used to measure mean velocity profiles at different downstream locations with different inflow conditions. A DC-generator was connected through a shaft to the rotor and using a resistor and other devices it was possible to vary the load and adjust the torque to appropriate values. Flow visualization allowed the researchers to take some of the first pictures of the tip vortex. Results of this work illustrate the presence of two different regions in the wake: a transition region and a decaying region. The latter is observable at a distance of two to five rotor diameters downstream. Here, the vortex breaks down and the wake starts to mix with the ambient turbulence. The level of turbulence occurs to be the main parameter that regulates vortex breakdown.

At the same institution *Montgomerie and Dahlberg* (2003) set up an experiment aiming to show the true paths of the trailing tip vorticity for different configurations, wind speeds and tip speed ratios. Different rotors were used but, due to the small wind tunnel, the diameter of each model was $180\mathrm{mm}$ only. The model was equipped with a generator and it was possible to record rotational speed, current and torque. Very detailed data of power and thrust coefficient are delivered. The effects of the increasing wind speed are reflected in the power and thrust coefficients curves, showing an increase of $C_{P_{MAX}}$ with increasing Re. The highest value of power coefficient achieved was $C_{P_{MAX}} = 0.28$. The vortex breakdown, due to the high turbulence level of the wind tunnel flow and the small scale of the model occurs earlier, at about 2 diameters downstream.

The same wind turbine model was used by *Medici and Alfredsson* (2005) in an experiment focused on the phenomenon of meandering. The authors claim a relation of this phenomenon to the bluff body vortex shedding. Meandering is not yet fully understood, other researchers relate it to the presence of large eddies in the atmospheric boundary layer.

In *Neff et al.* (1990), a selection of different rotor blades was evaluated using velocity and force measurements aiming to select the rotor model that could more closely represent the full-scale behaviour of a wind turbine. From their dimensional analysis it is suggested that the parameters that control wake behaviour are Tip Speed Ratio, Reynolds number, Thrust coefficient and Power coefficient. Also, since wake characteristics are strongly dependent upon the thrust perceived by the rotor disc, the authors suggest that the design criterion to be followed in the physical modelling

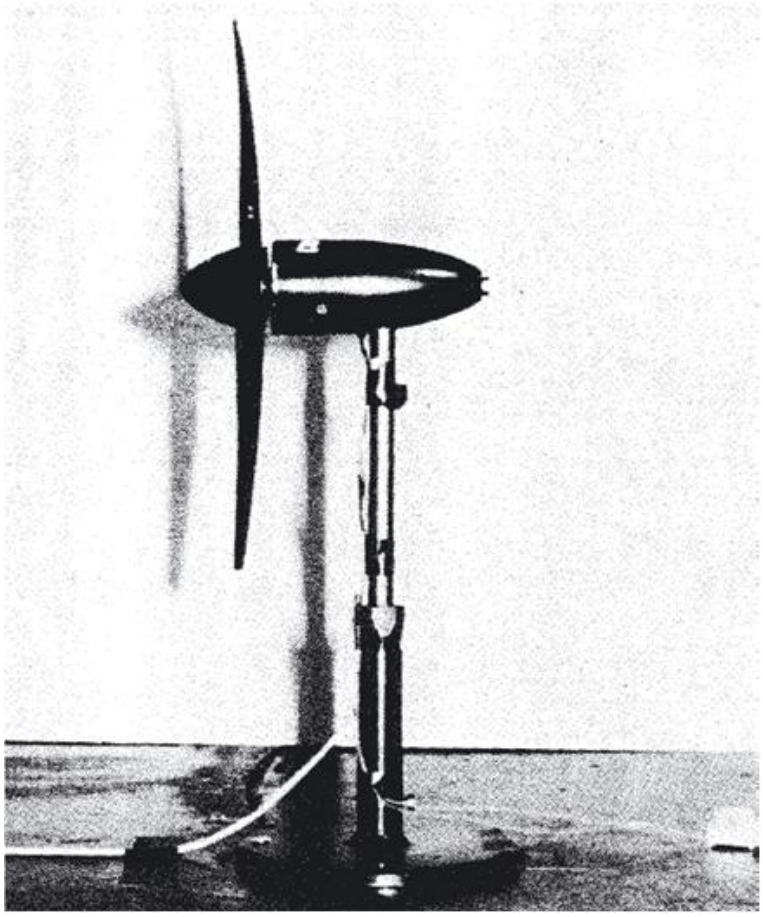

Figure 3.3.: Wind turbine model from *Alfredsson and Dahlberg* (1979)

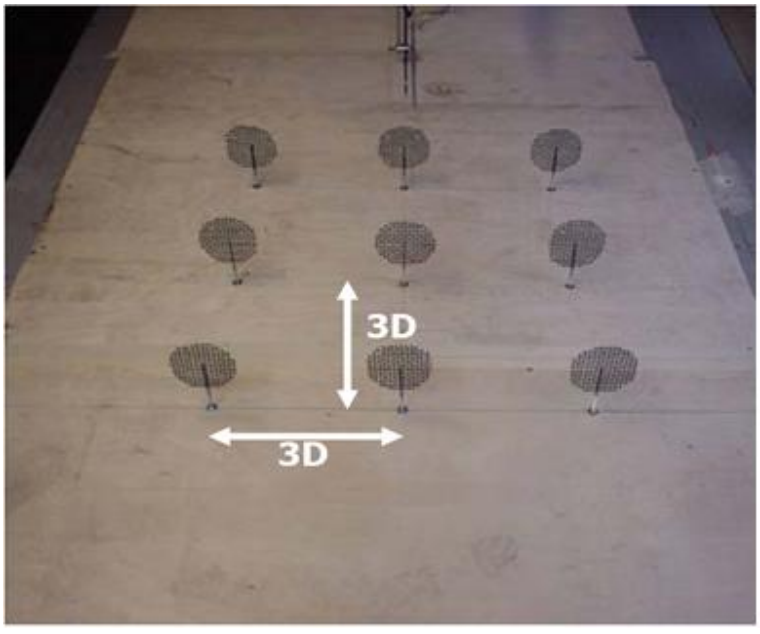

Figure 3.4.: Experimental setup from *Medici and Alfredsson* (2005)

of wind turbine wakes is to achieve thrust coefficient values of equivalent magnitude to full scale wind turbines.

In 2003 at ECN *Corten et al.* (2004) designed model wind turbines with $25\mathrm{cm}$ diameter. Rotors were made of fiber plastic. In order to have an adjustable pitch angle, 5 different rotors were built each with different pitch. The blades were designed using the airfoil NACA 0009 which delivered chord-based Reynolds number above 25000. This value is considered by the author a limit above which wake characteristics of that particular airfoil are Re-independent. It is important to stress that the authors paid attention to the aerodynamic characteristics at lower Reynolds number. The chord of the blade was extended in order to increase lift and efficiency. The increase of drag due to the larger chord seems to be neglected in the design procedure utilized. Since at low speed viscous drag can be comparable to form drag, this might result in lower performances. In order to guarantee constant torque over each revolution, the wind turbine models were equipped with three phase generators. Diodes allowed proper rotation speed to be adjusted. The aim of this experiment was to obtain measurements over a model wind farm, in presence of a simulated atmospheric boundary layer. The performances of these models were measured very accurately for such a small scale. This accuracy has been achieved by measuring only generator voltage and deriving C_T and C_P from the calibration of the four relevant electric signals. This experiment showed that the boundary layer above the wind farm takes far more than 5 rows to reach equilibrium and at this point the momentum above the farm continues to decrease.

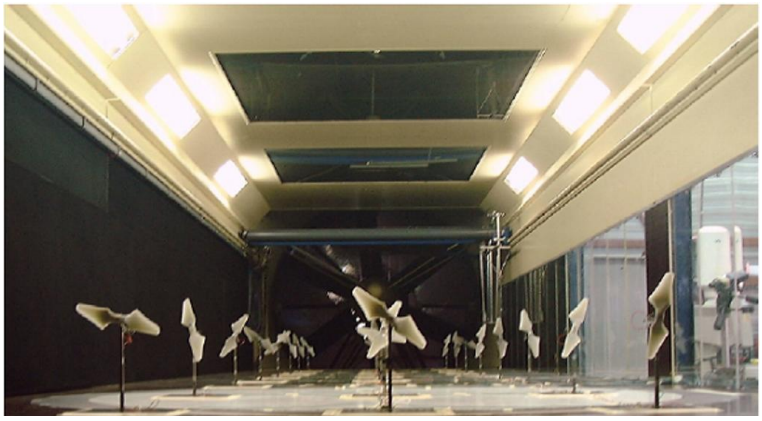

Figure 3.5.: Model Wind Farm, modified after *Corten et al.* (2004)

More recently *Pascheke and Hancock* (2007) focused on effects of stratification on the wake development. The low wind speed used in the tests might effect the development of the wake and the turbulent mixing of it. In order to increase the aerodynamic performances at low Re, see *Sunada et al.* (1997), the blades of this model consist in flat plates instead of airfoils. Although very efficient from an aerodynamic point of view, vibrations might occur at higher wind speed .

Figure 3.6.: Wind turbine model from *Pascheke and Hancock* (2007)

3.3. Large Scale Models

To avoid all the problems that are involved in the scaling process and to get rid of the uncertainties present in field tests two different but complementary projects have been developed to test large scale models in two of the largest wind tunnels in the world: the NASA-Ames wind tunnel in California and the LLF wind tunnel of the DNW in the Netherlands. The test section of these tunnels measure $28\mathrm{m}$x$43\mathrm{m}$ and $9.5\mathrm{m}$x$9.5\mathrm{m}$ respectively.

The first project, known as NREL Unsteady Aerodynamics Experiment, consists in the design, manufacturing and testing of a $10\mathrm{m}$-diameter wind turbine and subsequently a blind test for numerical modellers *Simms et al.* (2001). Great care was paid to the design of the model. In order to deal with uncertainties linked to blade geometry,the airfoil used, and the design procedure itself, preliminary projects were developed in this direction, see *Giguere and Selig* (1999). The resulting rotor satisfies better scientific constraints rather than representing completely a commercial one. The choice of this design is supported with a sensibility analysis that allowed a loss of about 5% in power performances with respect to the un-constrained design. Despite the amount of time spent in the wind tunnel, only few measurements were done in the wake but the large quantity of data focuses on pressure distribution along the span of the blades. In addition, a blind comparison among numerical models was undertaken. The required results were, among others, lift and drag coefficient distributions along the span of the blade. Numerical predictions ranged from 25% to 175% of the measured quantities. Fig.3.7 shows the model in the wind tunnel.

The second project, named Mexico (Model experiments in Controlled Conditions)*Snel and*

Figure 3.7.: The wind turbine model in the Ames wind tunnel. From http://wind.nrel.gov/amestest/Wconfig.htm

Schepers (2007) was carried out by a consortium of many European institutions and the NREL as invited participant. Despite some delay experienced in a 1-week campaign at the wind tunnel more than 100GB of data were recorded. The $4.5\mathrm{m}$-diameter rotor model, see Fig.3.8, was instrument with Kulite sensors along the sections of the blades and a large number of PIV measurements were done to monitor the inflow, the flow around the rotor and the near wake.

The resulting data have been studied within the MEXNETXT I *Schepers et al.* (2011) project and some further investigation is currently carried out within the MEXNETXT II project.

Figure 3.8.: Wind turbine model in the DNW wind tunnel, from *Snel and Schepers* (2007)

Part II.

Development

4. Phase 1 - Design of the Model

4.1. Wind Turbine Aerodynamics

This section gives an overview on the Actuator Disc Concept and on the Blade Element Momentum theory. These models are the most used in the modellers and manufacturers communities.

4.1.1. Actuator Disc Concept (ADC)

This model describes the wind turbine as a disc that extracts momentum from the passing flow field. Fig.4.1 illustrates this concept with a schematic.

From the physics point of view, the presence of the disc causes an increase of the pressure in front of the disc and a sudden drop of it when the air passes through the disc. The velocity slows down from unperturbed inflow value U_∞ to the value U_W in the far wake. Fig.4.2 shows the trend of these quantities along the path.

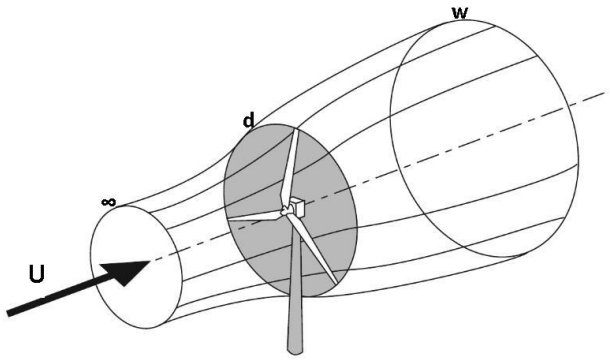

Figure 4.1.: Actuator disc concept-physical schematic. Modified after *Burton et al.* (2001)

Defining the axial induction factor $a = 1 - \frac{U_d}{U_\infty}$, where U_d indicates the velocity at the disc, and using the equation of mass, momentum and energy balance, we can write the next expressions for the mass flux $\dot{m}$, the thrust T and the kinetic energy E:

$$\dot{m} = \rho U A \tag{4.1}$$

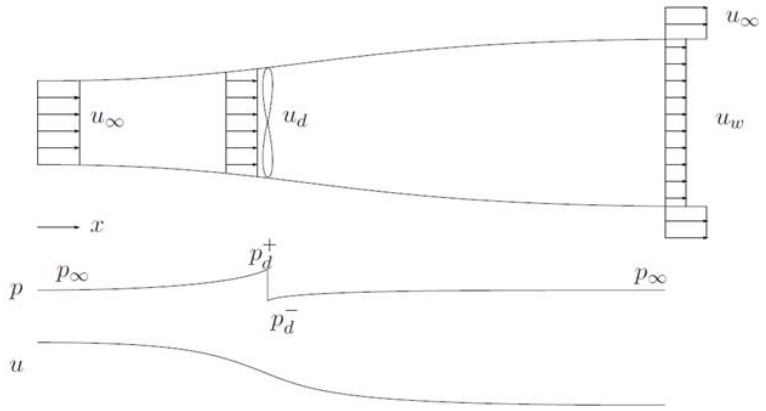

Figure 4.2.: Actuator disc concept-flow field schematic from *Sanderse* (2009)

$$T = \dot{m}(U_\infty - U_W) = (p_d^+ - p_d^-)A_d \tag{4.2}$$

$$E = \frac{1}{2}m(U_\infty^2 - U_w^2) \tag{4.3}$$

Where U and A are the velocity and the area at a general section of the stream-tube respectively. (p_d^+ and p_d^-) are the values of the pressure upstream and downstream of the disc, see Fig.4.2. Applying Bernoullli's theorem on both sides of the actuator disc and equalizing:

$$U_d = \frac{1}{2}(U_\infty + U_W) \tag{4.4}$$

Now it is possible to express U_W as a function of U_∞ and a:

$$U_W = (1 - 2a)U_\infty \tag{4.5}$$

Calculating the power as the rate of energy extracted in the unit of time and non-dimensionalising it by the wind speed and the rotor swept area we obtain:

$$C_P = \frac{P}{P_0} = \frac{\frac{1}{2}\rho A_d u_d (U_\infty^2 - U_w^2)}{\frac{1}{2}\rho A_d U_\infty^3} \tag{4.6}$$

and finally, by substituting the velocity terms by using the induction factor:

$$C_P = 4a(1 - a)^2 \tag{4.7}$$

Applying the derivative to this expression :

$$\frac{dC_p}{da} = 4(3a^2 - 4a + 1) \tag{4.8}$$

This expression shows that C_P exhibits a maximum for $a = 1/3$. This theoretical limit on the harvesting of the energy from the flow field is known as *Betz Limit*:

$$C_P = \frac{16}{27} \tag{4.9}$$

It is also useful to define the thrust coefficient as:

$$C_T = \frac{T}{\frac{1}{2}\rho A_d U_\infty^2} = 4a(1-a) \tag{4.10}$$

This theory applies only for $a <= 1/2$; beyond this value the velocity of the wake, as described in eqn.4.5, would result in zero or negative values and this is clearly in contrast with reality. Engineers deal with this limitation of the concept by using empirical modifications, see *Burton et al.* (2001).

4.1.2. Blade Element Momentum Theory (BEM)

This theoretical model describes the blade of the turbine as a sequence of elementary sections. The loss of momentum, in the axial and radial directions, is modeled as the result of aerodynamic forces of lift and drag acting on each blade element. The situation is shown in Fig.4.3

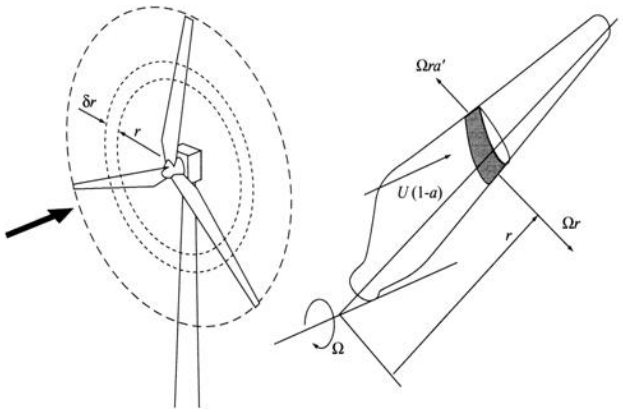

Figure 4.3.: Blade element theory-physical schematic from *Burton et al.* (2001)

The wind turbine rotates with angular velocity Ω. This generates a component of velocity in the tangential direction Ωr, where r is the radius. The air flow before encountering the turbine has no tangential component of the velocity; behind it, due to the reacting torque, a tangential component u_t is present. This component is generally expressed through the tangential flow induction factor defined as $a' = u_t/2\Omega r$. This means that rotational speed changes from zero value to u_t value passing along the profile; its average value is thus $\Omega r a'$. It is possible to express the tangential velocity experienced by the blade element as the sum of this contributions $\Omega r(1+a')$ and the total velocity of the air at the blade as the sum of tangential and axial components:

$$V_b = \sqrt{U_\infty^2(1-a^2) + \Omega^2 r^2(1+a')^2} \tag{4.11}$$

This is directed with an angle to the axis of rotation $\phi = \arctan \dfrac{U_\infty(1-a)}{\Omega r(1+a')}$. It is now possible to calculate the angle of attack $\alpha = \phi - \beta$ where β is the pitch angle. The situation is shown in Fig.4.4.

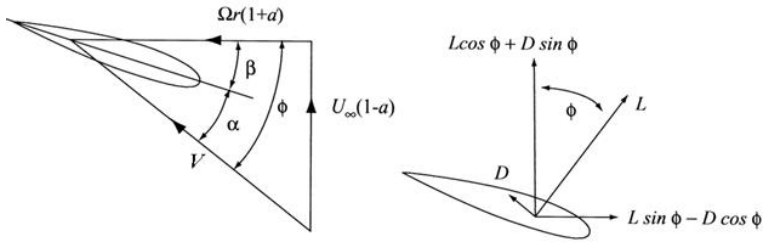

Figure 4.4.: Schematic of the forces and of the velocity components in the blade element from *Burton et al.* (2001)

To express the thrust (T) and the torque (Q), the 2-D values of drag and lift coefficient are used. Reminding that $V = U_\infty(1-a)/\sin\phi = \Omega r(1+a')/\cos\phi$ we obtain:

$$dT = \frac{1}{2}\rho c B (C_L \cos\phi + C_D \sin\phi)\left(\frac{U_\infty - (1-a)}{\sin\phi}\right)^2 dr \tag{4.12}$$

$$dQ = \frac{1}{2}\rho c B (C_L \sin\phi - C_D \cos\phi)\left(\frac{U_\infty(1-a)}{\sin\phi}\right)\left(\frac{\Omega r(1-a')}{\cos\phi}\right) r dr \tag{4.13}$$

where c is the chord length and B the number of blades.

Since drag and lift coefficient are non-linear functions of the angle of attack, to solve the equations above it is necessary to deduce thrust and torque also from momentum balance consideration. It is:

$$dT = (U_\infty - U_W) d\dot{m} = 4\pi r \rho u_\infty^2 (1-a) a dr \tag{4.14}$$

$$dQ = (u_t - u_{t\infty}) r d\dot{m} = 4\pi \rho U_\infty \Omega a (1-a') r^3 dr \tag{4.15}$$

where $u_{t\infty}$ indicates the tangential velocity of the unperturbed inflow.

Equalizing the respective equations it is possible to obtain a link between induction factors and aerodynamic coefficients setting up an iterative procedure to obtain all parameters needed.

This is generally done with the following steps:

- assigning a first step value of zero for a and a'
- determine ϕ
- reading the tabulated values of C_L and C_D
- calculate a and a' from 4.12=4.14 and 4.13=4.15

Once convergence is achieved, the power coefficient can be calculated as

$$C_P = \frac{Q\Omega}{\frac{1}{2}\rho\pi R^2 U_\infty^2}$$

The power curve is generally expressed showing the variation of C_P with respect to the tip speed ratio λ. A typical power curve of a commercial wind turbine is shown in Fig.4.5. Knowing the airfoil distribution along the span of the blade (the desired values of C_L and C_D are already defined), it is possible now to calculate the geometry of the blade in terms of chord distribution and twist angle distribution.

Although this theory is more detailed than the ADC, still there are a number of assumptions that have to be made in order to translate the complexity of physics into a procedure suitable for engineering use:

1. It is assumed that lift and drag can be calculated using 2-D airfoil data
2. Span-wise velocity is ignored
3. No 3-D effects are considered

These approximations might lead to uncertainties, particularly in the estimation of the angle of attack, and correction factors are widely used in the manufacturer community.

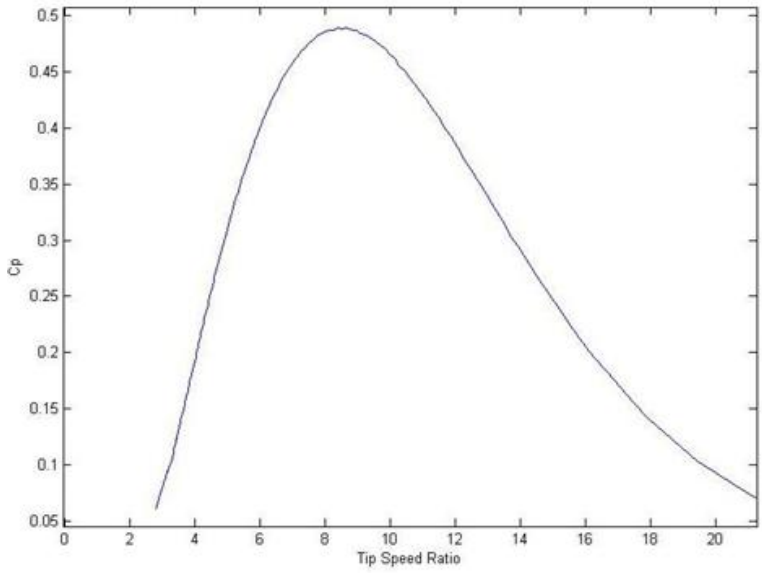

Figure 4.5.: Typical power curve of a wind turbine

4.2. BEM procedure

The scope of the theory explained in 4.1.2 is to offer a mathematical model that allows the calculation of the performances of the wind turbine once the momentum loss in the flow is estimated. Since the problem is non-linear, the estimation of the momentum loss needs an iterative procedure. This procedure calculates the induction factors of the blade as well as the angle of attack of the flow and, from tabulated data, it delivers the relative lift and drag coefficient of the airfoil. Once convergence is achieved for each blade element, it is possible to calculate the momentum loss and the power coefficient of the turbine.

The calculation loop is repeated for each operative condition, defined by the dimensionless parameter tip speed ratio λ, and it is possible to show the variation of the C_P with respect to λ, as shown in Fig.4.5.

The design tip speed ratio λ_D, defined as the TSR that delivers the maximum value of the power coefficient, is then used for the calculation of the chord distribution and twist angle distribution of each blade element. Thus, the geometry of the blade can be defined.

In particular, the design routine implemented with Matlab, following *Manwell et al.* (2009), needs as inputs:

1. the length of the blade, or the rotor radius
2. a characteristic value of the chord of the blade
3. the lift and drag diagrams of the airfoil used
4. the range of operative conditions of interest

The choice of the rotor radius is the first step of the design procedure. Since the final scope of this research project is to investigate the wake of a wind turbine in the presence of a simulated atmospheric boundary layer, the rotor radius is defined with respect to this constraint.

The part of the ABL that can be properly simulated in a boundary layer wind tunnel is the so called Prandtl Layer, which has a typical height in the order of $100\mathrm{m}$. This can be reproduced in the Wotan wind tunnel with scales in the range of $1:200 \sim 1:250$, see *Bastigkeit* (2011).

Modern wind turbines of the $3\mathrm{MW}$ class, such as Vestas $\mathrm{V112}$ (see Fig.4.6), Enercon E-115 or REpower $3.4\mathrm{M104}$, have blade length of about $50\mathrm{m}$ and hub height in the range $80\mathrm{m} \sim 120\mathrm{m}$. Therefore, the length of the blade of the wind turbine model was set to $210\mathrm{mm}$, this choice allows to take into account the size of the hub which, at the moment of the design, was not known. Since the expected wind speed was between of $5\mathrm{ms}^{-1}$ and $15\mathrm{ms}^{-1}$ The characteristic chord was set to $50\mathrm{mm}$, the Reynolds number resulting from this choice is $Re =\sim 4.1 \cdot 10^4$.

The aerodynamic characteristics of airfoils are Reynolds number sensitive, particularly in the range of the resulting Re. In fact, lift and drag coefficients of airfoils commonly used for full scale blades can be significantly lower at low Re, see also App.B. For this reason a geometric scaling of the blade is not advisable and the use of other airfoils and perhaps distorted geometries should be considered, as in this study.

Figure 4.6.: Vestas V112 wind turbine blade photography Vestas http://www.rechargenews.com/energy/wind/article236313.ece

A number of airfoils have been considered as options, from traditional shaped airfoils to folded plates as the ones tested by *Sunada et al.* (1997). Considering the manufacturing capabilities of our workshop, which lacks of a five-axis milling machine, the *Jedelsky EJ* 85 was chosen for the whole blade span. This airfoil is designed for low Re and its lower surface of this airfoil is straight. Although among the most performing airfoils at low Re, the EJ 85 has an aerodynamic efficiency (lift to drag ratio) ten times lower compared to the airfoils used at full scale. These latter achieve values of efficiency in the range of 150. Fig.4.7 shows the airfoil and its polars at different Re. The wind turbine model was equipped with a DC motor/generator which allows the investigation of a wide range of operative conditions.

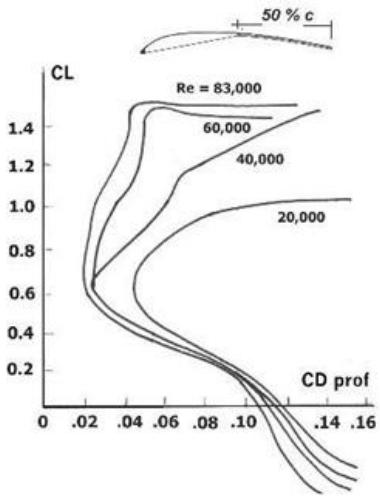

Figure 4.7.: Jedelsky EJ 85 polars

4.2.1. Results and geometry of the blade

Fig.4.8 shows the power curve of this model, the resulting λ is quite low. As shown by *Manwell et al.* (2009) and *Khan et al.* (2005), this result is typical for high solidity rotors, where the rotor solidity is defined as the total blade area divided by the rotor disc area.

Assuming as design conditions the tip speed ratio λ_{des} that delivers the maximum power coefficient it is possible to calculate the chord and the twist angle distributions along the span of the blade. These plots are shown in Fig.4.9 and Fig.4.10.

Some discontinuity close to the root is visible in Fig.4.10. The twist angle reaches high values in this region and, given also the lack of experimental data for this case, the iterative procedure does not achieve convergence for the first 10 blade elements. Thus, the distribution of the first $30\mathrm{mm}$ is obtained linearizing the trend of the twist angle φ, see Fig.4.11. The detailed geometry allows the blade to be digitally built and visualized. Fig.4.12 shows a 3D-rendering made using the *Dassault Systemes* software *Solidworks*.

Since the procedure does not take into account root or tip losses, the resulting solidity of the blade is very high. The choice of having such a solid blade was taken with the intent of extracting an higher momentum from the flow field and transforming it into torque. The idea behind is that since there are losses in terms of efficiency due to the low Re environment, dynamic similarity might be achieved by using more effective designs.

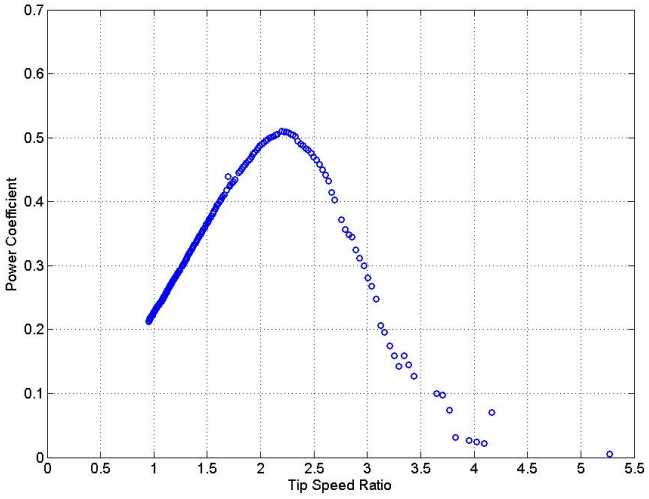

Figure 4.8.: Theoretical power curve of the wind turbine model

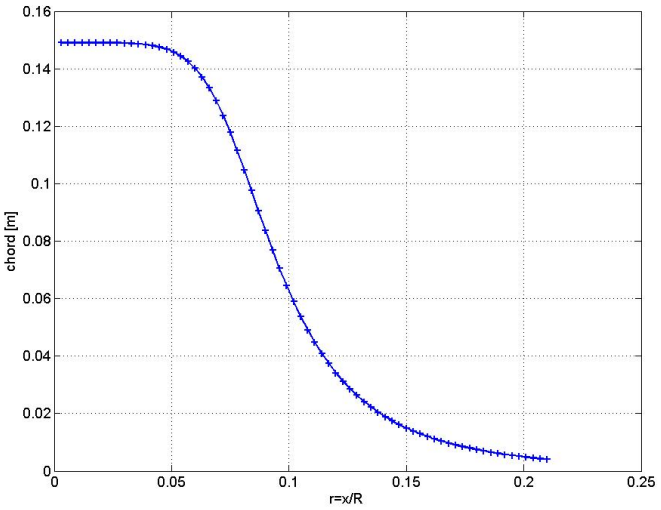

Figure 4.9.: Chord distribution along the span of the blade of the model

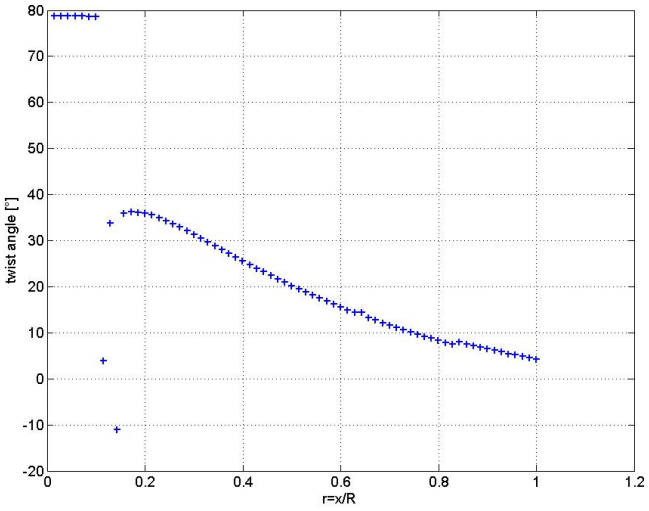

Figure 4.10.: Twist angle φ distribution along the span of the blade of the model

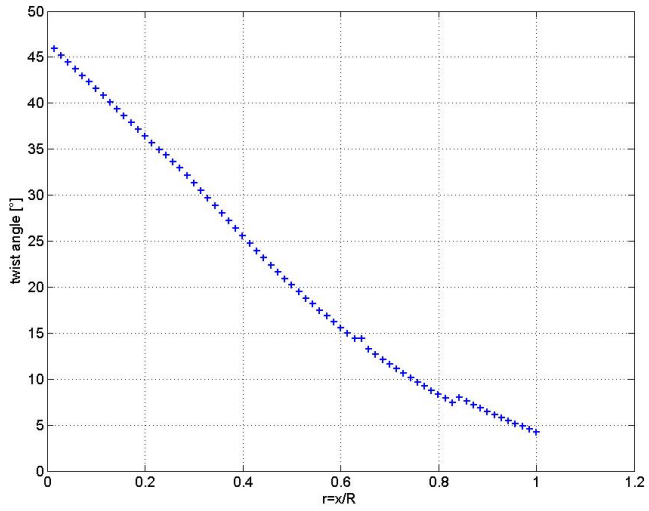

Figure 4.11.: Linearized β distribution along the span of the blade of the model

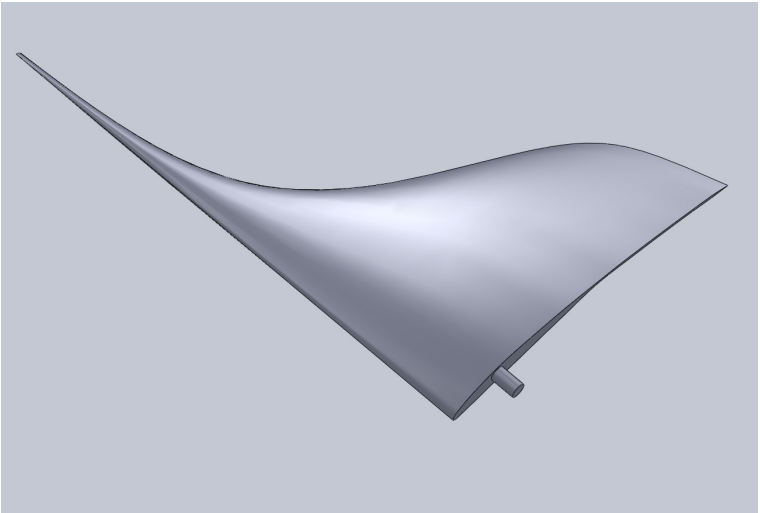

Figure 4.12.: 3D rendering of the blade of the model

4.2.2. Tower, DC motor and other components

Some of the components of the wind turbine model were not built in house. In particular, the *Varioprop* $12C$ hub of the company "Technik + Design Ramoser" was used. The motor (Faulhaber 3268 G0 24 BX 4) is a brushless DC-servomotor with a 4:1 gearbox. The rotational velocity can be controlled with a programmable speed controller (Faulhaber SC 2804). This allows the tip speed ratio to be adjusted by changing either the wind speed or the rotational speed of the turbine.

The tower of the turbine is a hollow frustum of a cone, its external diameter measures $60\mathrm{mm}$ at the bottom and $40\mathrm{mm}$ at the top, the thickness is $4\mathrm{mm}$. The tower is $360\mathrm{mm}$ long and the resulting hub heigth is $375\mathrm{mm}$. The nacelle is relatively long ($250\mathrm{mm}$) in order to hold the motor and to distance the tower from the blades. Fig.4.13 illustrates the tower-nacelle in a CAD rendering.

Figure 4.13.: 3D rendering of turbine without the rotor

5. Phase 2 - Preliminary experiments using prototypes: visualizations, measurements and sensitivity analysis

The design phase includes not only the aerodynamic design of the blade but also the study of the theory, the literature review, the implementation of the code, the search for the appropriate electric components, the definition of the geometry of the other parts and so on. This whole phase took about one year and, during this time, a number of experiments involving prototypes was carried out.

The first prototype was equipped with propeller blades and a basic layout of the tower-nacelle. The last prototype was used for a sensitivity analysis at the Prisme laboratory in Orleans as well as for the main wind tunnel campaign.

5.1. First prototype - visualization campaign

This campaign was carried out in the Göttingen-type wind tunnel, see App.A. In this experiment, a very basic wind turbine model was used, as shown in Fig.5.1. The components of the model have no fairing, propellers of aeroplane models were used as blades. During this campaign, two other rotors were tested. Both rotors were equipped with aluminium blades manufactured after the specifics of *Sunada et al.* (1997).

A bachelor thesis project was designed with the purpose of investigating different flow visualizations techniques. In particular, it aimed to visualize the wake by using:

- tufts method;
- release of titanium tetrachloride;
- laser lightsheet.

The first technique is used mainly to visualize streamlines and it may also give an insight about highly turbulent areas, see Fig.5.2. By releasing titanium tetrachloride from the tip of the blade, the second technique visualizes the flow streaklines. This technique may suggest the size of the wake, see Fig.5.3. The laser lighsheet is a very powerful flow visualization technique. Numerous preliminary attempts might be required to the definition of a suitable setup. Nevertheless, this technique allows turbulent structures to be visualized as well as the whole wake of the model.

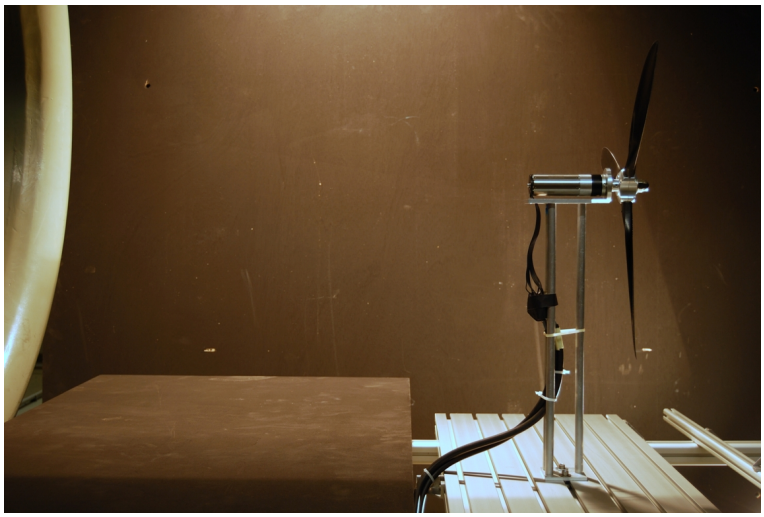

Figure 5.1.: First prototype in the Göttingen-type wind tunnel

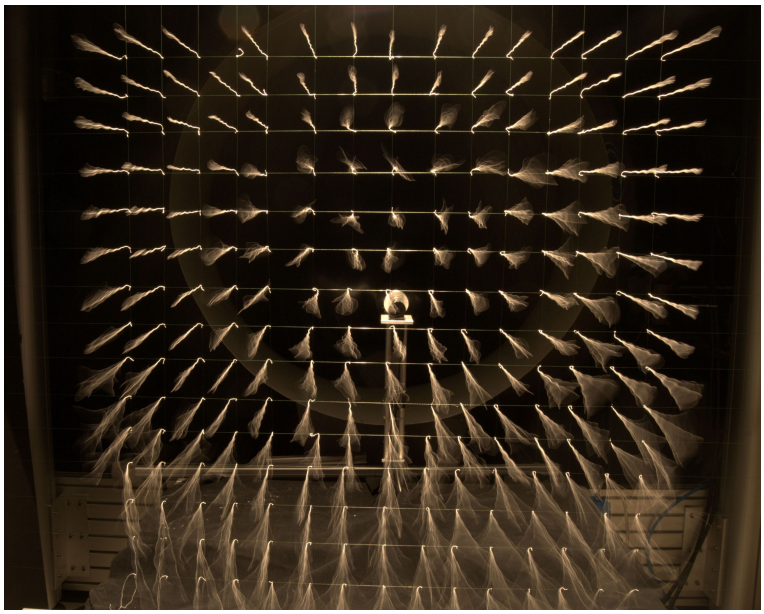

Figure 5.2.: Tufts showing larger direction variability visualize areas with higher turbulence

Figure 5.3.: Streaklines show the boundaries of the wake

5.2. Second prototype - experimental campaign

After improving the model, I designed and supervised a new project which was carried out as a Master Thesis project, see *Doerenkaemper* (2011). The figures shown in this section were developed under my supervision and were previously used in *Doerenkaemper* (2011).

The aim of this project was to investigate the wake of the wind turbine model in the open section wind tunnel. Velocity profiles were measured downstream of the rotor and changes were monitored for several operative conditions. In particular, a new rotor was mounted to the model. It was equipped with a set of blades manufactured by our workshop, using the EJ85 airfoil. Also, a new tower and a streamlined nacelle were used.

5.2.1. Experimental setup

The model was mounted into the test section of the Göttingen-type wind tunnel, see App.A. The rotor was fixed at a distance of $150\mathrm{mm}$ from the outlet of the wind tunnel. The tower of the model was fixed to a flat metallic plate below the level of the tunnel, avoiding any interference with the wind tunnel flow. In order to measure the reference value of the wind speed, a Prandtl tube was used. The probe, $150\mathrm{mm}$ long, was mounted $50\mathrm{mm}$ from the outlet of the tunnel in its upper side. An LDA system was used for velocity profile measurements, the laser probe was mounted to a traverse system above the wind tunnel. The mounting of the probe was chosen in order to minimize interferences with the flow and to minimize flow-induced vibrations. When measuring the U and the V component, the laser beams pointed downward (Fig.5.4), the tilt angle of the probe was less than 1°. Thus, the resulting uncertainty of the measured velocity components is less than 0.1%. Fig.5.4 shows the flow measurements setup.

The flow visualization campaign was carried out using a laser light sheet. The laser generator

was mounted above the tunnel realising a planar longitudinal sheet, focused at the height of the rotor. The laser light sheet, in this configuration, enabled to visualize up to a distance of three rotor diameter downstream of the turbine. Fig.5.5 shows the laser lightsheet setup.

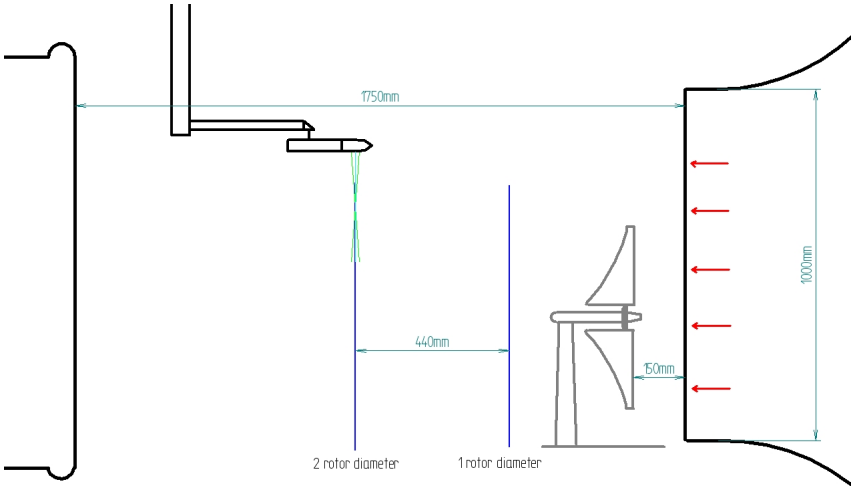

Figure 5.4.: Experimental Setup during the flow measurements, profile locations (blue lines). From *Doerenkaemper* (2011), M.Sc. thesis supervised by the author

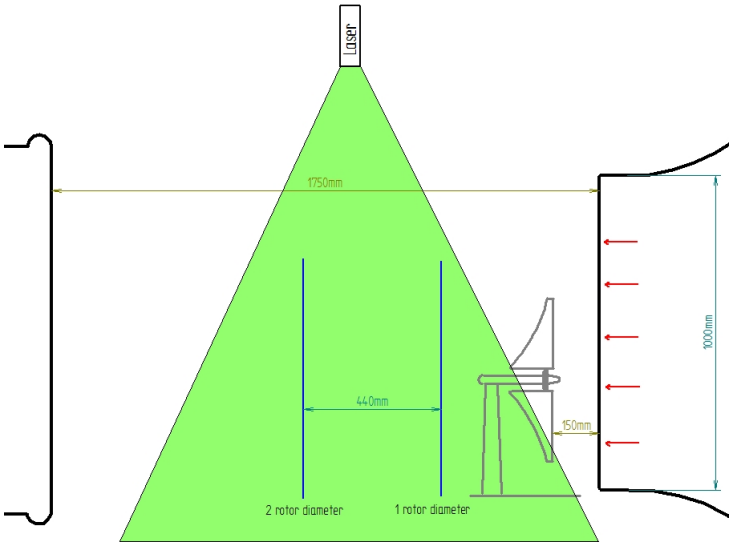

Figure 5.5.: Experimental set-up during the flow visualisation experiments. From *Doerenkaemper* (2011), M.Sc. thesis supervised by the author

5.2.2. Preliminary measurements

In order to characterize the free stream flow in the wind tunnel, several velocity profiles were recorded. More precisely, lateral and vertical profiles of the U and V-component were measured. The facility is a traditional aerodynamic wind tunnel, where turbulence is expected to be isotropic

and Reynolds number independent. Thus, the measurements for the empty tunnel were carried out at a wind speed of $12\mathrm{m\ s^{-1}}$ and not tested at lower values.

The center of the free stream at outlet of the tunnel was set as reference position. Measurements were carried out at position A (P_A) and at position B (P_B), respectively $100\mathrm{mm}$ and $1100\mathrm{mm}$ behind it. Fig.5.6 and Fig.5.7 show the non-dimensional longitudinal mean wind speed of the U and V components respectively. The values are constant ($U_{mean}/U_{ref} = 0.96$) for a wide range ($-400\mathrm{mm}$ to $+400\mathrm{mm}$) around the origin. At P_B the lateral component (V_{mean}/U_{ref}) shows a mixing with the surrounding air for $y > \pm 400\mathrm{mm}$. At this position, the velocity values show 10% reduction. In addition, the lateral component (V_{mean}/U_{ref} shows a decrease from the central to the outer part of the wind tunnel, see Fig.5.7. The measurements show that the inside area of the flow stream ($\pm 250\mathrm{mm}$) is not affected by the mixing of the flow with the surrounding air.

The turbulent mixing process is highlighted in Fig.5.8 and Fig.5.9. Here, the dimensionless turbulent quantities (U and V components) in the side areas double the respective values at the center of the flow. This effect is visible starting from $\pm 250\mathrm{mm}$ of distance from the center.

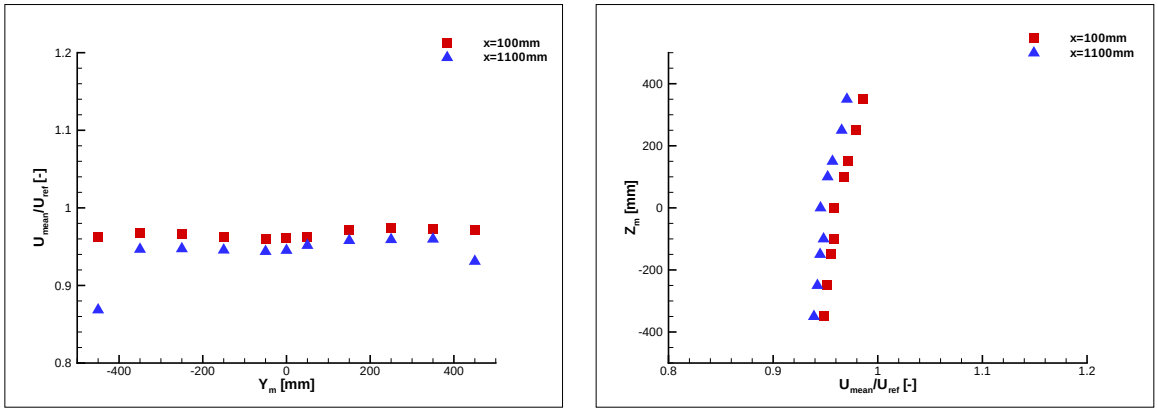

Figure 5.6.: Non-dimensional longitudinal wind speed component (U_{mean}/U_{ref}) lateral (left) and vertical (right) profiles at P_A and P_B. From *Doerenkaemper* (2011), M.Sc. thesis supervised by the author

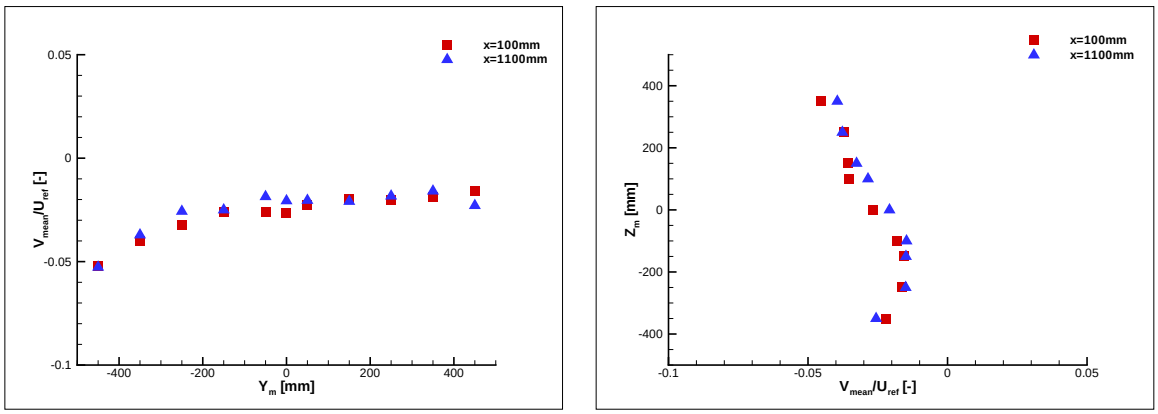

Figure 5.7.: Non-dimensional lateral wind speed component (V_{mean}/U_{ref}) lateral (left) and vertical (right) profiles at P_A and P_B. From *Doerenkaemper* (2011), M.Sc. thesis supervised by the author

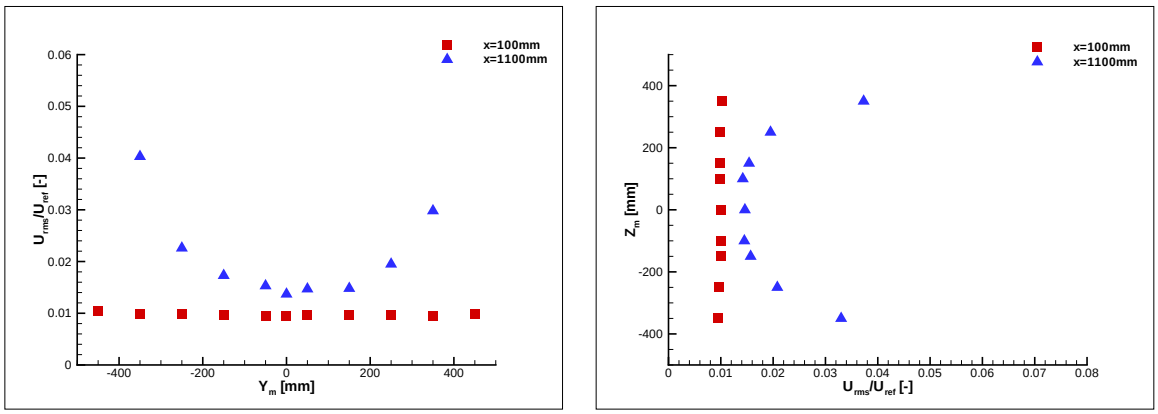

Figure 5.8.: Non-dimensional longitudinal turbulence (U_{rms}/U_{ref}) lateral (left) and vertical (right) profiles at P_A and P_B. From *Doerenkaemper* (2011), M.Sc. thesis supervised by the author

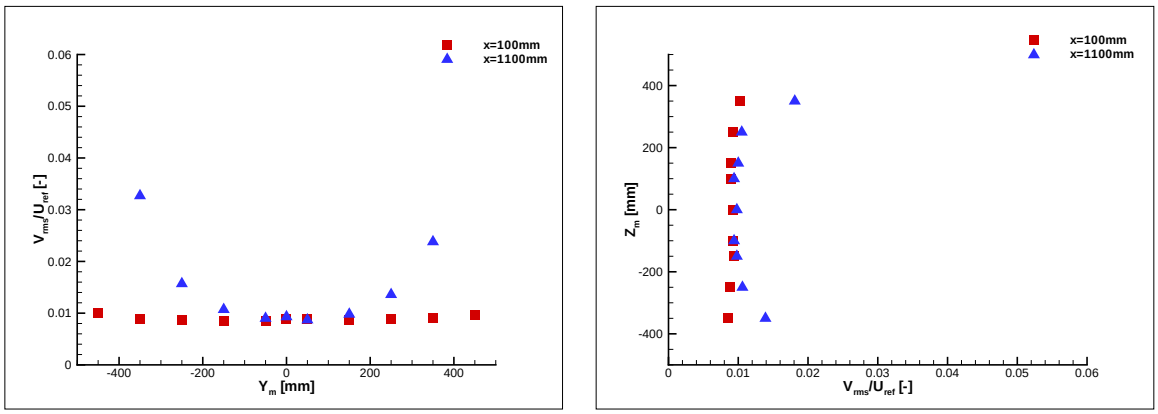

Figure 5.9.: Non-dimensional lateral turbulence (V_{rms}/U_{ref}) lateral (left) and vertical (right) profiles at P_A and P_B. From *Doerenkaemper* (2011), M.Sc. thesis supervised by the author

5.2.3. Flow visualization

In order to capture on camera the passing turbulent structures highlighted by the laser lightsheet, the wind speed was set in the range of $1\mathrm{m\ s^{-1}}$. A rotational speed of $120\mathrm{rpm}$ was consequently set, in order to achieve tip speed ratio values comparable to λ_{des}. During this experiment a value of $\lambda = 2.7$ was set.

There are different coherent structures dominating the wake flow of a wind turbine. One is the 'helical vortex street', the second is the tip vortex, a well known structure which develops at the tip of the blades. These structures are transported within the flow, as shown in sec.5.1. Both phenomena are visible in Fig.5.10. In particular, several coherent structures can be detected. In the upper part of the wake (highlighted with yellow circles), the vortex cores of three clearly defined tip vortices are visible. Also, a wavelike structure is located adjacent to the clean air above indicating the helical vortex street (blue curve). This structure passes the light sheet almost vertically and it creates areas of dense fog.
Any clearly defined structure can be detected in the central area of the wake. Strong turbulent mixing due to flow separation dominates the flow in this region. The wake widens within the illustrated area of about 2 rotor diameters.

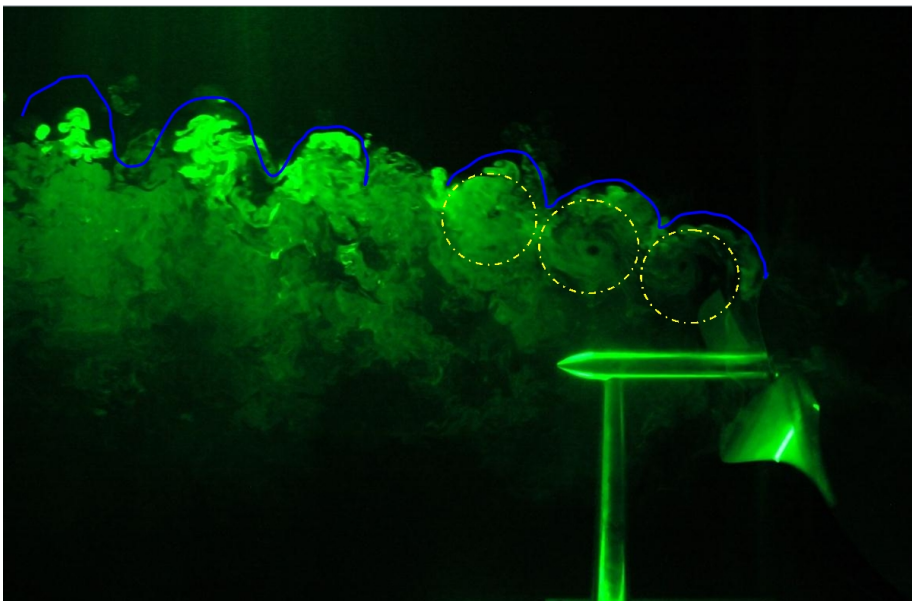

Figure 5.10.: Vertical laser light sheet wake flow visualisation - $\lambda = 2.9$ - several tip vortices and widening of the wake. From *Doerenkaemper* (2011), M.Sc. thesis supervised by the author

5.2.4. Flow measurements

Flow measurements were carried out using an LDA system by Dantec Dynamics, see App.A for details. At each location measures were recorded until fulfilling one of the criteria:

- 250000 acquired measures;
- $180\mathrm{s}$ of acquisition time.

An examination of the mean quantities as well as a statistical analysis of one time series were carried out. Taking as reference the leading edge of the blades, the planes at which the measurement have been carried out are at a distance of one and two rotor diameter downwind of the model. From now on, I refer to these measurement planes as $1D$ and $2D$.

For the analysis of the mean quantities of the wake flow we used the 'LDA-analysis' program, see *Fischer* (2012) for details. The program needs as input the time series recorded during the measurement for each point, as well as the reference wind speed. The aim of this section is to describe the influence of several operative parameters (pitch angle and TSR) on the velocity measurements in the wake.

Repeatability of the experiments

Before systematic measurements, in order to assure the repeatability of the experiments and determine the related uncertainty, repetitive measurements have been carried out. The same velocity profiles have been measured at different days, keeping the operative conditions constant (wind tunnel speed, rotational speed, pitch angle, etc.). Fig.5.11 to Fig.5.14 show U and V component for lateral and vertical profiles.

At position $2D$ the variability of all analysed parameters is less than 10%, indicating a good reproducibility. At position $1D$ instead, the turbulent quantities (see Fig.5.12 and Fig.5.14) show a scatter up to 30% located mainly in the inner part of the wake.

A probable cause is that the blades at pitch angle $\beta = 0^\circ$ are working in stalled conditions and this, together with the influence of the long nacelle, might cause a very turbulent and inhomogeneous flow. In fact, due to the particular twist angle distribution of the blades it is expected that the situation shown is the worst-case one.

For mean quantities, see Fig.5.11, the area were the lowest reproducibility occurs is the inner region of the blades. At $2D$ the U-component shows a lower reproducibility than the V-component, this characteristic is not observed for the turbulent quantities.

The resulting maximum deviations from these reproducibility tests are considered as the resulting maximum uncertainties and used in the following figures as error bars. The reproducibility of the experiments in the region of the nacelle clearly suggests that a convergence analysis of the time series should be considered in future experiments.

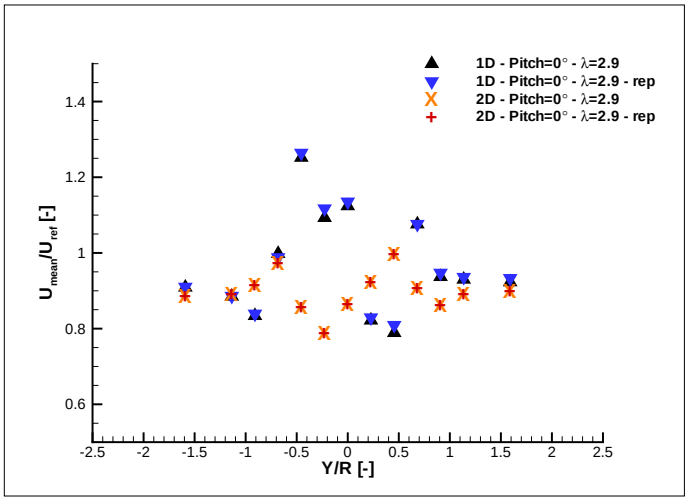

Figure 5.11.: Reproducibility of the experiments - Lateral profiles - mean U component. From *Doerenkaemper* (2011), M.Sc. thesis supervised by the author

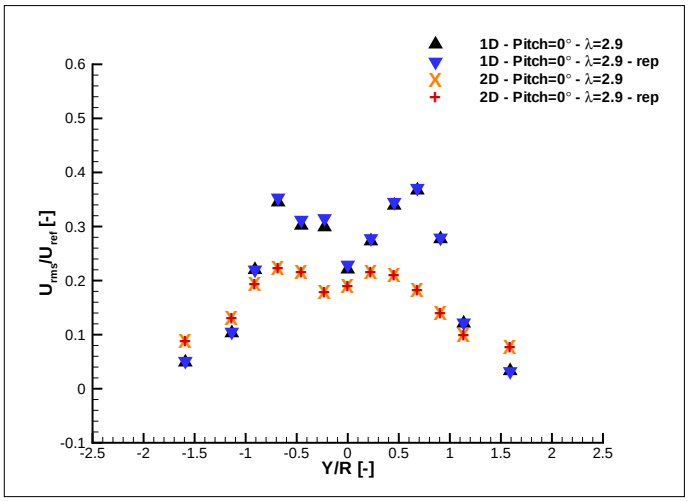

Figure 5.12.: Reproducibility of the experiments - Lateral profiles - turbulent intensity - U component. From *Doerenkaemper* (2011), M.Sc. thesis supervised by the author

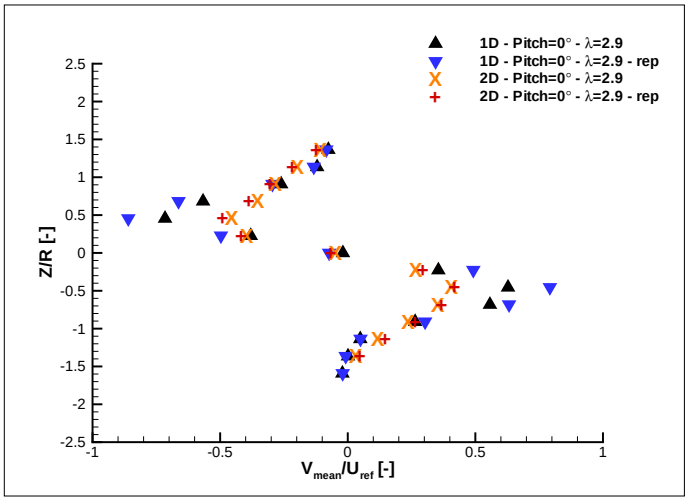

Figure 5.13.: Reproducibility of the experiments - vertical profiles - mean V component. From *Doerenkaemper* (2011), M.Sc. thesis supervised by the author

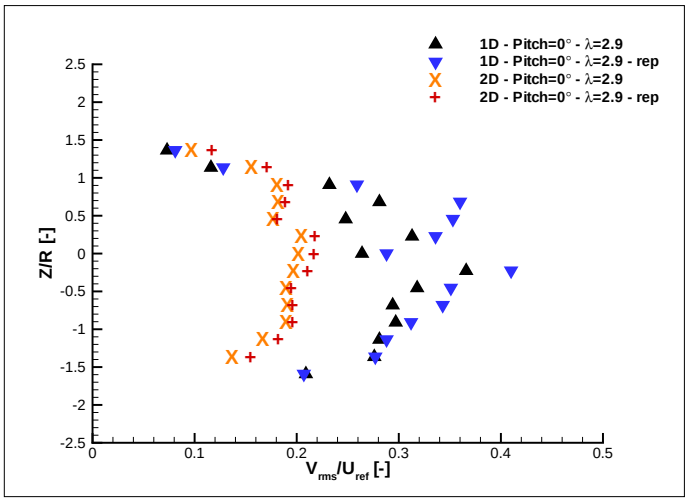

Figure 5.14.: Reproducibility of the experiments - vertical profiles - turbulent intensity - V component. From *Doerenkaemper* (2011), M.Sc. thesis supervised by the author

Development of the wake

The length of the test section allows to investigate the wind turbine near wake only . Fig.5.15 and Fig.5.16 show lateral and vertical profiles at pitch angle $\beta = 20°$, while the turbine was operated at the design tip speed ratio ($\lambda_{des} = 2.9$).

The horizontal profile (Fig.5.15 left) shows that the U-component of the velocity reaches a maximum value in the range of $U_{mean}/Uref = 1.0 - 1.2$ at about $y/R = 0.8$. The highest velocity deficit occurs in the inner part of the wake where hub and nacelle block significantly the flow stream.

Also the turbulent fluctuations show a similarly shaped distribution (Fig.5.15 right). Their maximum and minimum values occur at the same position of the mean velocity plot. In addition, both quantities exhibit a reduction in their maximum value from the measurements at $1D$ to the one at $2D$. In particular, the maximum turbulence is reduced by about half, while the maximum mean velocity decreases of about 20%.

Non-dimensional velocity (U_{mean}/U_{ref}) profiles are typically used to characterize the wake flow of a wind turbine and for comparisons. Fig.5.16 shows the vertical profiles of the U-component (left) as well as turbulence (right). These plots also highlight an M-shaped structure and the influence of the tower for $z/R < -1.0$. Comparing this area with the part above the axis of rotation ($z/R > 1.0$) a decrease in the mean wind speed is noticeable, while the turbulence reaches higher values.

The development of the transversal wind speed component V is shown in Fig.5.17. On the left plot, the measurements in the horizontal planes are shown. The rotation of the wake is clearly indicated by the change of sign in the non-dimensional velocity.

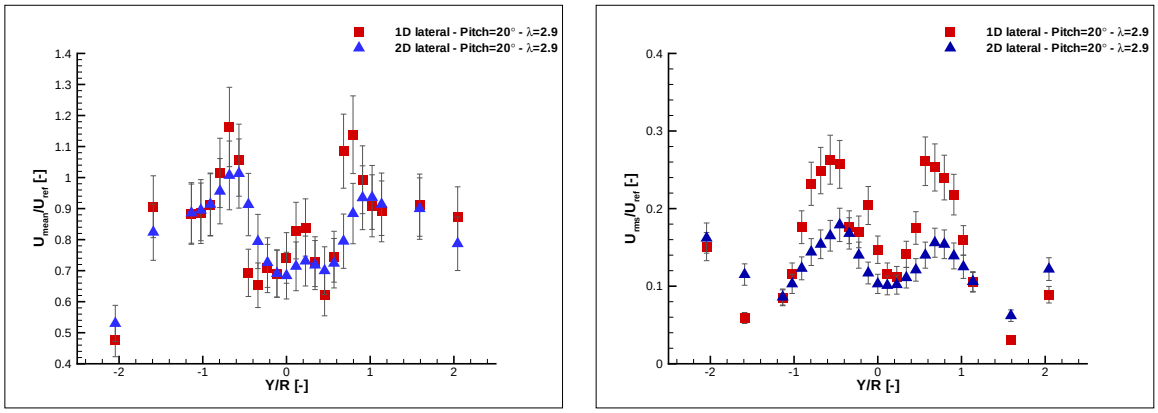

Figure 5.15.: Lateral development of the U-component wind speed (left) and turbulence intensity (right) of the wake, Pitch angle $20°$, design TSR, scatter-bars indicate uncertainty resulting from repeatability measurements. From *Doerenkaemper* (2011), M.Sc. thesis supervised by the author

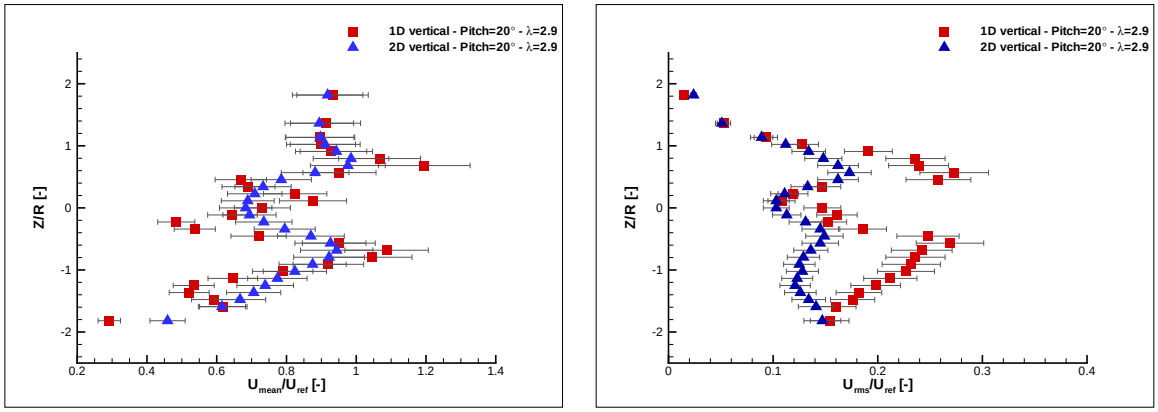

Figure 5.16.: Vertical development of the U-component wind speed (left) and turbulence intensity (right) of the wake, Pitch angle $20°$, design TSR, scatter-bars indicate uncertainty resulting from repeatability measurements. From *Doerenkaemper* (2011), M.Sc. thesis supervised by the author

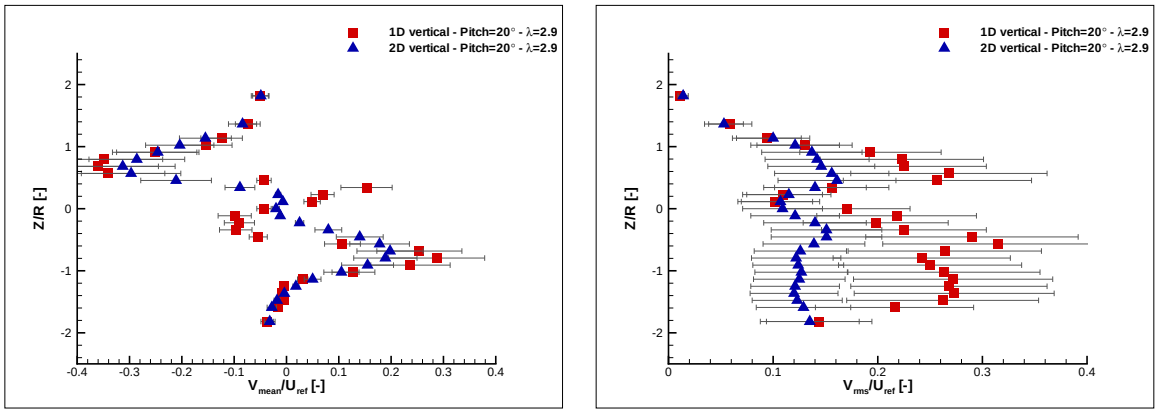

Figure 5.17.: Vertical development of the V-component wind speed (left) and turbulence intensity(right) of the wake, Pitch angle $20°$, design TSR, scatter-bars indicate uncertainty resulting from repeatability measurements. From *Doerenkaemper* (2011), M.Sc. thesis supervised by the author

Influence of the pitch angle on the wake

In order to investigate the influence of the pitch angle β of the blades on the wake flow, the velocity measurements were repeated at the same locations for three different values. Due to the relatively large chord of the rotor blades close to the root, the pitch angle is expected to be of significant influence on the wake flow. In fact a higher value of β corresponds to a larger projected area. Thus, to a stronger blockage effect.

Fig.5.18 shows the measurements of the U-component of the wind speed in the horizontal profile, at $2D$ for $\lambda = \lambda_{des}$. The biggest influence is observed in the central area. Also, a decrease of about 50% of the U component can be observed between the case at $\beta = 0°$ and the one at $\beta = 30°$.

The same measurements were taken without powering the turbine model. A wind speed in the range of $[3 - 5]\mathrm{m\ s^{-1}}$ is sufficient to drive the wind turbine model at $\beta = [20° - 30°]$, while in the case of $\beta = 0°$ a wind speed of $8\mathrm{m\ s^{-1}}$ is needed.

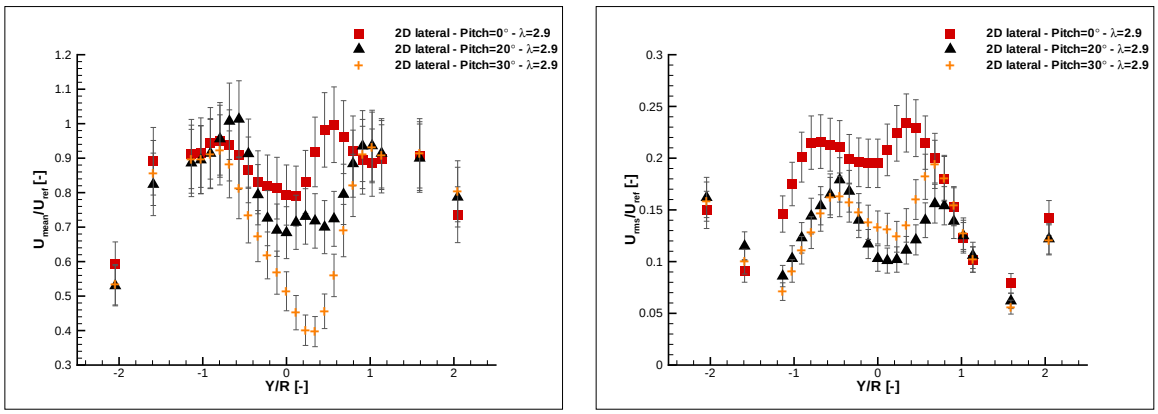

Figure 5.18.: Influence of the pitch angle , Pitch angle $0°, 20°, 30°$, design TSR, scatter-bars indicate uncertainty resulting from repeatability measurements. From *Doerenkaemper* (2011), M.Sc. thesis supervised by the author

Influence of the tip speed ratio on the wake

Different TSR were tested to quantify the influence of this parameter on the wake flow. Fig.5.19 shows the mean (left) and RMS (right) streamwise component of the wind speed for three different TSR at $2D$. The most visible effect is the widening of the wake as a result of the increasing λ. The maximum value of both the mean and the RMS value move outside in the radial direction: this maximum values are found at $y/R = 1$ of distance from the center for $\lambda = 4$. At lower TSR values instead, they can be found between 60% and 80% of the rotor span.

For the design operative condition $\lambda = 2.9$ (black triangles in Fig.5.19), an almost symmetric structure was obtained. The U_{RMS}/U_{ref} shows a maximum for this condition, although it must be pointed out that the deviation from the other values of λ tested is very low and in the range of uncertainty of the measurement. The flow visualisation experiments were carried out at this operative condition. A strong mixing and distinctive turbulent structures like the tip vortices was observable during the flow visualization experiments.

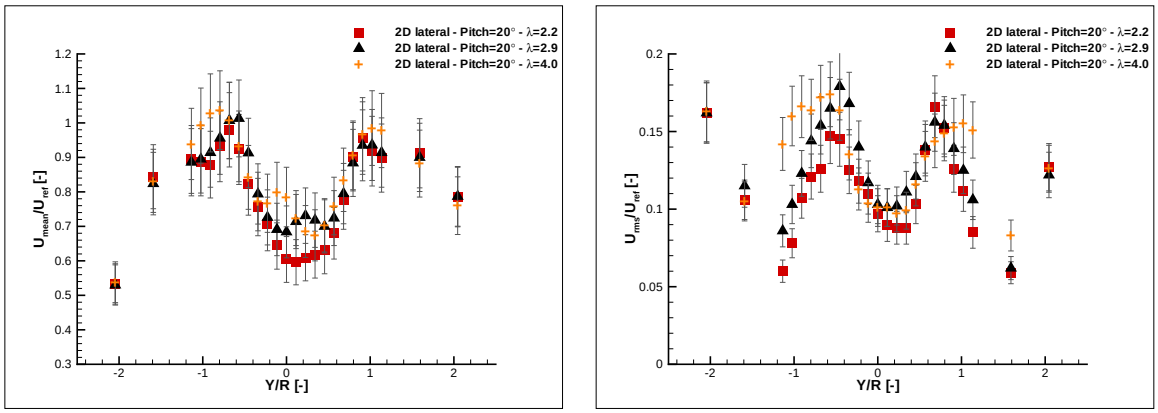

Figure 5.19.: Influence of the tip speed ratio , Pitch angle $20°$, three different TSR ($\lambda = 2.2, 2.9, 4.0$), scatter-bars indicate uncertainty resulting from repeatability measurements. From *Doerenkaemper* (2011), M.Sc. thesis supervised by the author

5.2.5. Time series analysis

At each measurement point time series of up to 250.000 values were recorded. In order to find the best compromise between data rate and accuracy of the measurement, different configurations of flow seeding level and of LDA laser power were investigated. Thus, sampling frequencies varies in the range of $1 - 5 \cdot 10^3 \mathrm{Hz}$.

Time-series are made non-dimensional using the reference wind speed (U_{ref}) and then re-sampled for further use in numerical routines. The high data sampling rate of about $3200\mathrm{Hz}$ allows the application of a spectral analysis. Fig.5.20 shows an example of a recorded time series at position P_1. This measurement point is located at $z/R = 0.9$ where z is the vertical coordinate and R the radius of the rotor (the tip region of the blade).

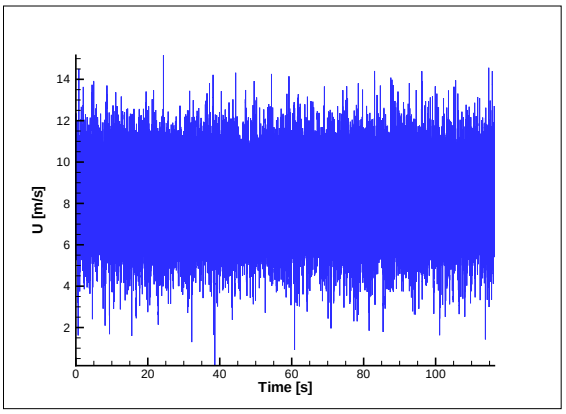

Figure 5.20.: Time series of the U-component wind speed recorded at P_1 - λ=2.4, $\beta = 30°$. From *Doerenkaemper* (2011), M.Sc. thesis supervised by the author

The Fourier transform (FT) is of common use for analysing the time series in terms of frequency content and related energy distribution. The use of FT allows to highlight the dominating frequencies in a time series and thus the size of the dominating eddies present in the flow.

The Fourier transform of a continuous signal with finite energy content can be defined as:

$$\hat{u}(f) = \int_{-\infty}^{\infty} u(t) \exp(-2\pi i f t) dt$$

The discrete version of this equation is known as the discrete Fourier transform (DFT) and commonly applied to various data sets. In practice a (numerically faster) recursive algorithm known as fast Fourier transformation (FFT) is used. Further details can be found in *Bendat and Piersol* (2011) and in *Brigham and Morrow* (1967).

Fig.5.21 shows unfiltered spectra derived with a FFT algorithm of the U (left) and V (right) component in a time series consisting of 250.000 points. Measurement location is P_1 at plane $1D$, operative conditions are Tip Speed Ratio (TSR) $\lambda_{des} = 2.9$ and pitch angle $\beta = 20°$. Both plots show a clear peak in their spectra at $35\mathrm{Hz}$ which is three times the rotational speed of the turbine in this experiment suggesting this being the signature of the blades.

There are different methods to estimate the power of a signal at different frequencies, we used

the Welch method which has the advantage of filtering the signal from the noise. In this method the power spectral density is estimated by splitting the time series into (overlapping) elements where periodograms are computed, averaged and used to produce the power spectral density estimate.

Fig.5.21 shows the unfiltered spectra, while Fig.5.22 shows the spectra that result from the application of Welch's filtering method with $L = length\ of\ timeseries/2^4$ elements.

All time series show a clear peak in the tip region of the rotor at the rotational speed of $5\mathrm{Hz}$. A second (less pronounced) spike can be observed at about $70 - 80\mathrm{Hz}$.

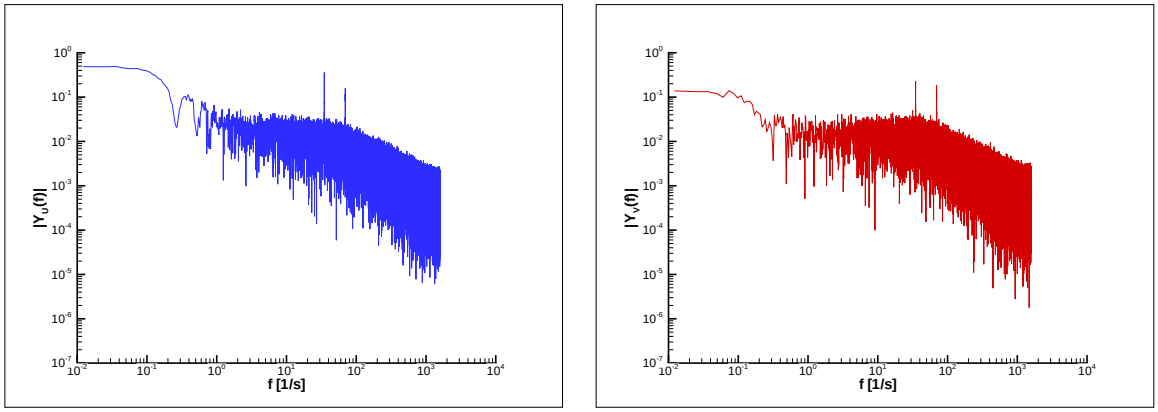

Figure 5.21.: Unfiltered spectra for the U(left) and V(right) component derived from the dimensionless time series recorded at P_1 , $\lambda_{des} = 2.9$, $\beta = 20°$. From *Doerenkaemper* (2011), M.Sc. thesis supervised by the author

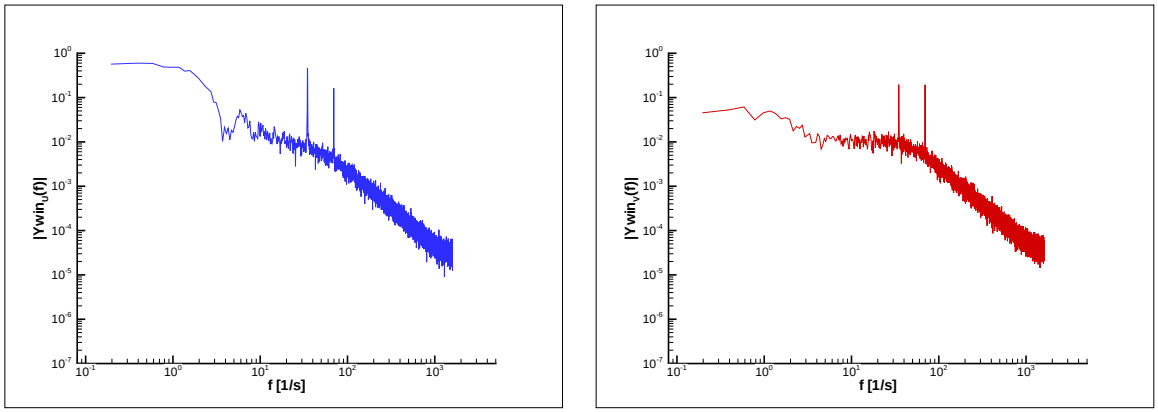

Figure 5.22.: Windowed spectra for the U(left) and V(right) component derived from the dimensionless time series recorded at P_1 , $\lambda_{des} = 2.9$, $\beta = 20°$. From *Doerenkaemper* (2011), M.Sc. thesis supervised by the author

Fig.5.23 and Fig.5.24 show different filtered spectra at different positions around the turbine at the same operative conditions. Fig.5.23 shows on the left the spectra at $1D$ at about $z/R = 0.1$. Here the presence of the nacelle induces the higher level of turbulence. Fig.5.23 on the left is taken at the same location of Fig.5.22 but at plane $2D$, the vanishing of the second spike is also clear. Fig.5.24 on the left presents the spectra of a horizontal profiles in the tip region, the shape

is essentially the same as for the vertical profile (Fig.5.22), with two distinct spikes. On the right, Fig.5.24 shows the plot at about one third of the blade length. In this area the chord length shows the greatest decrease, where visualization experiments showed intensive turbulent mixing.

In the tip region of the blade a second distinct maximum is found, which can not be detected in other regions around the blade and vanishes downstream. This can be seen as an evidence of the presence of the tip vortex. Dividing the wind speed by a particular frequency it is also possible to evaluate the size of the perturbation passing through the measurement point. Regarding the second spike visible in Fig.5.24 (left) and Fig.5.22, the size of the vortex would be in the range of $5 - 10\mathrm{cm}$, given a wind speed of $6\mathrm{m\ s^{-1}}$. This dimension can be related to the tip vortex, as visualized in Fig.5.10.

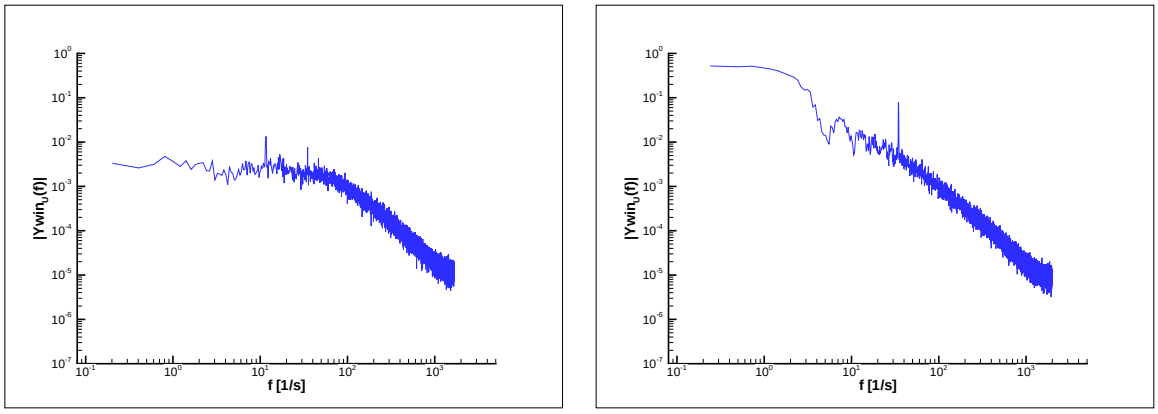

Figure 5.23.: Windowed spectra for the U-component derived from dimensionless time series at $1D$ $Z/R = 0.1$ (left), $2D$ $Z/R = 0.9$ (right). Operative conditions $\lambda_{des} = 2.9$, $\beta = 20°$. From *Doerenkaemper* (2011), M.Sc. thesis supervised by the author

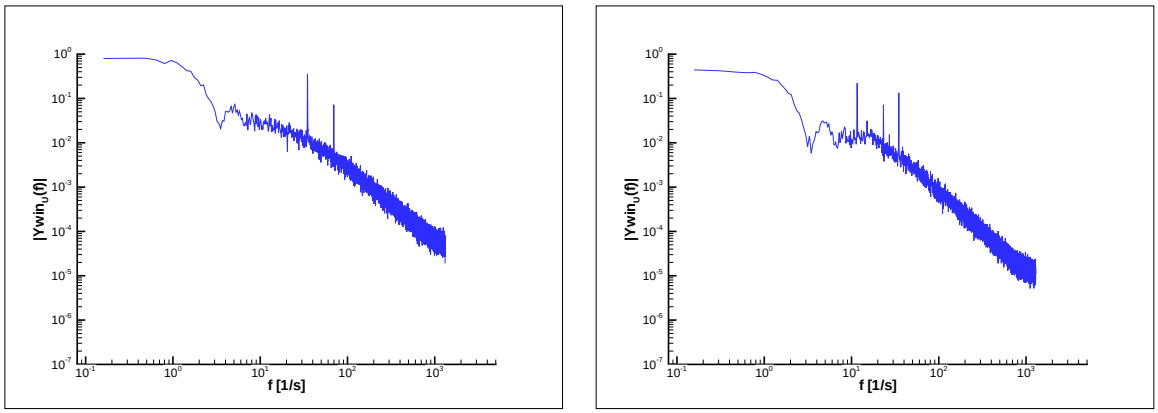

Figure 5.24.: Windowed spectra for the U-component derived from dimensionless time series at $1D$, $Y/R = 0.9$ (left), $1D$, $Y/R = 0.34$ (right). Operative conditions $\lambda_{des} = 2.9$, $\beta = 20°$. From *Doerenkaemper* (2011), M.Sc. thesis supervised by the author

6. Phase 3 - Sensitivity Analysis

This section is based on *Cuzzola et al.* (2012) presented at EAWE Conference "The Science of Making Torque from Wind", Oldenburg 2012.

6.1. Introduction

The large number of degrees of freedom involved in the simulation of the wake of a wind turbine in atmospheric boundary layer flow (see Ch.1), suggested to investigate the performances of the wind turbine model at different operative conditions.

As previously discussed in Ch.1, the four similarity parameters of the wind turbine wake flow are Reynolds number Re, Tip Speed Ratio (TSR) λ, power coefficient C_P and thrust coefficient C_T. The latter is thought to be the most effective one, see *Neff et al.* (1990). For this reason the scope of this experiment was to carry out a sensitivity analysis of the thrust coefficient C_T on the changing operative conditions. The evaluation of C_T was carried out with two methods: first using force measurements and then using velocity measurements. The evaluation of C_T with velocity measurements is based on a mathematical approximation and force balance measurements provide a reference. In addition, velocity measurements allow to distinguish if the momentum loss in the flow field is transformed into torque or not.

6.2. Experimental setup

The experiment was carried out in the "Malavard" wind tunnel at the PRISME Laboratory of the University of Orléans, see App.A for details. In this study, the main test section (2m high, 2m wide and 5m long) of the wind tunnel is used. In order to perform measurements in homogeneous isotropic turbulent flow, a turbulence grid is placed at the entrance of the test section. The turbulence grid is made of metallic square section bars of diameter $25\mathrm{mm}$ and mesh size $100\mathrm{mm}$. The approaching mean wind speed is $U_0 = 10\mathrm{m\ s^{-1}}$ and the turbulence intensity is $Iu_0 = 3\%$ (ratio between the standard deviation of streamwise velocity and its time average) at the rotor location.

Aerodynamic loads are measured with a 6-components force balance located below the test section. The mast of the model ($34\mathrm{mm}$ in diameter) is used to link the balance to the model. The precision of the balance is estimated to be $0.16\mathrm{N}$ for the drag component and $0.48\mathrm{N}$ for the lift component. The sampling frequency is fixed to $500\mathrm{Hz}$, and 25000 samples are acquired for each configuration. The measurement of the three components of velocity was carried out using a

Dantec triple hot-fiber probe, connected to the Dantec StreamLine system. The probe was fixed on an automated traverse system. More information about hot wire anemometry (HWA) are given in App.A.

In addition to the blade designed for highest power coefficient C_P, see sec.4, a second set of blades was also manufactured. The blades share the same Jedelsky $EJ85$ airfoil, the length of $210\mathrm{mm}$, the wetted surface of $0.303\mathrm{m}^2$ and the twist angle distribution which is a linear approximation of the optimum distribution. The only geometric parameter which changes is the chord distribution. From now on we refer to these blades/rotor as Optimum Blade **OB** and Linear Chord blade **LC**. The latter blade was designed as a reference in assessing the importance of the chord distribution for models of such small scale. Fig.6.1 and Fig.6.2 show the experimental set-up and the model wind turbine with the two rotors.

The wind turbine model is equipped with a DC motor (see sec.4.2.2) which allows the rotational velocity Ω to be controlled using a power supply. Fig.6.3 shows the almost perfect linear dependency of the rotational speed with the increasing voltage supplied in the no wind case. If disconnected from the power supply, the motor would also work as a generator transforming the torque into electricity. In the latter configuration the turbine is driven by the wind only. From now on, this two operative configurations of the model will be named *active status* and *passive status* respectively. In this experiment the three configurations described in Tab.6.1 were examined.

The systematic variation of parameters such as λ, the tunnel wind speed U_∞ and the pitch angle β allows to describe the dependencies of the C_T with respect to the operating conditions. In the present experiment, first U_∞ and β were set then Ω was adjusted to the desired value of λ and data have been collected.

Table 6.1.: Wind turbine operative conditions investigated

$U_\infty(\mathrm{m\ s^{-1}})$	λ	Wind turbine status
10	[0.2-2]	active
2.5	7	active
10	2.5	passive

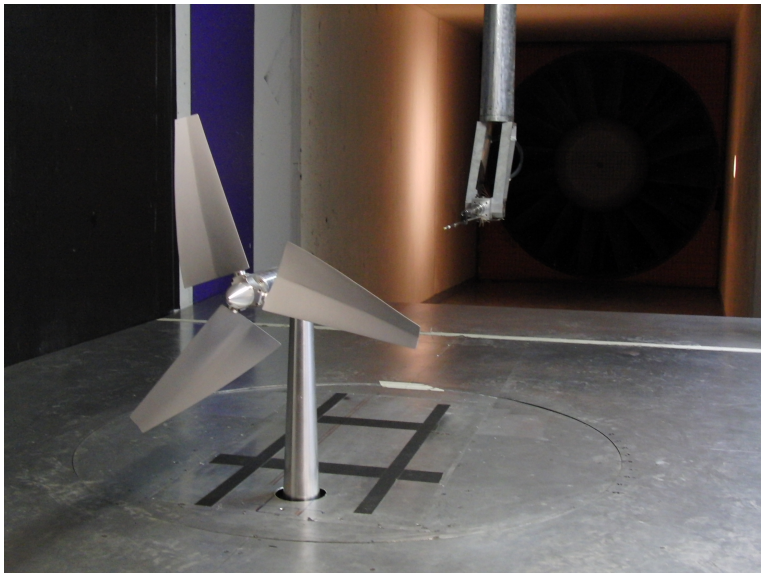

Figure 6.1.: **LC** configuration and experimental set up.

Figure 6.2.: Model wind turbine with **OB** rotor.

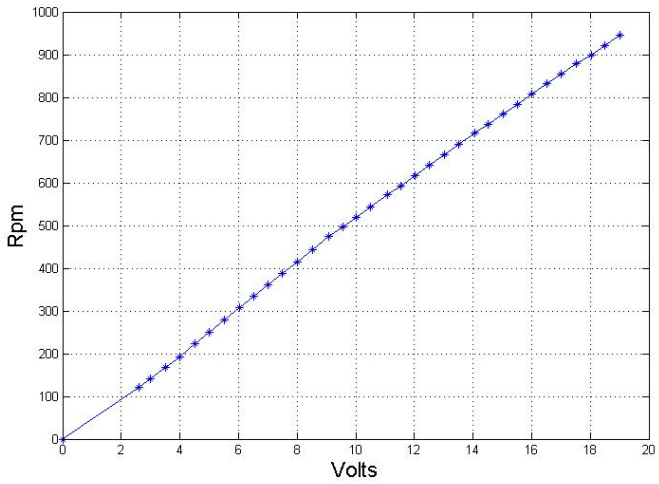

Figure 6.3.: $RPM - Voltage$ curve for the model wind turbine

6.3. Force measurements

In this section, results of the force measurements are presented for both active and passive status of the wind turbine model.

Wind turbine model in active status - wind speed $10\mathrm{m\ s^{-1}}$

Fig.6.4 and Fig.6.5 show the variation of the thrust coefficient for **LC** and **OB**. The **LC** rotor shows higher (30% to 50%) C_T values than **OB** for a given value of λ. Also, for certain values of the pitch angle β, the $C_T - \lambda$ curve show different trend for the two rotors, as shown in Fig.6.6 and Fig.6.7.

The **OB** rotor can operate up to pitch angle values $\theta = 70°$. The **LC** rotor, due to the larger tip area of the blade, operates only for pitch angles up to $\theta = 60°$.

From these measurements it is clear that the chord distribution has a very important influence on the thrust coefficient and on the C_T-TSR dependency. Furthermore, the graphs show that the value of the TSR corresponding to the maximal value of the thrust coefficient $C_{T_{MAX}}$ increases with increasing pitch angle. Also, at higher β, the trends suggest that $C_{T_{MAX}}$ might be found in a higher range of values of the tips speed ratio λ. Unfortunately, the motor and the available supply system do not allow higher rotational speed to be achieved and higher values of λ could not be investigated at $10\mathrm{m\ s^{-1}}$ wind speed.

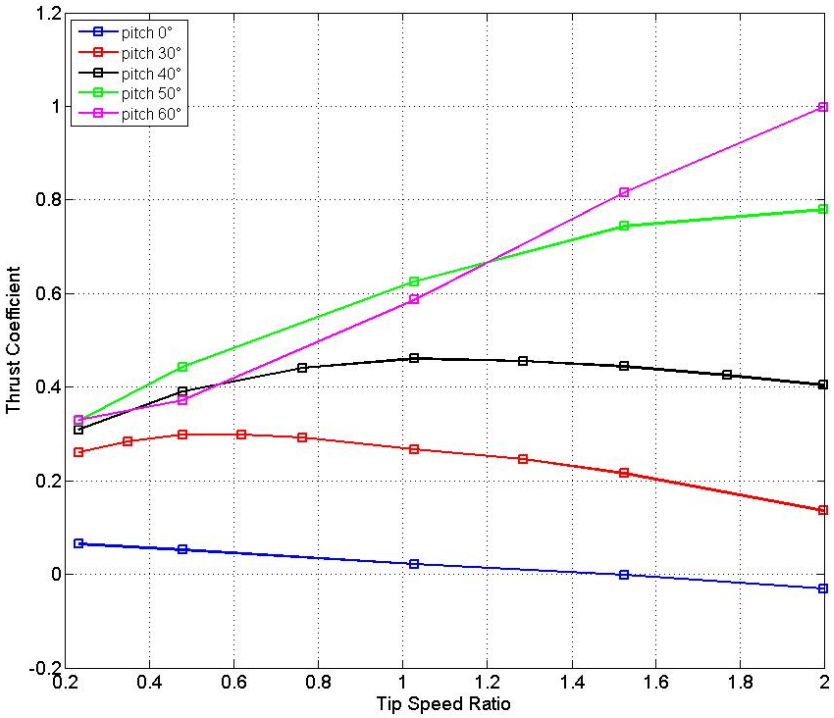

Figure 6.4.: Effects of the pitch angle on the $C_T - \lambda$ curve for **LC**, $U_\infty = 10\mathrm{m\ s^{-1}}$, active status

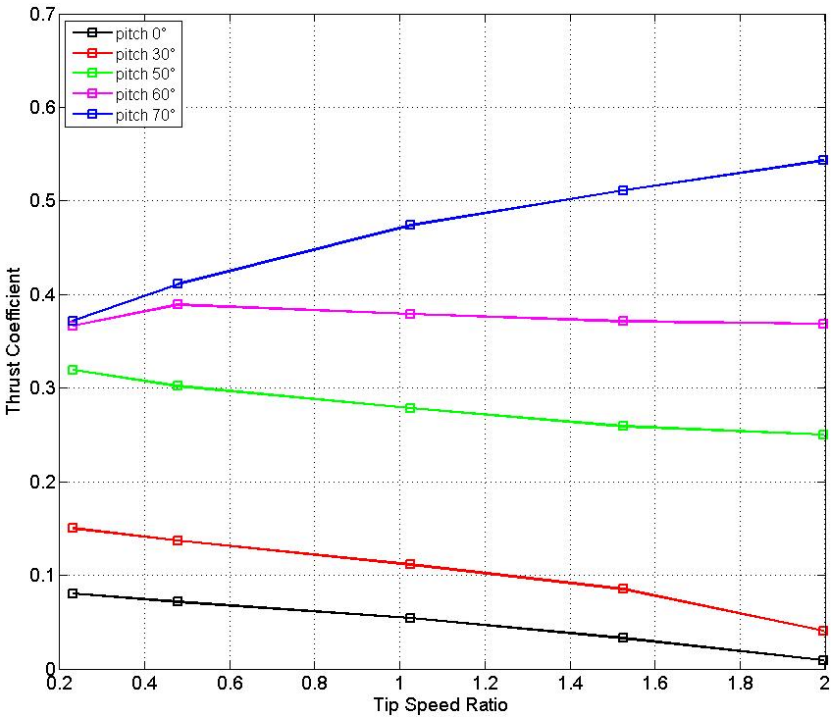

Figure 6.5.: Effects of the pitch angle on the $C_T - \lambda$ curve for **OB**, $U_\infty = 10\mathrm{m\ s^{-1}}$, active status

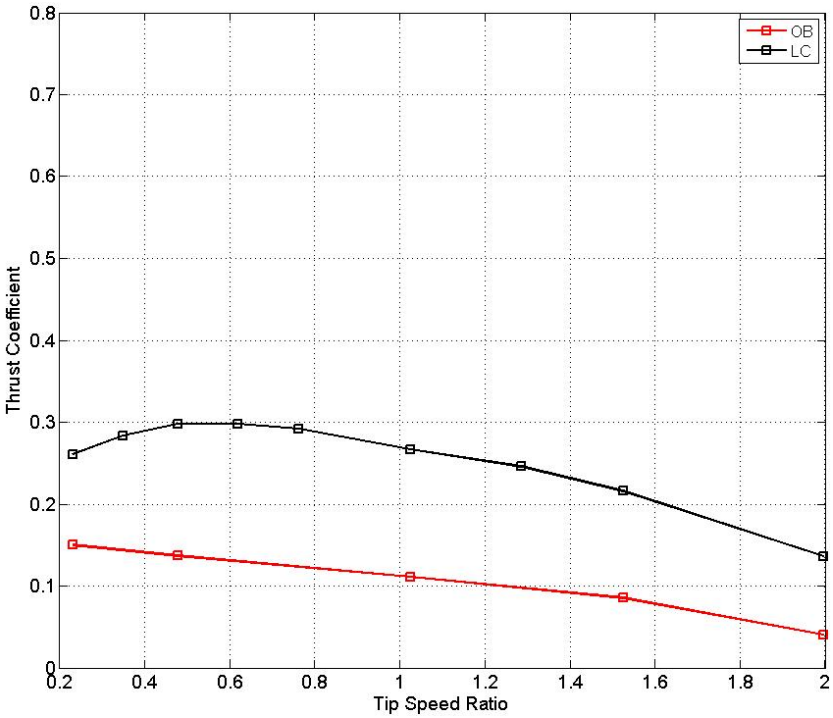

Figure 6.6.: $C_T - \lambda$ curve comparison at $theta = 30°$, $U_\infty = 10\text{m s}^{-1}$, active status

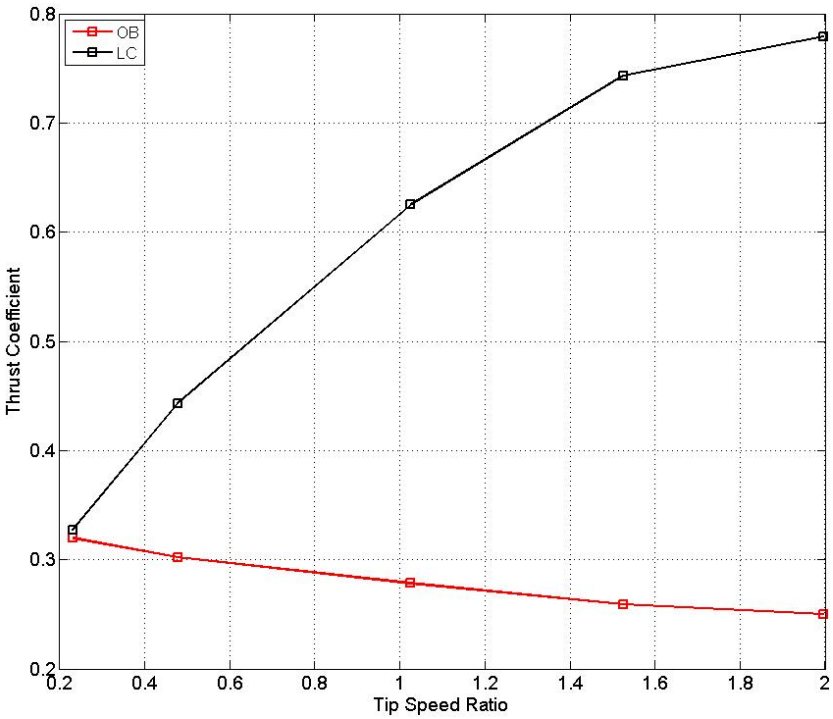

Figure 6.7.: $C_T - \lambda$ curve comparison at $theta = 50°$, $U_\infty = 10\text{m s}^{-1}$, active status

Wind turbine model in passive status - wind speed $10\mathrm{m\ s^{-1}}$

Disconnecting the power supply the rotational speed of the model rotor depends on the wind speed and on the resistance applied to the DC motor/generator output. In case of a short circuit the internal torque of the motor increases, blocking the shaft. Thus, the turbine stops rotating. On the other hand, the application of a resistance to the output lowers the internal torque. Theoretically, if an infinite resistance is applied, the internal torque tends to zero.

Fig.6.8 shows the C_T vs β curves in this latter configuration. Both curves exhibit a change at $\theta = 40°$ where the thrust coefficient starts increasing with a steeper trend. The increase of pitch angle increases the area of the blade that is directly exposed to the flow, the aerodynamic drag increases and this explains the trend. The velocity measurements shown in the next section give a better insight on this aspect.

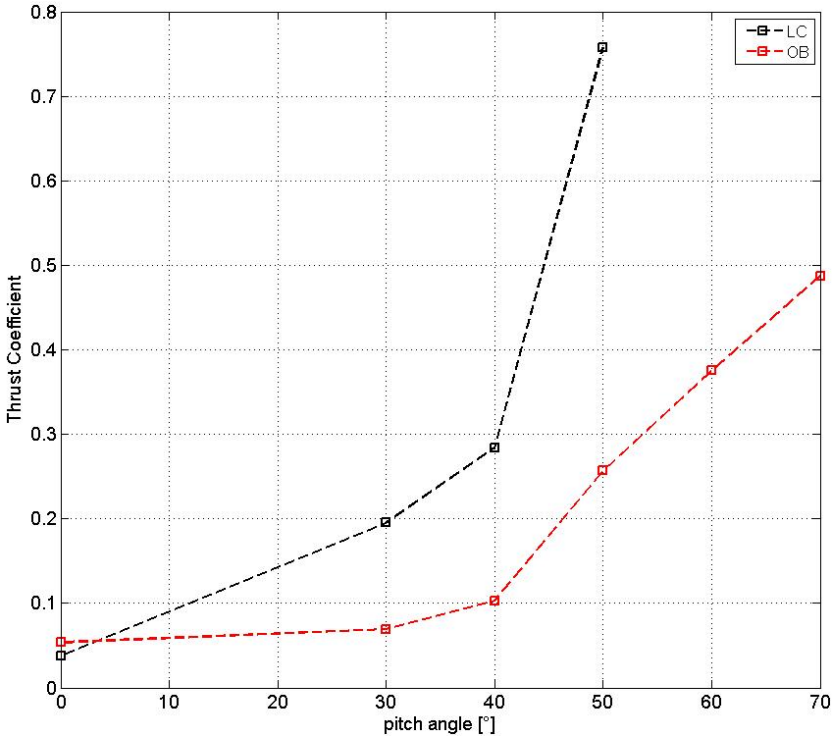

Figure 6.8.: $C_T - \theta$ curves, $U_\infty = 10\mathrm{m\ s^{-1}}$, passive status

6.4. Velocity measurements

Horizontal velocity profiles have been measured at a distance of $708\mathrm{mm}$ downstream of the rotor plane, which corresponds to three rotor diameters.

6.4.1. Results at $10\mathrm{m\ s^{-1}}$ - passive status

The graphs of Fig.6.9 and Fig.6.10 show the velocity deficit along the blades for the two rotors. The abscissa is $r = x/R$ where R is the radius of the rotor and x the radial distance. The velocity deficit increases with increasing pitch angle.

Fig.6.11 and Fig.6.12 highlight the differences between the rotors. The wind speed recovers smoothly in the **OB** configuration. The trend shown is consistent with previous experiment, such as *Chamorro and Porté-Agel* (2009) and *Sanderse* (2009), and with field experiments, see *Mann* (2010). The **LC** configuration, which at $\theta = 50°$ delivers a remarkably high C_T, shows a different wake behaviour, with the maximum of the velocity deficit occurring in the outer part of the blade.

Fig.6.13 and Fig.6.14 present the root mean square curves of the U component of the velocity. **OB** rotor has lower turbulence intensity than **LC**. Also, it shows a spike in correspondence of the blade elbow. In this area at about 60% of the blade span, vortex shedding was recorded in previous experiments (see sec.5.2.3). The **LC** rotor shows instead an increase of the turbulence intensity in the outer part ($r = [0.6 - 1]$) of the blade. At $\theta = 50$ this increase is much higher than in the case of **OB**, as can be seen in Fig.6.15.

For the above stated reasons, these graphs indicate that the **LC** rotor might generate its velocity deficit by converting the momentum into turbulence, rather than into torque.

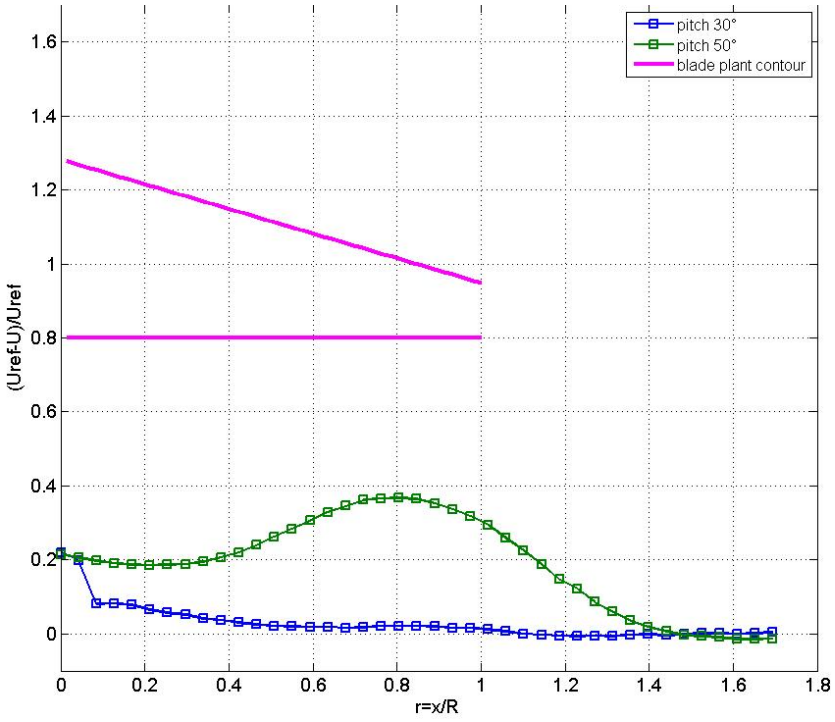

Figure 6.9.: Velocity deficit curves for **LC**. $U_\infty = 10\mathrm{m\ s^{-1}}$, passive status

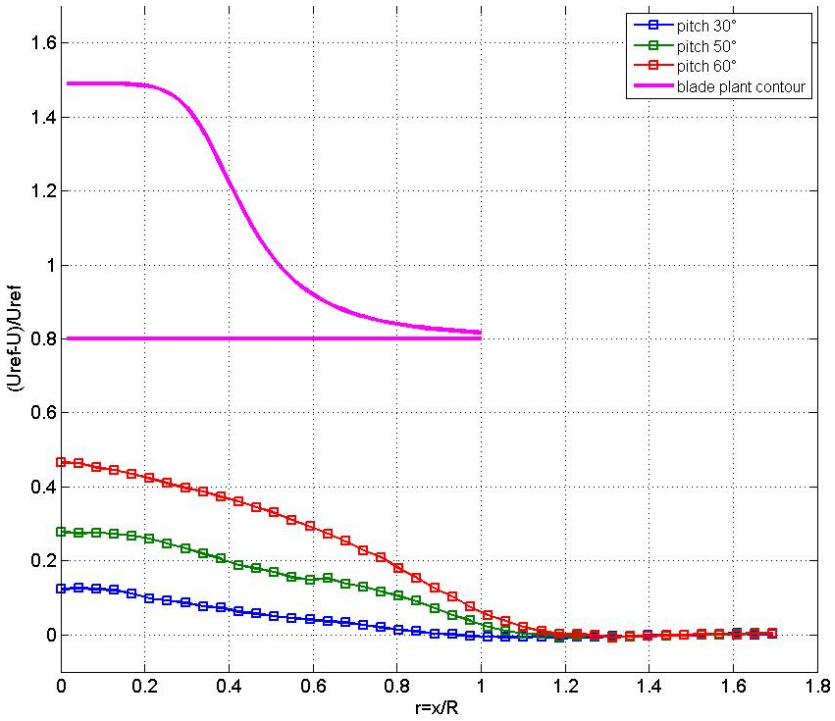

Figure 6.10.: Velocity deficit curves for **OB**. $U_\infty = 10\mathrm{m\ s^{-1}}$, passive status

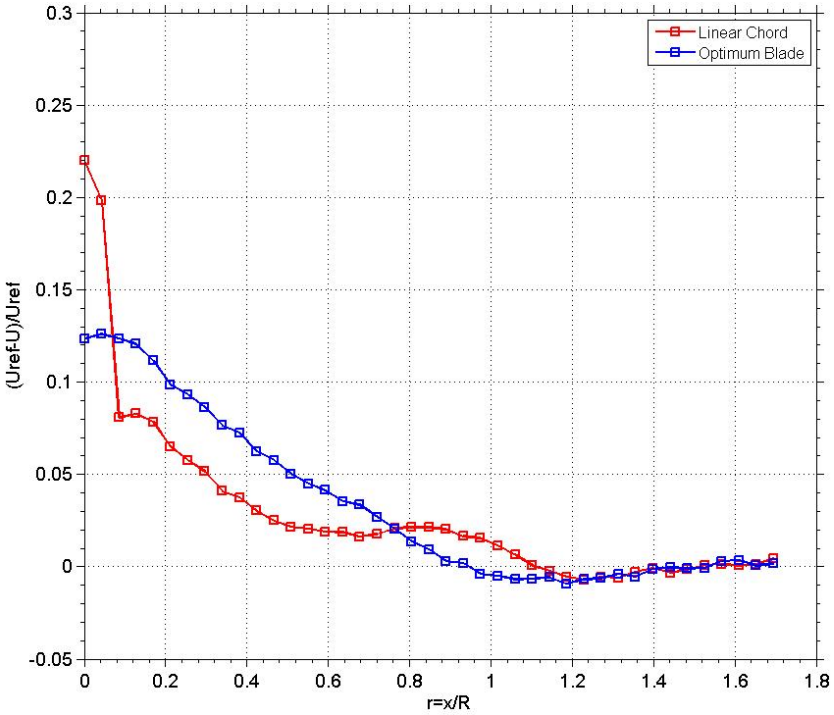

Figure 6.11.: Velocity deficit comparison at $\theta = 30°$. $U_\infty = 10\text{m s}^{-1}$, passive status

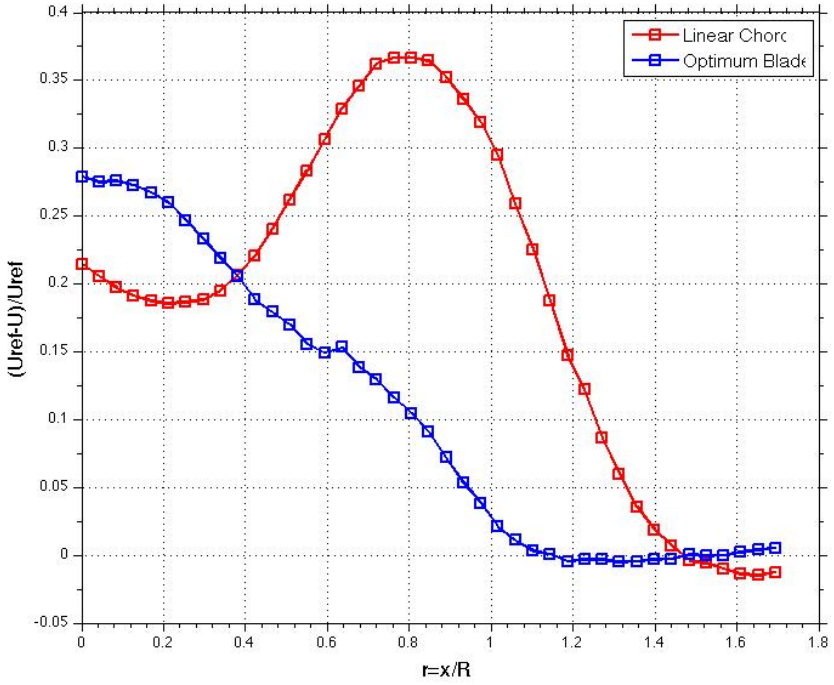

Figure 6.12.: Velocity deficit comparison at $\theta = 50°$. $U_\infty = 10\text{m s}^{-1}$, passive status

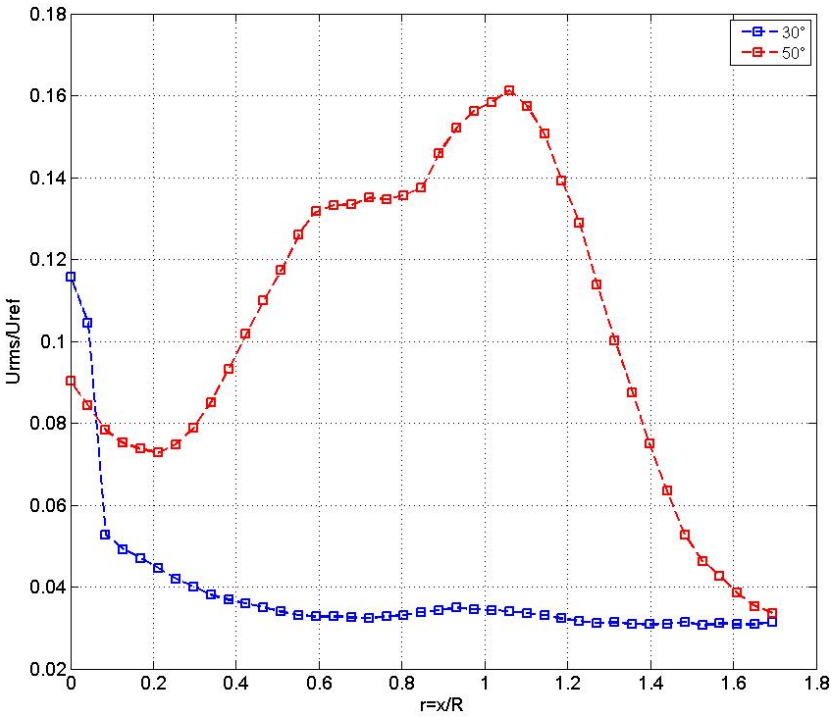

Figure 6.13.: Turbulence intensity for **LC**. $U_\infty = 10\mathrm{m\ s^{-1}}$, passive status

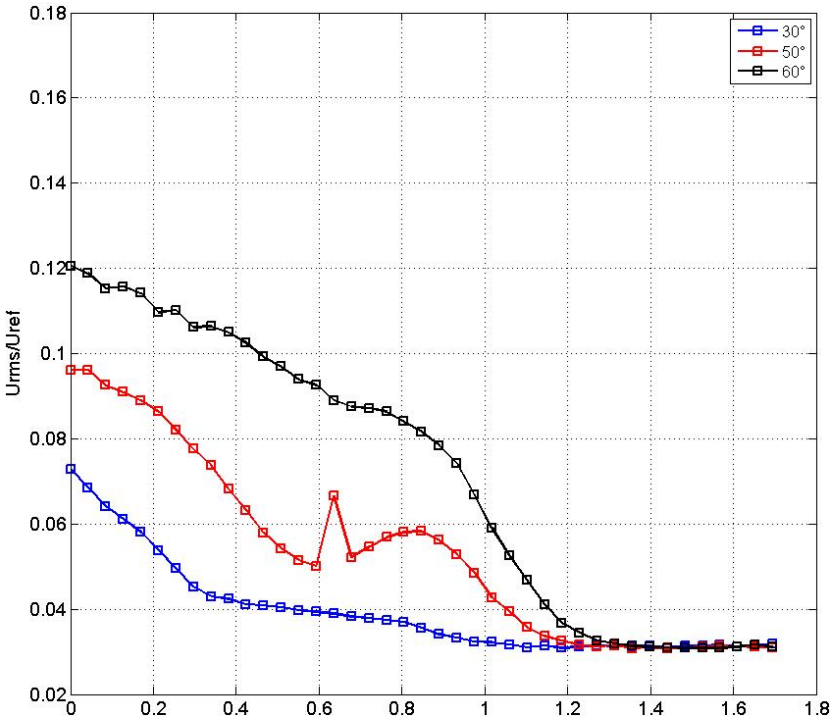

Figure 6.14.: Turbulence intensity for **OB**. $U_\infty = 10\mathrm{m\ s^{-1}}$, passive status

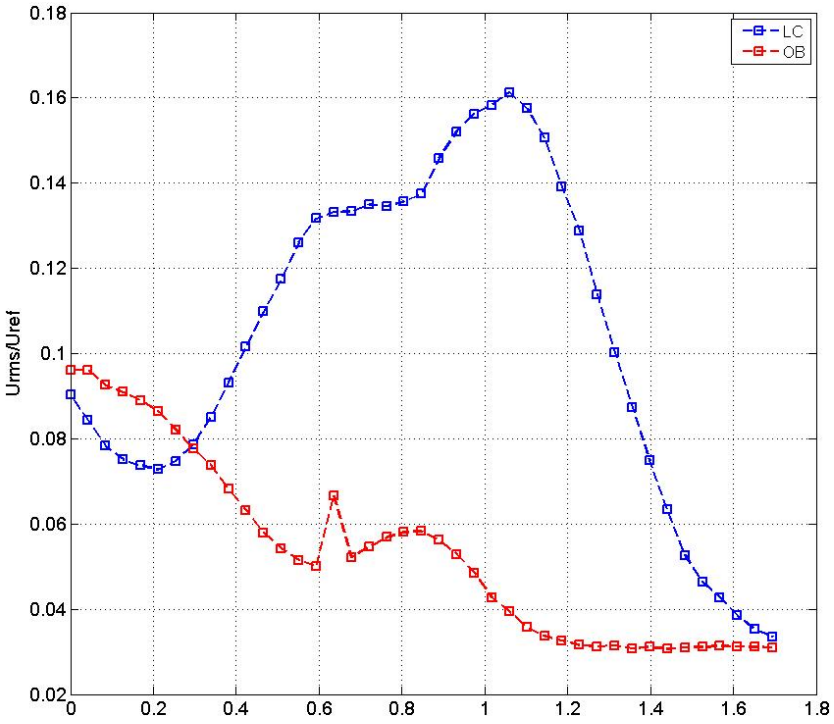

Figure 6.15.: Turbulence intensity comparison at $\theta = 50°$. $U_\infty = 10\mathrm{m\ s^{-1}}$, passive status

6.4.2. Results at $2.5\mathrm{m\ s^{-1}}$ - active status

In order to investigate the wake at $\lambda = 7$, a value of the tip speed ratio in use also for commercial wind turbines, the wind speed was set to $U_\infty = 2.5\mathrm{m\ s^{-1}}$ and the rotational speed to $\Omega = 708\mathrm{rpm}$. The result, presented in Fig.6.16, shows that the turbine does not extract energy from the flow field but it is accelerating the flow. The axial force acts in the opposite direction of the stream and the model is not behaving as a turbine but as a propeller. Thus, for this model wind turbine, an attempt to match the similarity parameter λ by actively driving the rotation of the motor has to be considered as inappropriate. From this experiment, only operative configuration of *passive status* are representative of the real behaviour of a wind turbine. The quantitative matching of the thrust coefficient can not be considered as a sufficient condition for similarity. A prove that the model transforms the axial momentum of the flow field into torque, thus harvesting energy, has to be included.

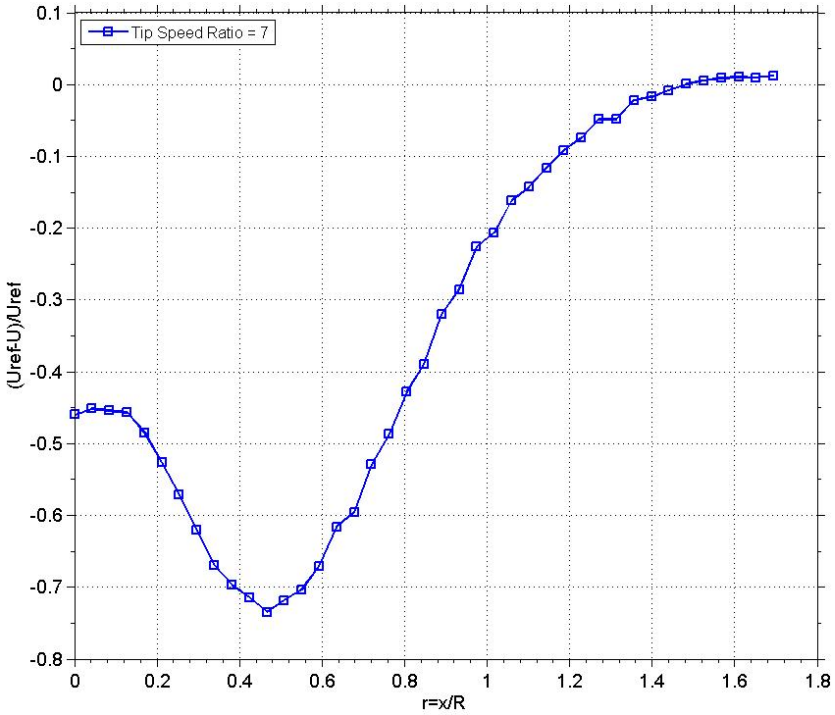

Figure 6.16.: Velocity deficit for **LC** at $\theta = 30°$ and $\lambda = 7$. $U_\infty = 2.5\mathrm{m\ s^{-1}}$, active status

6.4.3. Calculation of the thrust coefficient

At the distance of three rotor diameters downstream of the wind turbine model, the V and W components of the velocity are less than 5% of U (see Fig.6.17) and can be neglected in the calculation of the thrust coefficient. According to the blade element momentum theory, see *Aubrun et al.* (2007), the thrust coefficient can be calculated using the relation:

$$T = 2\pi \int_0^\infty \rho U_{mean}(r)(U_\infty - U_{mean}(r))r\,dr \tag{6.1}$$

Tab.6.2 shows a comparison between the values of the thrust coefficient evaluated respectively from the force measurements and from the velocity ones.

Table 6.2.: Thrust coefficient calculation - summary table

rotor	**LC**	
measurement type	**Force**	**Velocity**
$\theta = \mathbf{30}°$	0.19	0.047
$\theta = \mathbf{50}°$	0.75	0.62

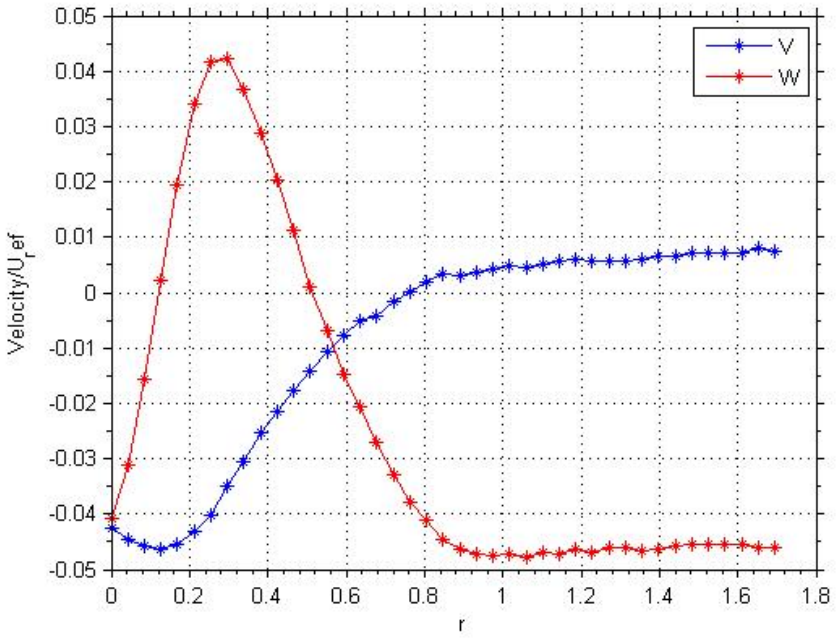

Figure 6.17.: V and W Dimensionless velocity components three diameters downstream of the **LC** rotor. $U_\infty = 10\text{m s}^{-1}$, passive status

6.5. Conclusions

The chord distribution has a big influence on the performances and on the wake of the model. In particular the **LC** rotor delivers a higher thrust coefficient than the **OB** one. However, only the latter configuration shows velocity profiles consistent with previous literature. In addition, the velocity profiles of the **LC** rotor suggest that the blades are working in stalled conditions. For these reasons the **OB** rotor should be considered as a more appropriate choice for simulating the wake of a wind turbine in a wind tunnel.

Besides this result it must be pointed out that, if a wind turbine rotor model is used, the matching of the thrust coefficient needs to be integrated with velocity measurements. These measurements have to assure the transformation of the axial momentum of the flow field into torque, hence harvesting energy. Also, the matching of the tip speed ratio should not be achieved by means of powering the motor and driving the rotation of the turbine. This operation may result in a change in the overall behaviour of the turbine adding energy to the flow.

Experimental power curves

The experimental prove that an active driving of the model has to be avoided, suggests to investigate more in detail the performances of the wind turbine model in *passive status*. Thus, another experiment was carried out in the Göttingen-type wind tunnel in Hamburg. This experiment aims to give a qualitative overview of the performances only. Following the conclusions, the **OB** rotor has been used. Details about the internal electronics of the DC motor are not released. Therefore,

interpretations of the behaviour can be based on the trend of the power curve measured only.

The application of a series of electric resistances to the output of the DC motor/generator allows the internal torque of the motor to be adjusted. Also, the electric output can be monitored and registered in terms of frequency and voltage by using an oscilloscope. Using this quantities it is possible to calculate C_P and λ. In particular resistors between 22 and 138 Ohms have been applied to the model and the wind speed varied between $3.5\mathrm{m\ s^{-1}}$ and $11.2\mathrm{m\ s^{-1}}$.

Fig.6.18 shows the trend of the tip speed ratio with respect to increasing electric resistance, at various wind speeds. The growth of λ is monotonic with respect to both parameters. Fig.6.19 illustrates the corresponding power curves of the turbine at the same operative conditions.

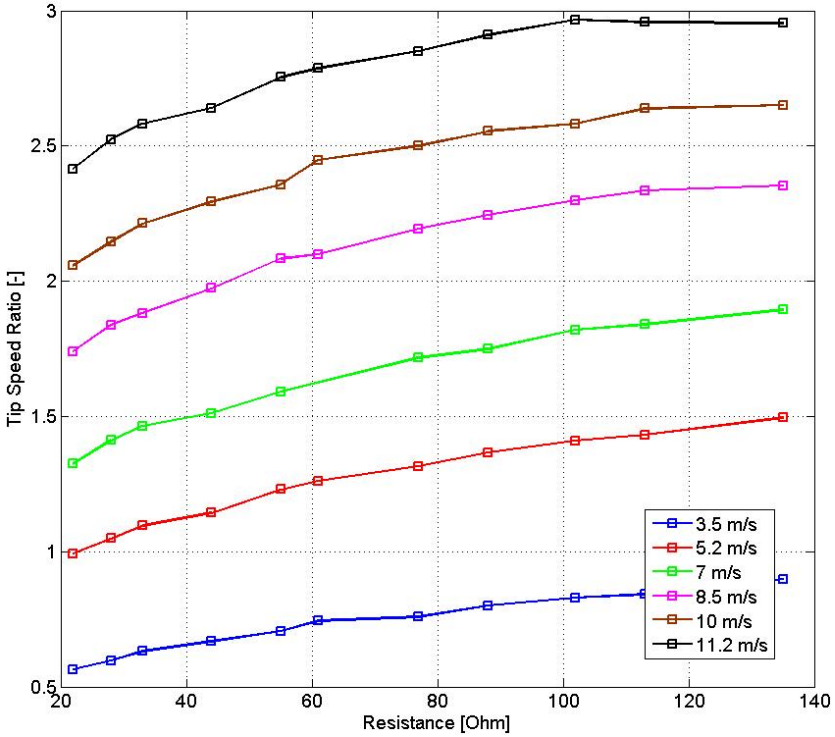

Figure 6.18.: influence of the electric load on the tip speed ratio - **OB** rotor

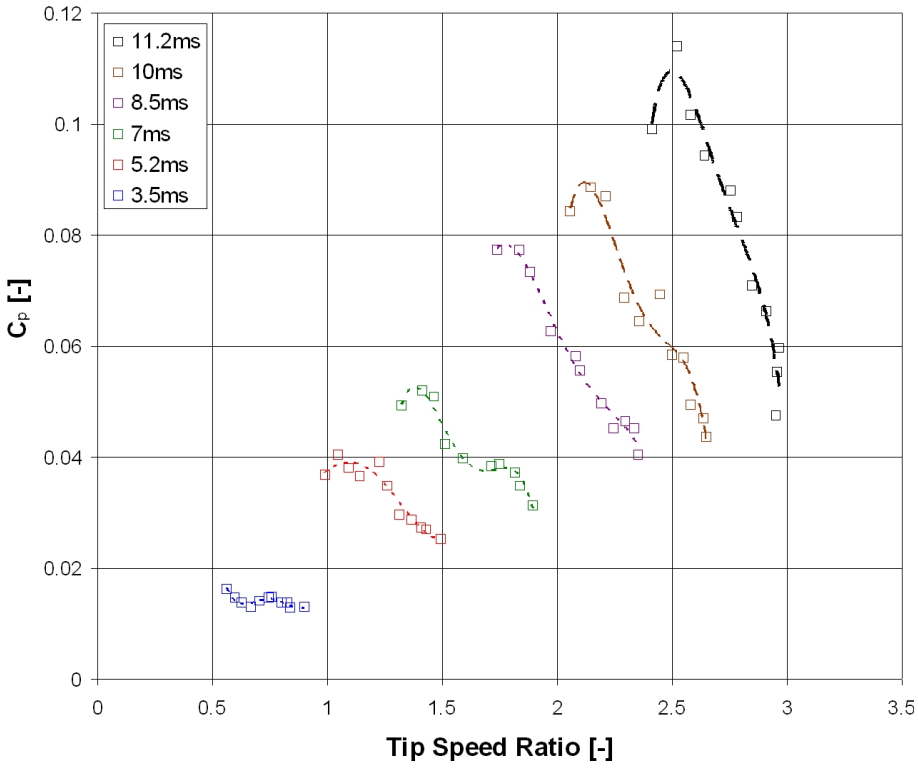

Figure 6.19.: power curves of the wind turbine model - **OB** rotor

7. Phase 4 - Wake of a Wind Turbine and Atmospheric Boundary Layer Effects

In this chapter the experimental campaign in the ABL wind tunnel "Wotan" is described. First, informations about the experimental setup and operative conditions are given. Then, velocity measurements in the wake of the wind turbine model are presented.

7.1. Experimental setup and operative conditions

The model

The operational condition of the model was chosen based on the previous experiments, see Chap.6. Thus, the optimum blade **OB** was used and the pitch angle set to $\beta = 50°$. The wind speed was set to $10\mathrm{m\ s^{-1}}$ and resistors were applied to the electric output. An oscilloscope was used to monitor the electric output of the motor, as in sec.6.5.

For the free stream case, in order to place the rotor above the boundary layer developing along the wind tunnel floor, an extended tower was used.

Tab.7.1 summarizes the main operative parameters.

Table 7.1.: Wind turbine configurations investigated

	Free Stream	ABL
Hub Heigth	$725\mathrm{mm}$	$375\mathrm{mm}$
θ	$50°$	$50°$
Resistance	28Ω	28Ω

Fig.7.1 and Fig.7.2 show the model in a close-up image and from the inlet of the wind tunnel respectively. The dimensions of the model with respect to the tunnel are noticeable. Fig.7.3 illustrates the setup for 2 wind turbines in the free stream case.

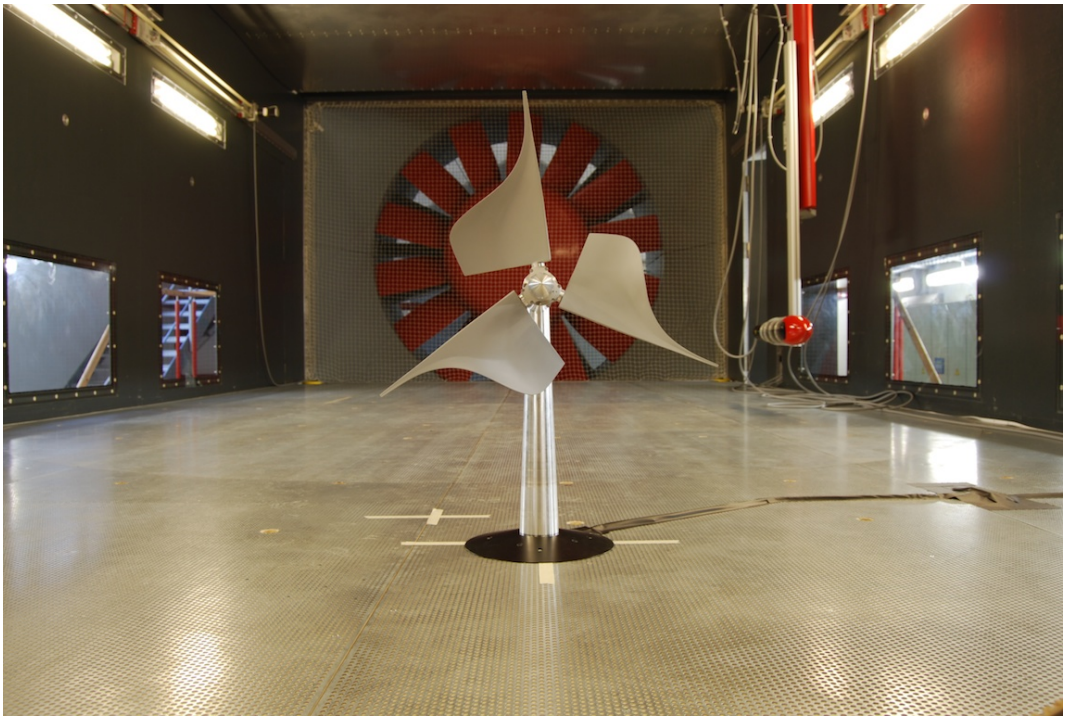

Figure 7.1.: The model wind turbine ready to be tested, ABL case

Figure 7.2.: Total view of the model from the inlet of the Wotan wind tunnel

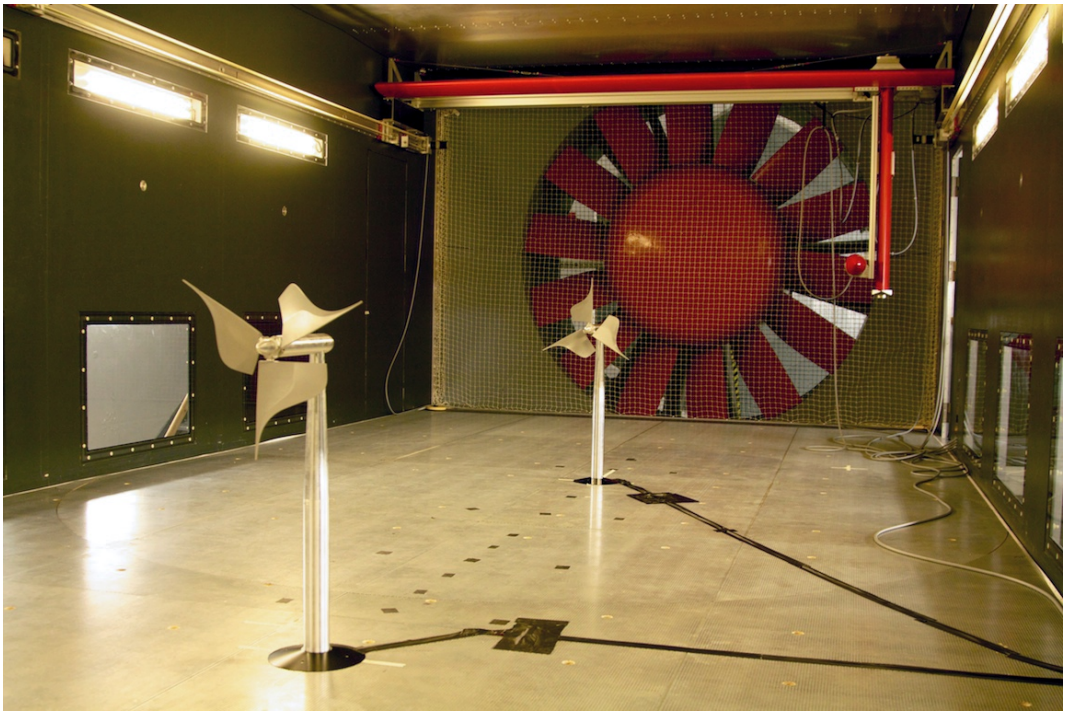

Figure 7.3.: 2 models in the free stream case, the higher towers are noticeable.

The wind tunnel

General information about the tunnel are given in App.A, as well as specifics about the LDA system. In this particular campaign we used the general set up of the Wotan wind tunnel for a velocity measurement campaign, see Fig.7.4.

A focal distance of $500\mathrm{mm}$ was used for the laser probe, the reference wind speed is taken at the tunnel inlet using a Prandtl tube. Its location is illustrated in Fig.7.5 together with the spires set up in use for the ABL case.

The traverse system uses a coordinate system to identify the measurement points. The origin of this coordinate system is set at a distance of $14,25\mathrm{m}$ from the inlet of the tunnel (x coordinate), at its centerline (y) on the floor (z).

The velocity profiles are measured at several cross-wind planes behind the model. The reference position used for the exact identification of these planes is set at the hub center. Fig.7.6 shows the coordinates of the reference point. Here it is also possible to see how the electric wires are taped to the floor in order to avoid any aerodynamic interference. From now on, we refer to this coordinate system as *reference system*.

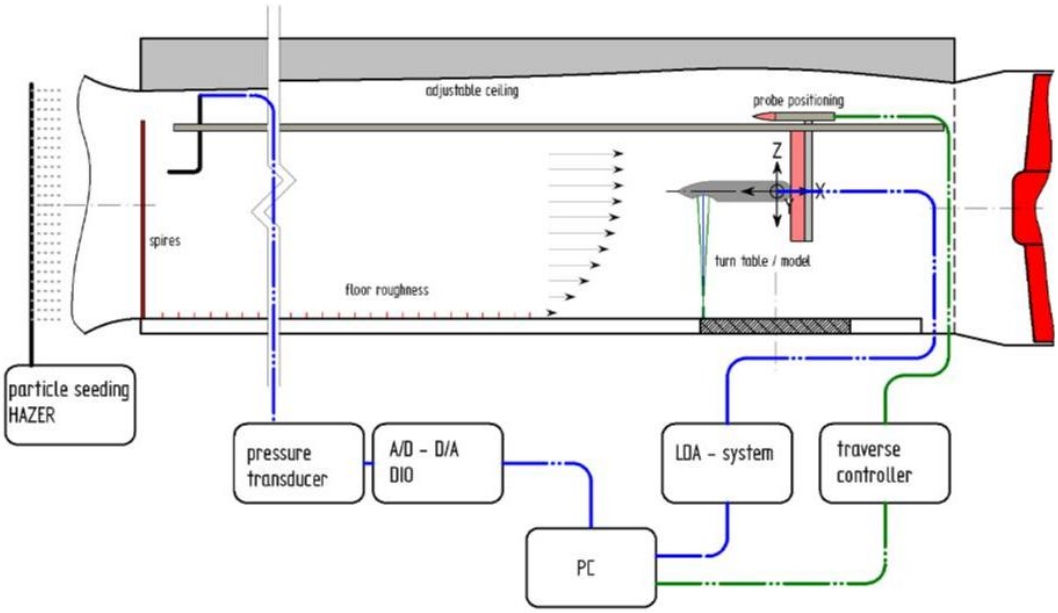

Figure 7.4.: The general experimental set up in the Wotan wind tunnel

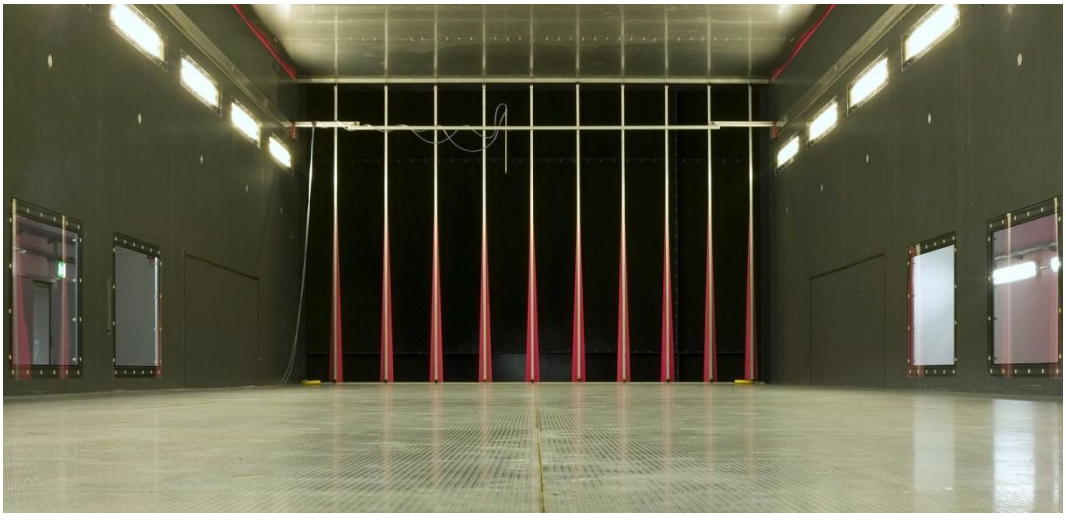

Figure 7.5.: Inlet of the tunnel with spires and Prandtl tube

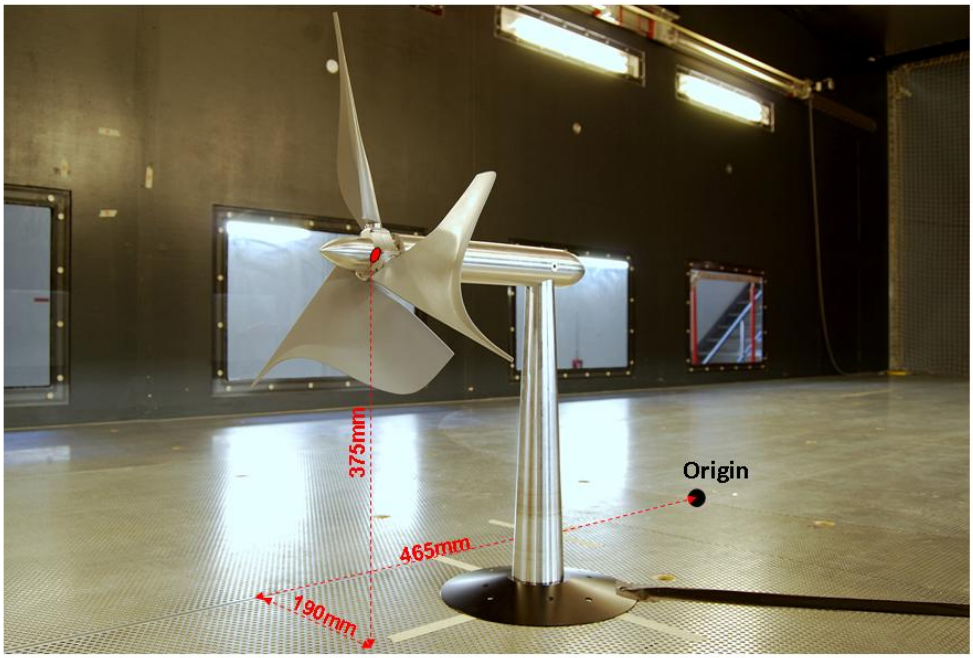

Figure 7.6.: Coordinates of the center of the hub and turbine model set up

7.1.1. Preliminary measurements

Before the start of the campaign a set of preliminary measurements was carried out. In this section informations about the inflow conditions and repeatability of the experiment are given. Also, the measurement plan is described.

The inflow conditions

As already discussed in Ch.1, one of the key aims of these tests is to assess the influence of the atmospheric boundary layer (ABL). Hence, tests were carried out for both the free stream and the ABL case.

The ABL is generated using spires and floor plates as can be seen in Fig.7.5 and Fig.7.7 respectively.

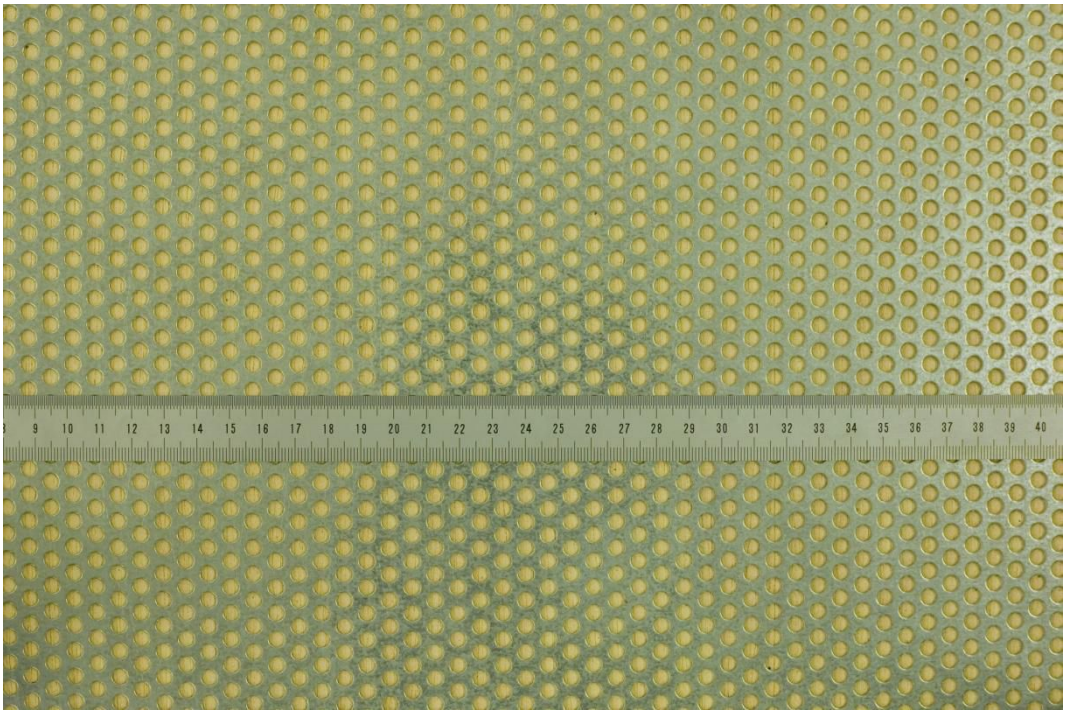

Figure 7.7.: Floor plates with metallic mesh

Free stream case The behaviour of the wake is often studied in the very ideal case of homogeneous free stream, a pure aerodynamic condition that does not occur in reality. In order to have a reference case when assessing the influence of the ABL, these conditions were modelled as well.

In order to document the lateral homogeneity of the flow inside the tunnel vertical velocity profiles were taken at four locations. The profiles were measured at the plane corresponding to hub center location ($x = 0$ of the reference system). In particular four profiles were measured: at the center ($[x = 0, y = 0, z]$) and in other three locations: $y = -450\mathrm{mm}$, $y = 450\mathrm{mm}$ and $y = 1000\mathrm{mm}$. The results, illustrated in Fig.7.8, show that the measured velocities at the

different locations are within the uncertainties range. However, for $z > 300\mathrm{mm}$, the velocity tends to higher values from left ($y = -450\mathrm{mm}$) to right ($y = 10000\mathrm{mm}$).

The Wotan wind tunnel is an ABL wind tunnel, specifically designed for wind engineering purposes, and not a purely aerodynamic tunnel. This small asymmetry is always compensated when modelling the ABL by using spires at the inlet. Nevertheless, even beyond the design boundaries of the wind tunnel, the lateral homogeneity is whithin $\pm 2.5\%$.

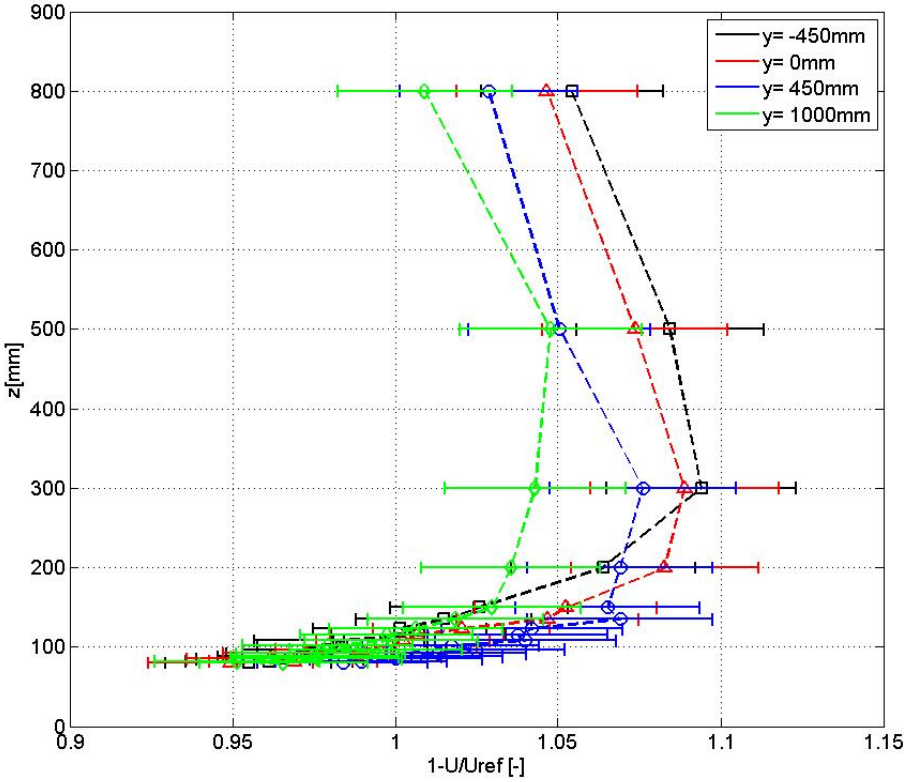

Figure 7.8.: Lateral homogeneity of the flow, non-dimensional U component vertical profiles

Atmospheric Boundary Layer case As pointed out in Ch.1 this experiments shared the same ABL flow with another research project. The whole detailed description of the inflow conditions can be found in *Petersen* (2013). Here, velocity profile plots of the U component at different locations in the plane $x = 0$ are presented. Fig.7.9 shows the lateral homogeneity of the flow. The circles identify the measurements from *Petersen* (2013) which extend closer to the floor of the tunnel.

Also from *Petersen* (2013), Fig.7.10 presents the turbulence quantities graphs.

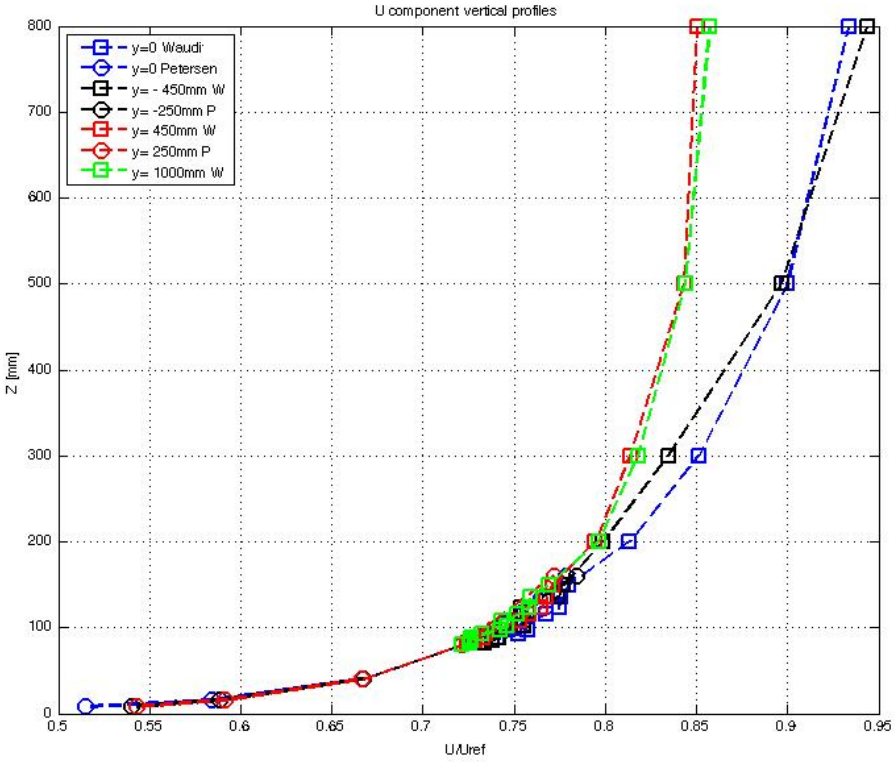

Figure 7.9.: Vertical profiles of the U component of the velocity

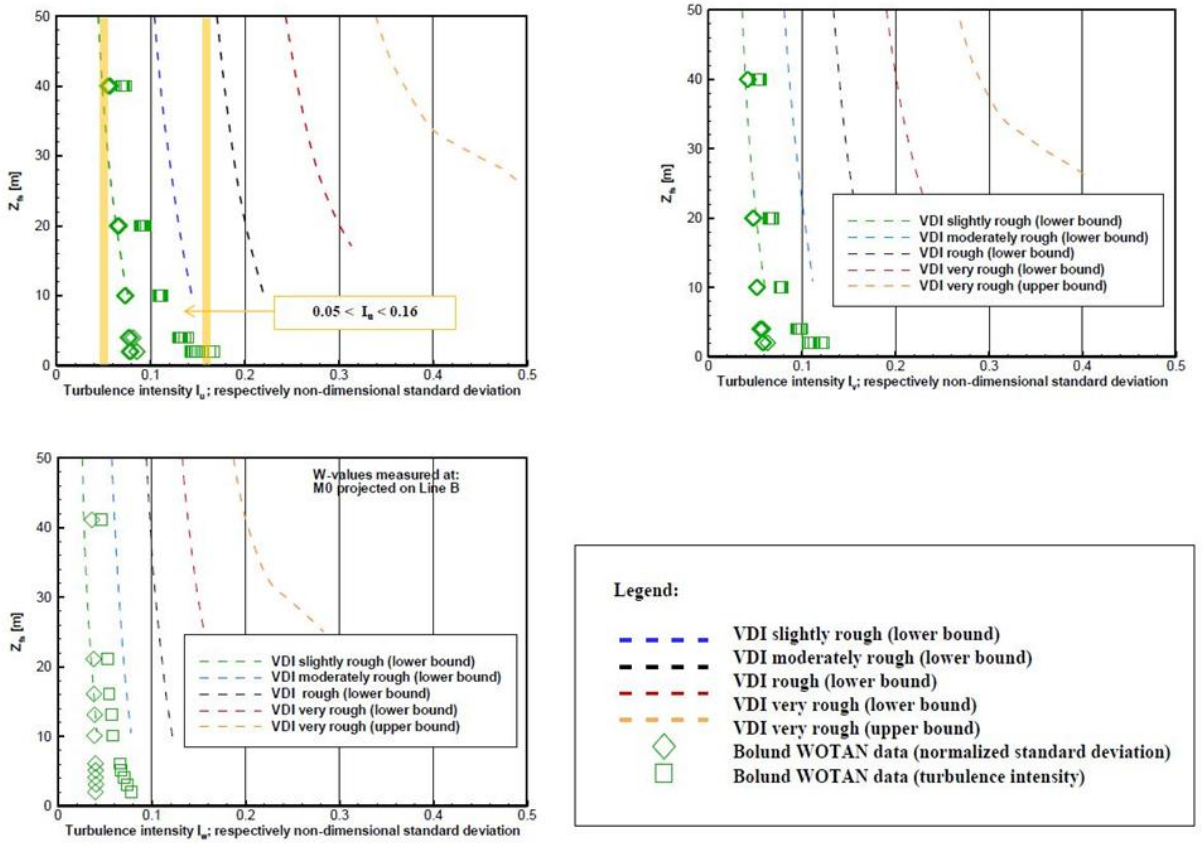

Figure 7.10.: Turbulence intensity in the atmospheric boundary layer modelled - from *Petersen* (2013)

The convergence tests

In order to define the number of velocity samples necessary for the achievement of a precise mean value, a long duration (6 minutes) time series was recorded. About 200000 events are included. The time series was transferred into non-dimensional form in order to be independent on the wind speed.

The convergence plots show the trend of the non-dimensional mean values with respect to the non-dimensional ensemble size (ES). The graphs clearly show how after $1/3$ of the ensemble size the non dimensional value of the U component of the wind speed has negligible variations: in the case of the empty tunnel is $U/\bar{U}_{ref} = 1.064 \pm 0.002$, in the case of the wake it is $U/\bar{U}_{ref} = 0.523 \pm 0.003$.

Therefore we defined the desired non-dimensional ensemble size as 67000, which corresponds at the desired wind speed to a measurement time scale as 2 minutes. This time range allows the non dimensional mean value to be assessed with a precision of $\pm 1\%$.

The convergence test, for the case of the wake, was carried out at a distance of 1.5 rotor diameters from the model, at 20% of the span of the blade. At this location the influence of the hub/nacelle and of the rotation of the blades is very high. Thus, this location represents a worst-case condition for the repeatability of the experiment. The measurement time resulting from this test can be then considered conservative and it can be applied to all other measurement locations.

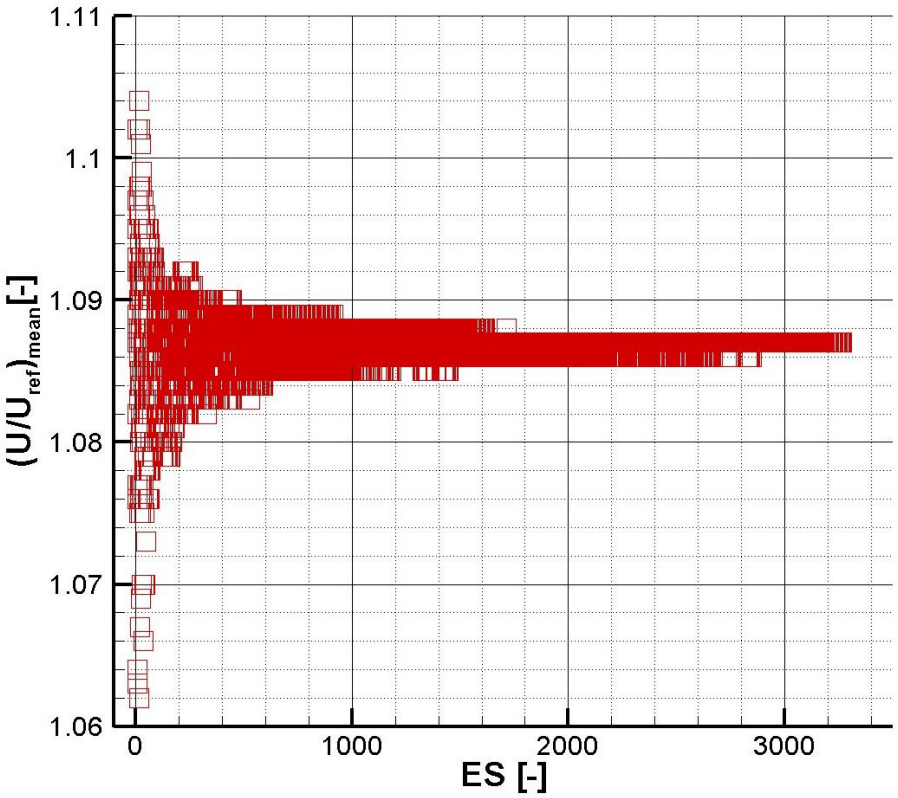

Figure 7.11.: Convergence of the non-dimensional mean value in the empty tunnel as a function of the ensemble size

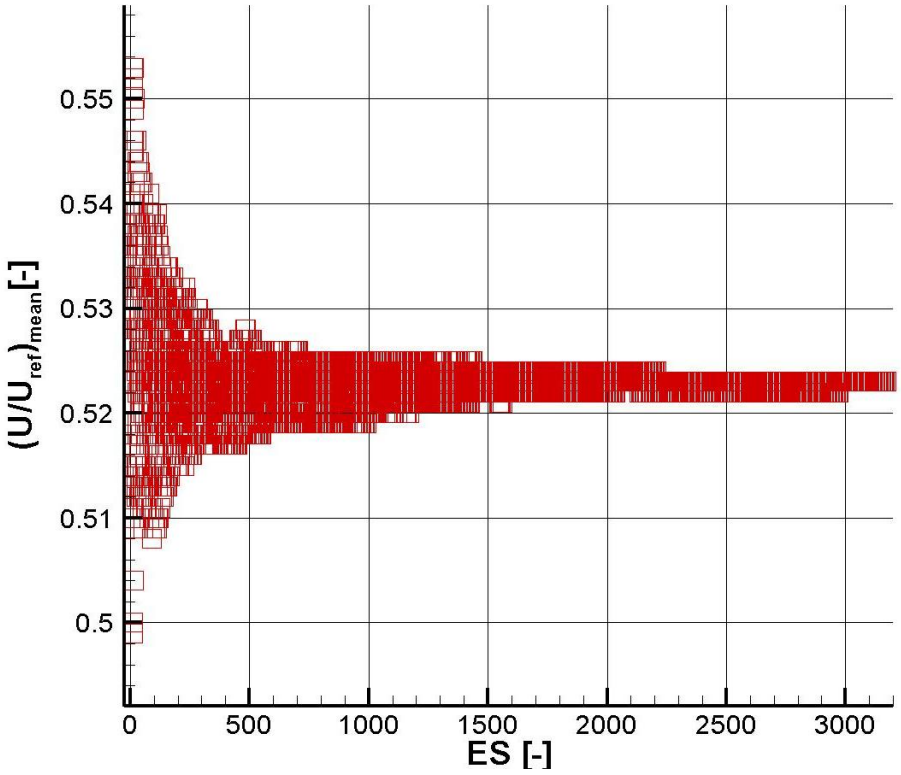

Figure 7.12.: Convergence of the non-dimensional mean value in the wake of the wind turbine model as a function of the ensemble size

The measurement plan

The measurement plan was designed with the intent to describe the velocity field by measuring at several planes downstream of the models. For each plane vertical and horizontal velocity profiles were measured. Four particular locations representative of near wake (1.5D), far wake (8D) and transitions zones (3D and 5D) were chosen. At these planes the three components of the velocity in the horizontal, vertical, diagonal $45°$ and $135°$ profiles were measured. Fig.7.13 summarizes the measurement campaign plan.

Additionally, to allow for spectral analysis of the time series, a number of measurements with increased data rate were performed.

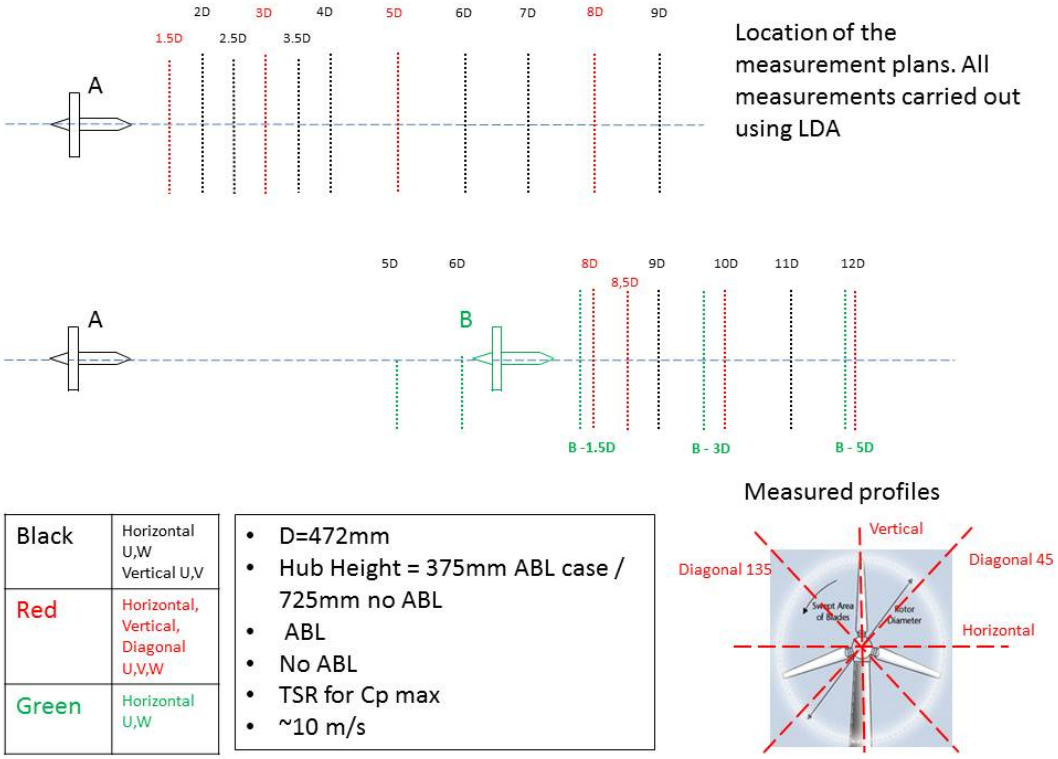

Figure 7.13.: Summary of the measurement campaign plan

Repeatability and reference velocity

Assessing the repeatability of velocity measurements in a very long wind tunnel campaign is a complex task. For time reasons, it is impossible to investigate the repeatability of each measurement point of the the whole ensemble. To deal with this problem, velocity profiles close to the model, where all the sources of uncertainty are maximized, were analysed.

The measurements were repeated on different days, at different times of the day. With this procedure, uncertainties in the calibration of the Prandtl tube, changes of ambient pressure and/or

temperature during the measurements, incidental misalignments of the laser probe and/or of the model can be accounted for.

Next, plots showing repeatability characteristics are presented. Fig.7.14 shows vertical profiles of the U component at 1.5 diameters of distance downstream of the wind turbine model, in atmospheric boundary layer flow. At each measurement point, data have been collected seven times: the maximal variation of the non dimensional U component is $\pm 0.75\%$.

At the same distance from the rotor, Fig.7.15 illustrates the horizontal profiles of the U component in free stream flow. The measurement series in black, named 1.5Dv, shows a scatter of $\pm 2.66\%$. Unlike the other measurements, in this case the UV setup (see App.A) was used. When this setup was used, the laser probe exhibited a higher interference in the wake which may explain the higher deviation.

The V and W components of the velocity vary much less. In the case of two model, the uncertainty is $\pm 0.3\%$. Fig.7.16 presents horizontal profiles of the W component at 1.5 diameters of distance downstream of the second wind turbine model.

In order to be conservative, the uncertainty bars in the plots in the following sections are based on the largest uncertainty range $\pm 2.66\%$.

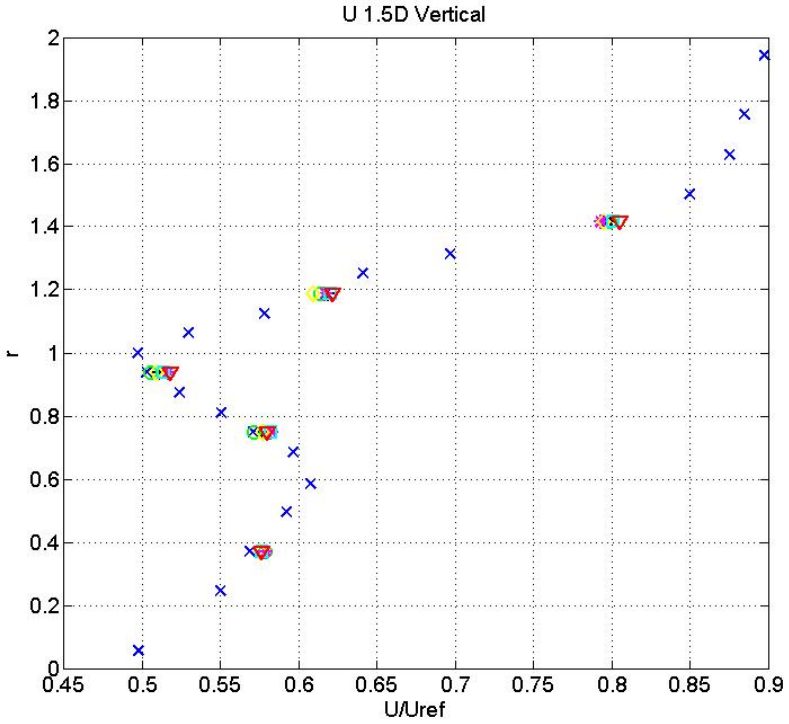

Figure 7.14.: Repetition measurements at 1.5 diameter downstream of the rotor in the case of the vertical profile of 1 wind turbine model in ABL flow

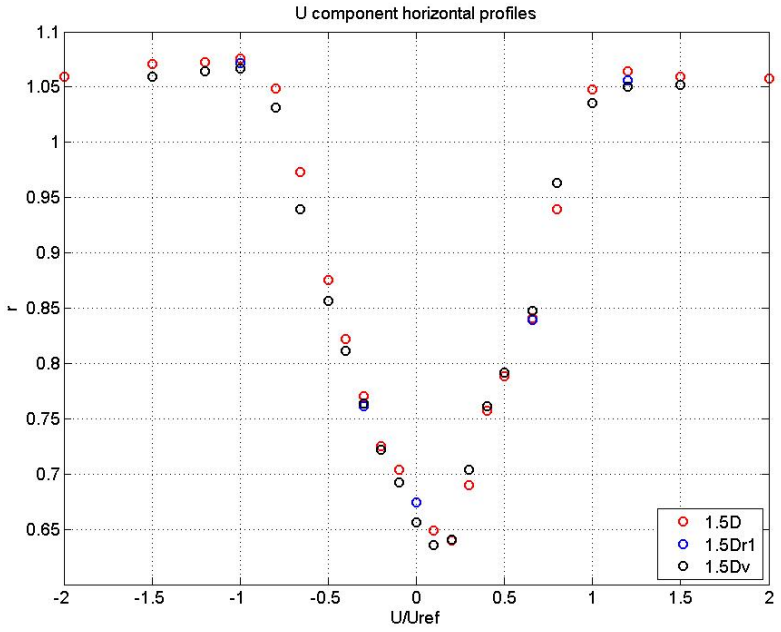

Figure 7.15.: Repetition measurements at 1.5 diameter downstream of the rotor in the case of the horizontal profile of 1 wind turbine model in free stream flow

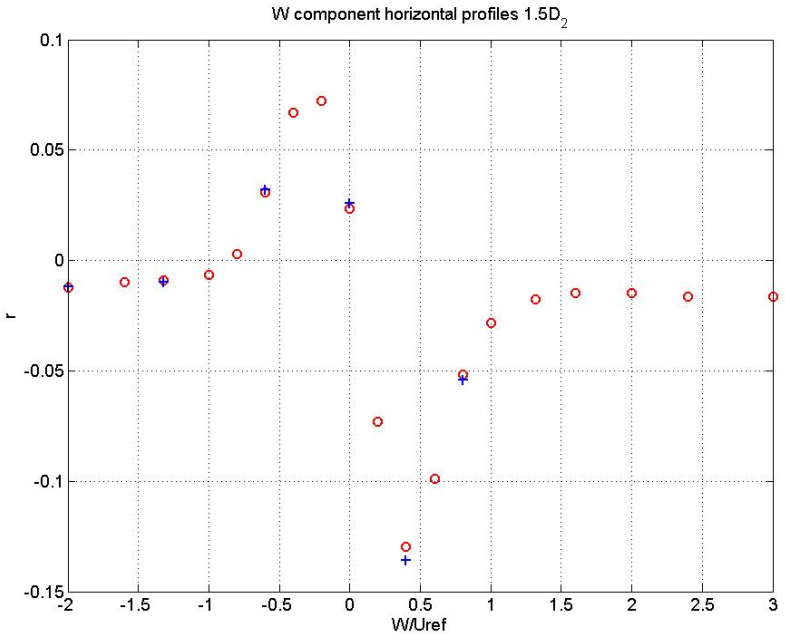

Figure 7.16.: Repetition measurements at 1.5 diameter downstream of the second rotor in the case of the horizontal profile of 2 wind turbine models in ABL flow

Reference velocity The reference velocity was measured using a Prandtl tube which, as illustrated in Fig.7.4 and Fig.7.5, is positioned at the inlet of the tunnel. In order to have a reference position within the ABL, the measurement of the Prandtl tube was linked to the location **L** at [0, 0, 500]. This location lies between the heights of the rotor hub in the two model configurations (ABL configuration $375\mathrm{mm}$, free stream configuration $725\mathrm{mm}$).

Fig.7.17 illustrates the situation. Being U_P the velocity at the Prandtl tube and U_{ref} the velocity at the reference location, the non-dimensional mean value of the velocity in the wake can be calculated as $U_{ad} = k * \frac{U_m}{U_P}$. A constant value of the ratio $k = U_P/U_{ref}$ is assumed, U_{ref} is measured during the preliminary tests without the model ("undisturbed" conditions).

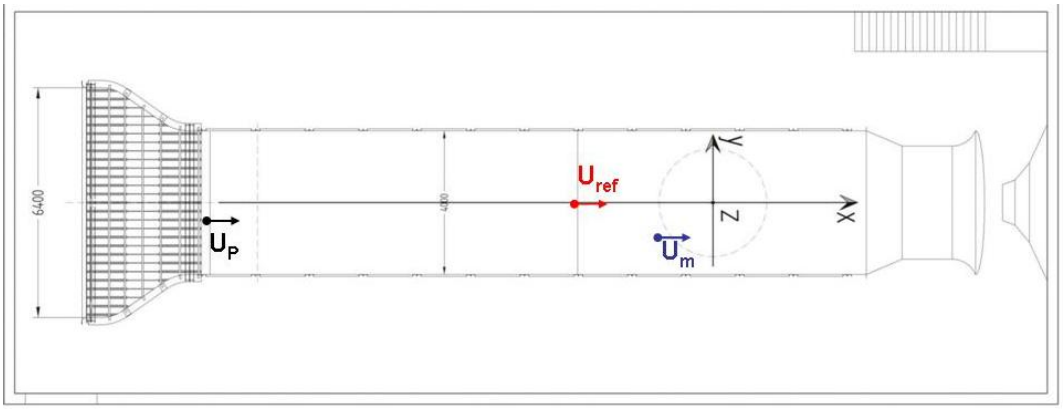

Figure 7.17.: Schematic of the velocity measurement locations

7.2. Velocity measurements

In this section, profiles of the velocity deficit and of the turbulence intensity of the non-dimensional velocity are shown. Given the vast amount of data collected, only selected measurements are presented. In particular, to help visualize the differences, profiles at four selected locations only (see sec.7.1.1) are shown. In particular cases, additional plots are provided. Captions specify also the particular setup of the probe. More information can be found in App.A.

The scale of the plots is not the same in each figure. Instead, it is tuned to highlight the differences among the profiles. The velocity profiles span is presented in terms of normalized rotor radius $r = C/R$, where C is the radial distance from the center and R the rotor radius. In particular, $r = 0$ indicates the rotation axis whereas $r = 1$ is the tip of the blade.

It must also be pointed out that, at each plane, the velocity profiles are centred geometrically at the x-axis of the coordinate system (see Fig.7.17), which coincide with the axis of rotation of the turbine. The wake flow may shift from this symmetry axis; therefore, any conclusion about the physical behaviour should account for this situation.

Comparisons between the different study cases are presented in the following Ch.8.

7.2.1. Results - 1 Wind Turbine - free stream

In this section results for the case of one wind turbine model in the free stream are presented.

Velocity deficit plots

The next figures show the horizontal and vertical profiles of the U component of the velocity. Fig.7.18 shows the wake shifting to the right side. This phenomenon can be explained by the small inhomogeneity of the flow (see sec.7.1.1). A misalignment of the model may be another possible cause. In this latter case however, a bend towards the center of the tunnel should be observable in the wake.

Fig.7.19 shows the vertical profiles of the U component. The asymmetry of the wake is visible. Also, the profile smooths in the far wake. In particular, the maximum value of the velocity deficit decreases (the velocity recovers) of the 53% from the value at 1.5D to the one at 8D. From now on we refer to the maximum value of the velocity deficit as $V_{D_{max}}$. Within this range of distances, the $V_{D_{max}}$ point moves downwards of about the 50% of the blade length. The low pressure area that surrounds the wake may be the cause for this physical behaviour. Also, the wake of the tower might influence the wake flow. Further experiments would be required for a clearer insight, see sec.9.2.

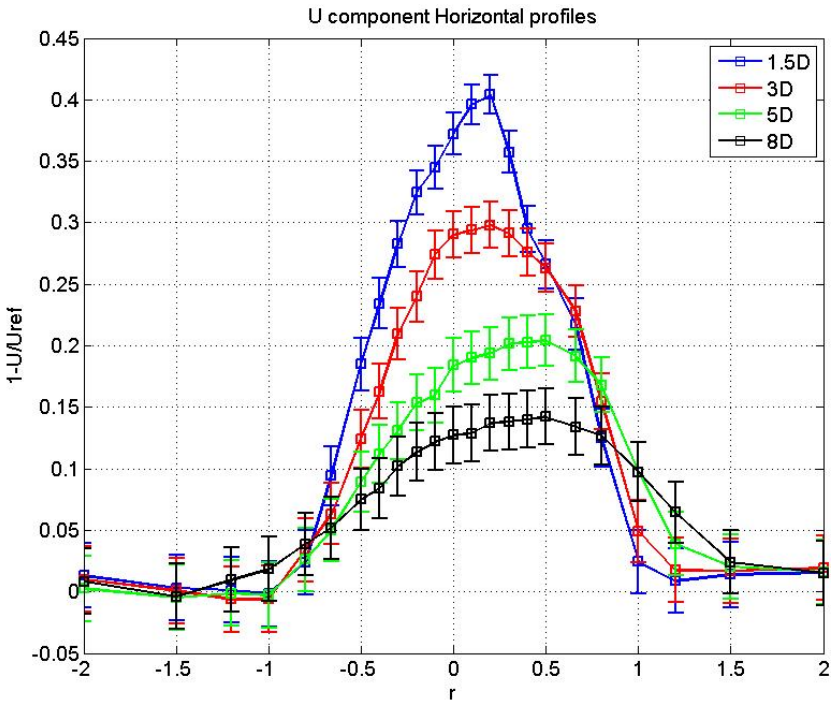

Figure 7.18.: Horizontal profiles velocity deficit - U component - Free stream UW setup

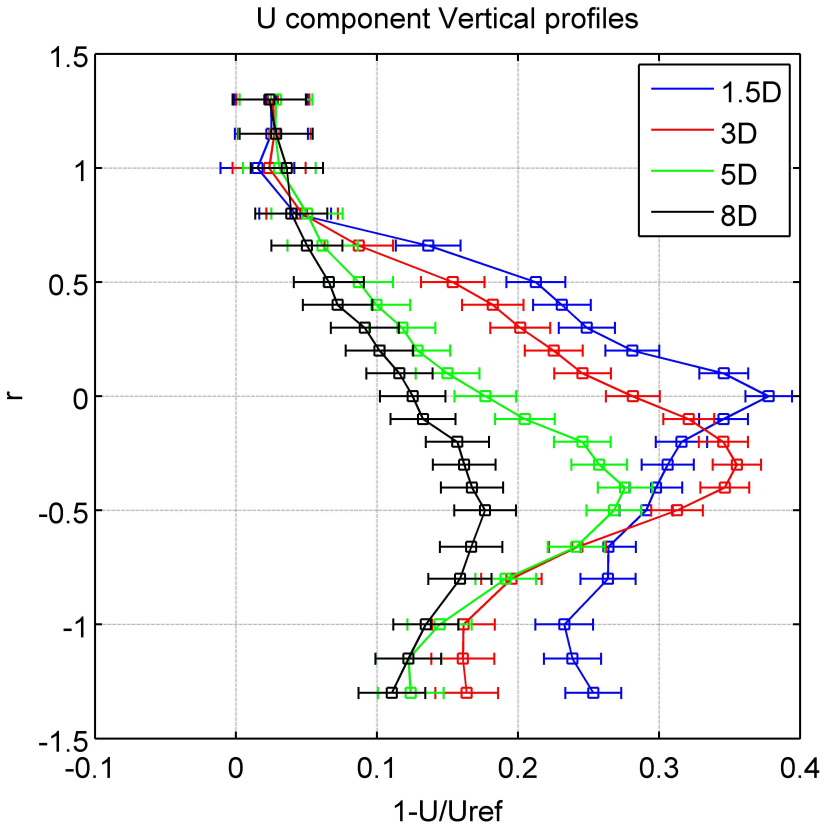

Figure 7.19.: Vertical profiles velocity deficit - U component - Free stream UW setup

Non-dimensional velocity plots

Fig.7.20 and Fig.7.21 show the horizontal and vertical profile of the non-dimensional W and V component respectively. Also these plots show an asymmetry of the wake, consistently with the measurements of the U component.

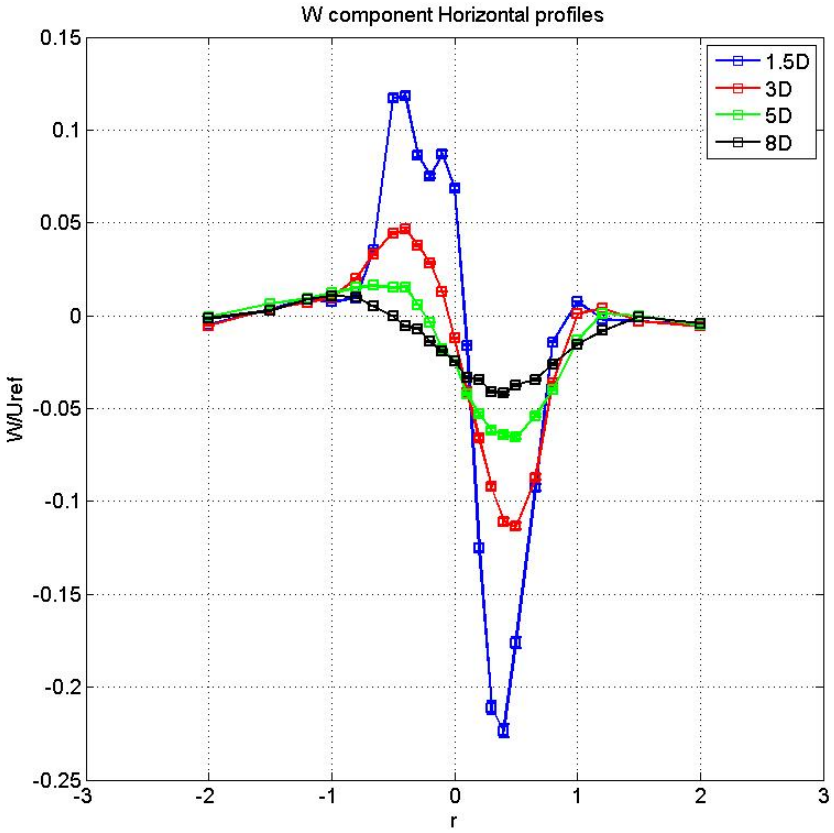

Figure 7.20.: Horizontal profiles non-dimensional velocity - W component - Free stream UW setup

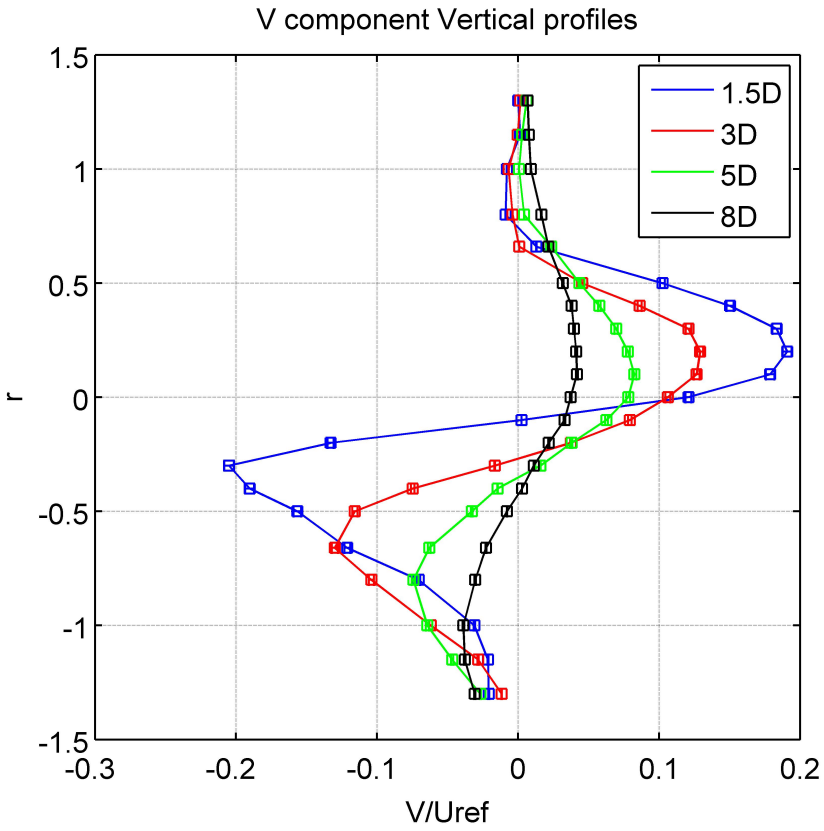

Figure 7.21.: Vertical profiles non-dimensional velocity - V component - Free stream UV setup

Turbulence intensity plots

The horizontal profiles of the turbulence intensity clearly show a non-symmetrical distribution, particularly at the closer planes, Fig.7.22 and Fig.7.24. To explain this phenomenon flow visualization coming from experiments and CFD are needed.

Fig.7.26 shows the helical structure of the wake. The picture was taken at the National Renewable Energy Laboratory, during a flow visualization campaign in the field. A nucleus of turbulence (the tip vortex) is present in area of the tip of the blade, and it moves downstream creating an helix. In Fig.7.27 the root vortex is also visible.

Summarizing:

- profiles were measured at planes perpendicular to the axis of rotation. Thus, the external nucleus of turbulence hits the plane at one location only in the outer part of the profile;
- the central part of the profile, due to the presence of the root vortex, exhibits higher turbulence intensity.

Thus, the non-symmetrical distribution of the turbulence is to be expected.

The vertical profiles (Fig.7.23 and Fig.7.25) also show a secondary peak, up to 3 diameters downstream, in the higher part of the profile. As in the horizontal profiles, this peak is located at about the 65% of the blade length where the vortex is shedding, see Ch.6.

The lower part of the profiles exhibits a different trend. In the near wake, where the tower also influences the flow, there is an increase of the turbulence. 1.5 rotor diameters downstream of the rotor, the turbulence level is higher closer to the ground than in the hub region. This effect is more visible for the V component of the velocity, Fig.7.25.

Further investigation of the tower-nacelle-hub system should be considered in order to quantify the turbulence in the central area of the profile. In addition, considering that the vortex sheds around the 65% of the blade span in the rotor used, its size is larger than a vortex shedding from the tip of the blade. Thus, in order to investigate the effect of the chord distribution on the turbulence characteristics of the profile, new tests with slender blades should be performed.

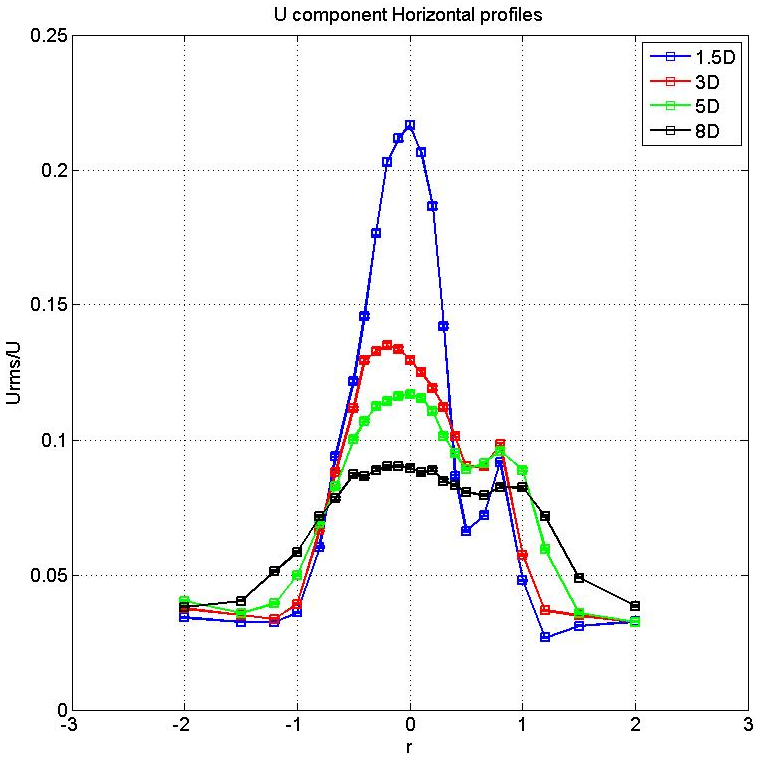

Figure 7.22.: Horizontal profiles turbulence intensity - U component - Free stream UW setup

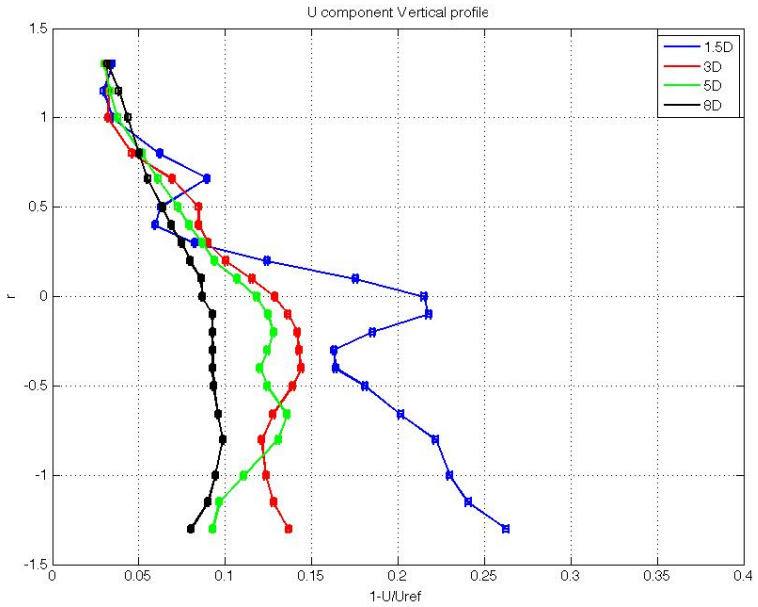

Figure 7.23.: Vertical profiles turbulence intensity - U component - Free stream UW setup

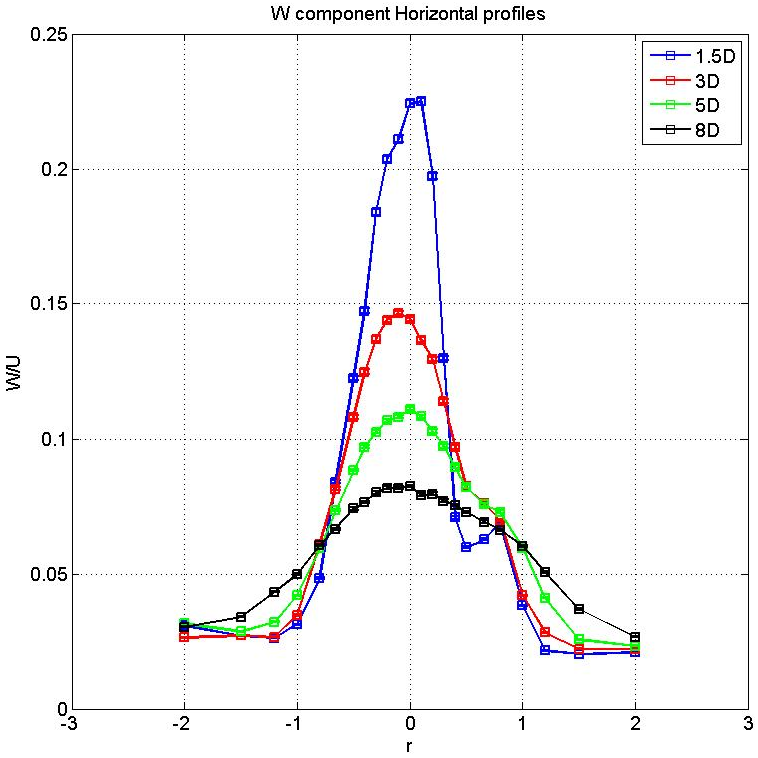

Figure 7.24.: Horizontal profiles turbulence intensity - W component - Free stream UW setup

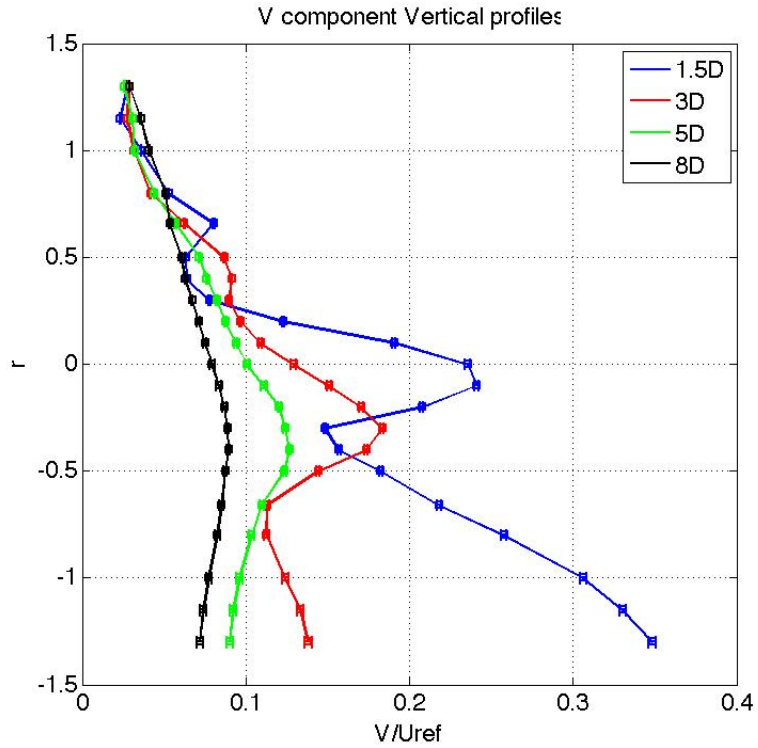

Figure 7.25.: Vertical profiles turbulence intensity - V component - Free stream UV setup

Figure 7.26.: Flow visualization on the field. ©NREL

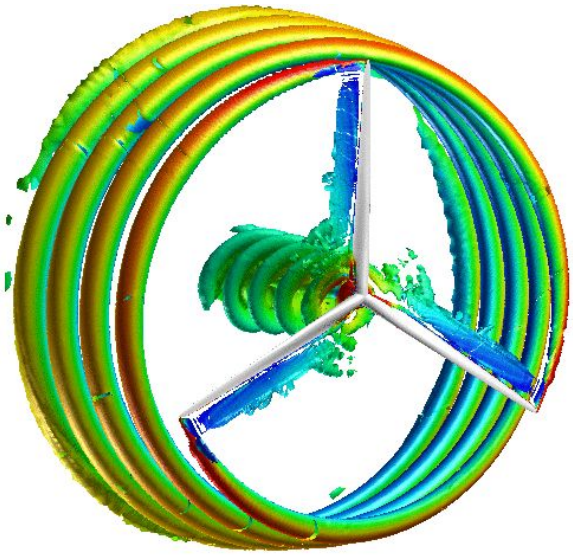

Figure 7.27.: CFD visualization of the near wake made by Acusim software. ©(http://www.acusim.com/images/apps/windTurbSiting.icon.gif)

7.2.2. Results - 1 Wind Turbine - ABL flow

In this section the results for the case of one wind turbine model in ABL flow are presented.

Velocity deficit plots

When the atmospheric boundary layer is modeled, the flow is more homogeneous as shown in sec.7.1.1. Therefore, the wake remains aligned with the flow.

Fig.7.28 shows the horizontal profiles of the U component. Differences are noticeable between the profile at 3D and the one at $5D$. While the velocity deficit of the first one behaves similarly to the closest profile (at $1.5D$), the latter is more similar to the most far profile (at $8D$). In addition, Fig.7.29 shows the profiles at 3, 4, and 5 rotor diameters downstream. The widening of the wake is visible in the latter profile only. This behaviour suggests that the transition between near and far wake is found at about four diameters of distance from the rotor.

A clear description and identification of the influences that each of the similarity parameters has on this transition can only be done with further experiments. In fact, a systematic variation of the similarity parameters requires different rotors to be designed and manufactured. A second campaign with a more slender blade, which allows higher values of λ to be investigated, is recommended.

The vertical profiles of the U component show again the motion of the maximum-deficit point towards the ground, also confirmed by the diagonal profiles (Fig.7.31 and Fig.7.32). In the case of atmospheric boundary layer flow, this phenomenon is well known and described. Generally, it is linked with the *non-uniform velocity distribution of the incoming flow*, see *Chamorro and Porté-Agel* (2010). *Rhethore* (2009) shows that it can be seen with numerical models as well.

Attention must be drawn to the vertical profiles of the U component, see Fig.7.30. The velocity deficit in the bottom half of the profiles tends to increase as in the free stream case, but this trend is exhibited already at half of the blade length, $r = 0.5$. This behaviour might be caused by the ground which is closer to the rotor, due to the smaller height of the tower. However, to distinguish and quantify the effects of the ground from others, such as the low pressure area out of the wake and the influence of the tower wake, local pressure measurements sustained by on-purpose designed numerical simulations should be carried out.

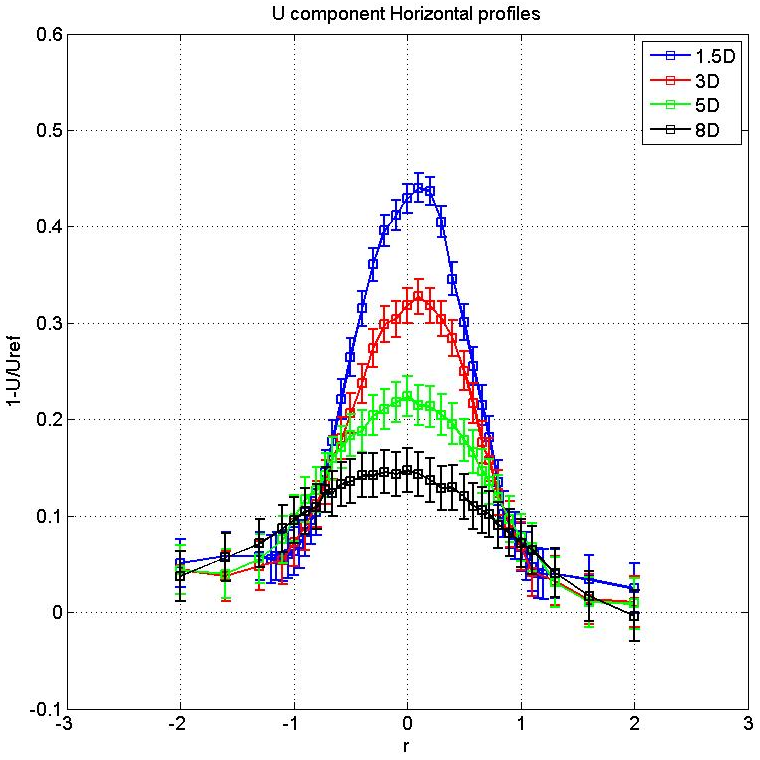

Figure 7.28.: Horizontal profiles velocity deficit - U component - ABL flow UW setup

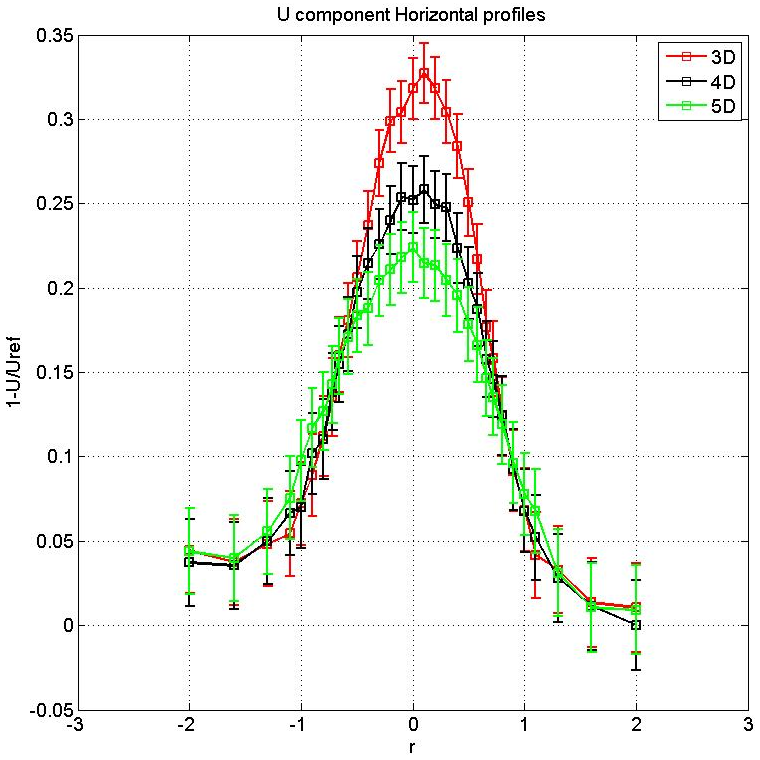

Figure 7.29.: Horizontal profiles velocity deficit - U component - ABL flow UW setup

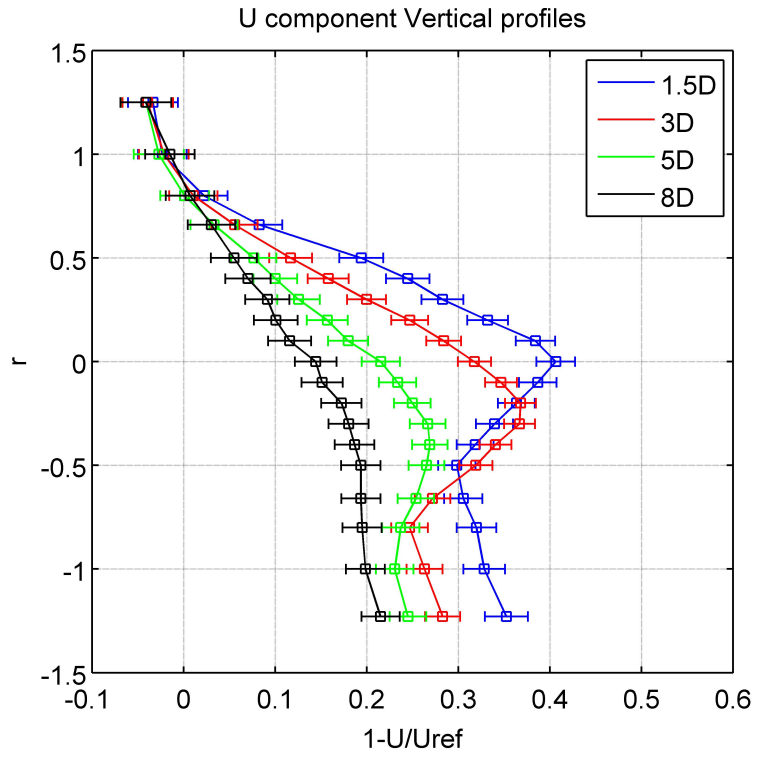

Figure 7.30.: Vertical profiles velocity deficit - U component - ABL flow UW setup

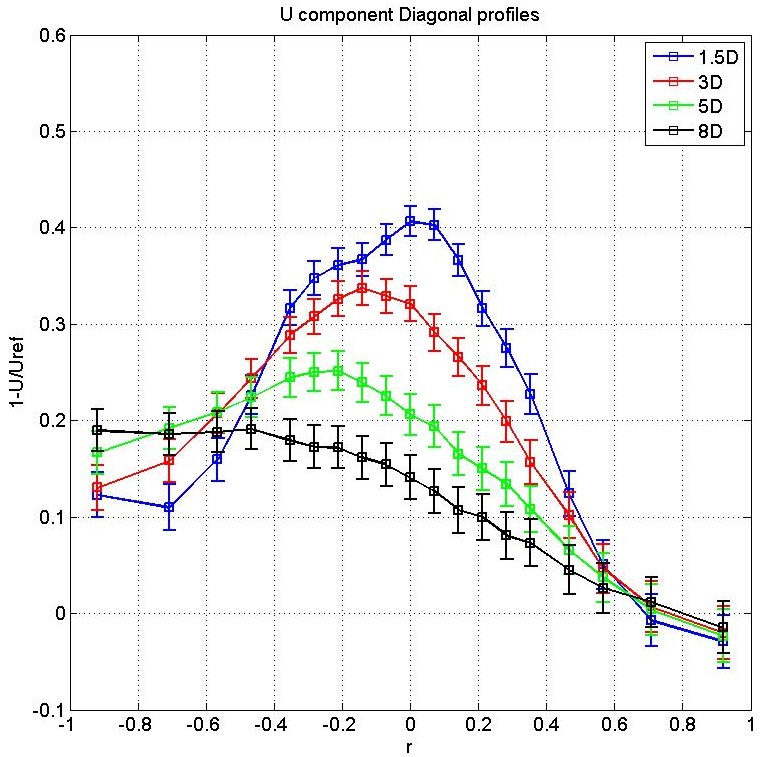

Figure 7.31.: Diagonal profiles velocity deficit - U component - ABL flow UW setup

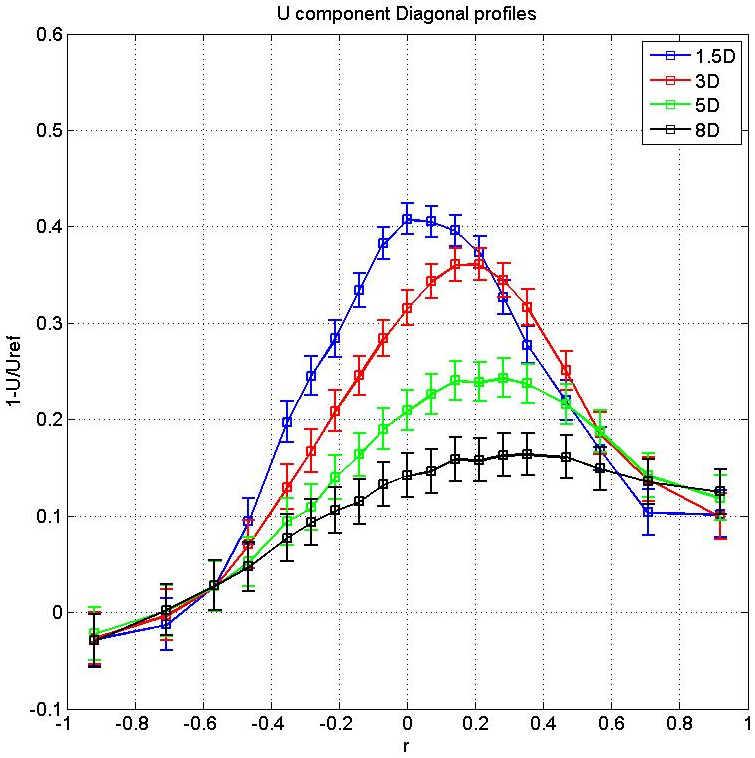

Figure 7.32.: Diagonal profiles velocity deficit - U component - ABL flow UW setup

Non-dimensional velocity plots

Non-dimensional velocity profiles of the W and V component are shown in Fig.7.33 and Fig.7.34 respectively. The profile at $1.5D$ in Fig.7.33 shows an asymmetry which is not observed in the other profiles.

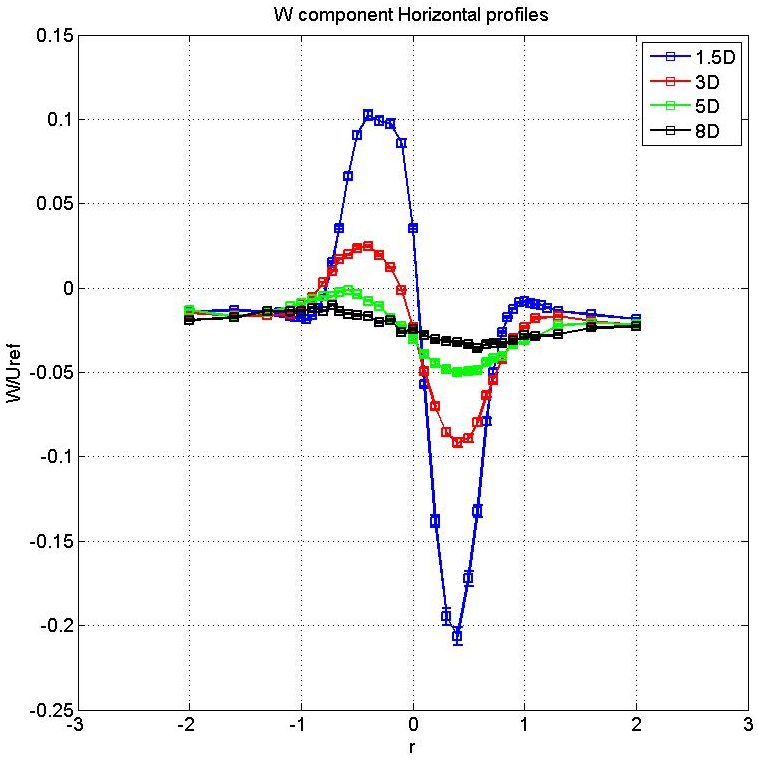

Figure 7.33.: Horizontal profiles non-dimensional velocity - W component - ABL flow UW setup

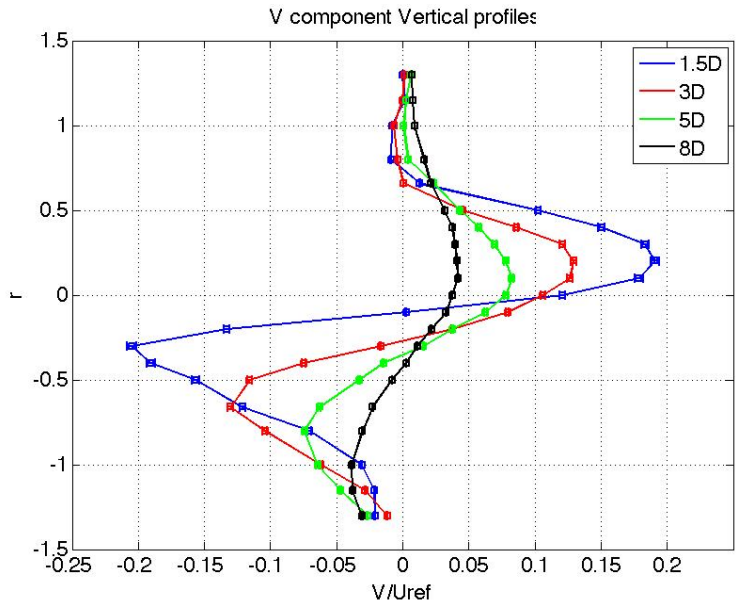

Figure 7.34.: Vertical profiles non-dimensional velocity - V component - ABL flow UW setup

Turbulence intensity plots

Focusing on Fig.7.35, it is possible to see that at 1.5 diameters of distance from the rotor the non-symmetrical distribution of the turbulence intensity is similar to the case of free stream flow. Adding here the profile at $2D$, it is possible to see that the second peak is destroyed. A recovery towards an homogeneous distribution of the turbulence is observed. The turbulence intensity profiles show also the widening of the wake which eight diameters downstream of the rotor has a width of about 2 rotor diameters.

The plots in Fig.7.36, Fig.7.37 and Fig.7.38 consistently confirm the described behaviour: a minor peak is visible in the near wake which is smoothed already at $3D$.

I refer to Ch.8 for the comparison with the free stream flow case.

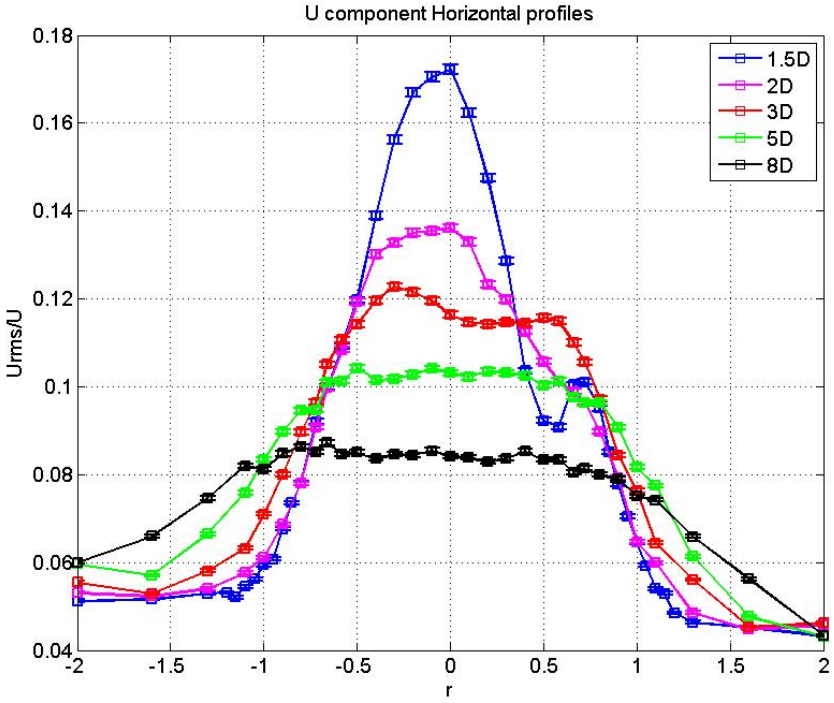

Figure 7.35.: Horizontal profiles turbulence intensity - U component - ABL flow UW setup

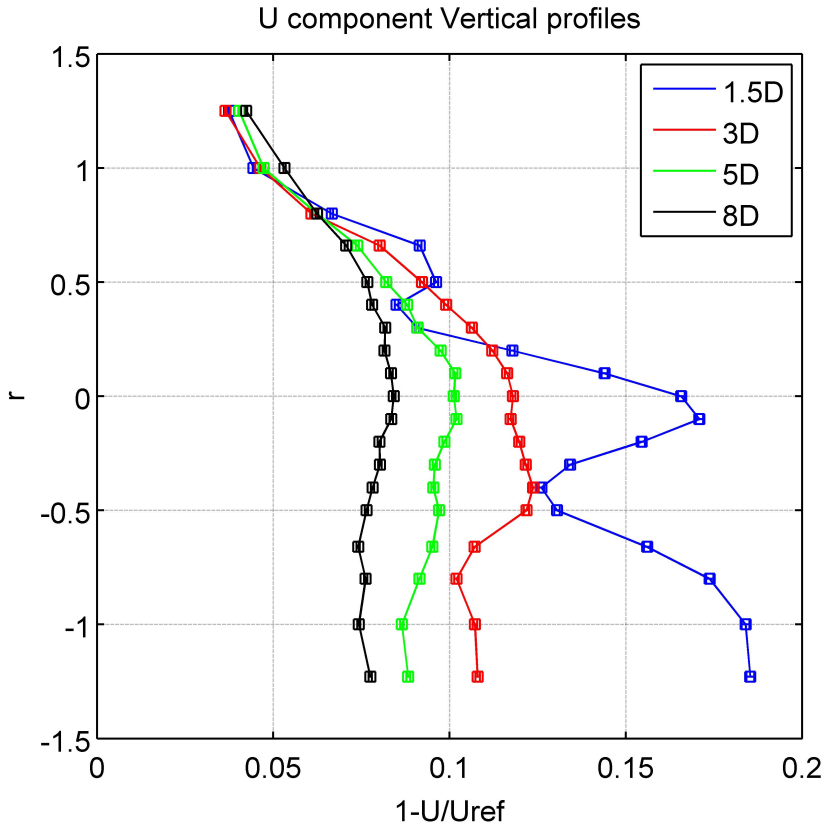

Figure 7.36.: Vertical profiles turbulence intensity - U component - ABL flow UW setup

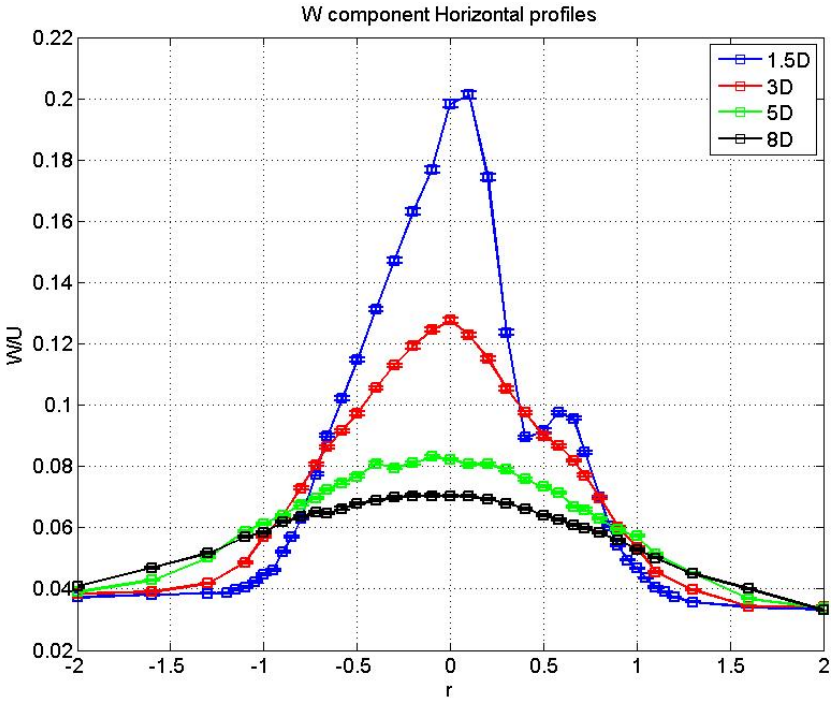

Figure 7.37.: Horizontal profiles turbulence intensity - W component - ABL flow UW setup

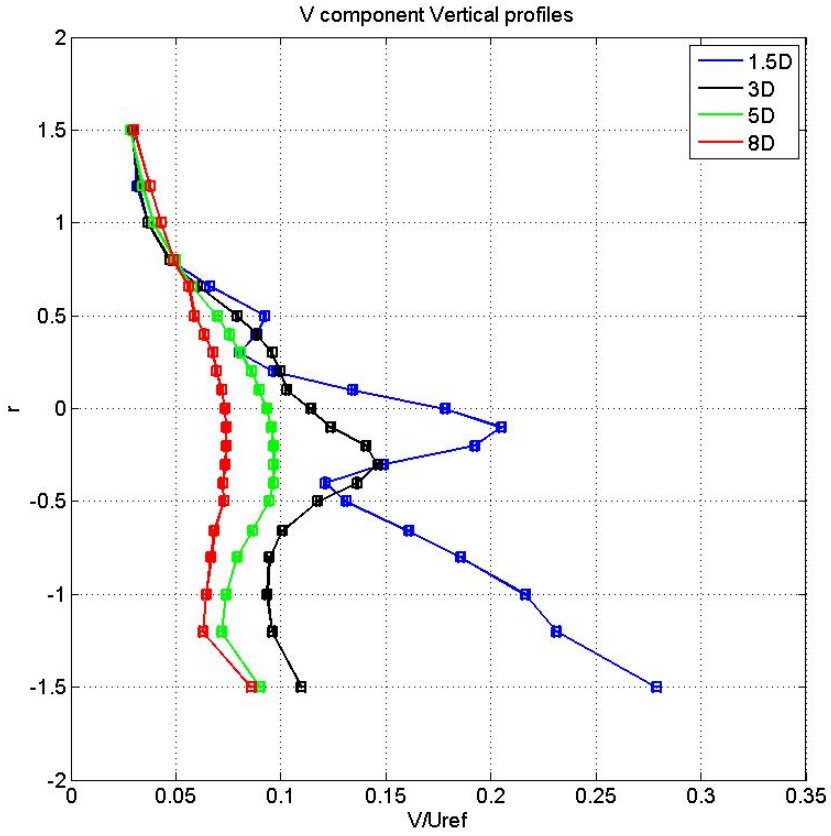

Figure 7.38.: Vertical profiles turbulence intensity - V component - ABL flow UV setup

7.2.3. Results - 2 Wind Turbines - free stream

In this section the results for the setup with two wind turbines are presented. In particular the free stream case is shown. For the model placed in the second row, the velocity deficit has to be calculated with respect to its inflow.

Also, legends show the distance of each profile from the **first** rotor. Comparison between profiles placed at the same respective plane (e.g. profiles at 3D from the first rotor and 3D from the second rotor) are presented in Ch.8.

Reference inflow conditions for the second wind turbine model

As the second wind turbine model is placed 6.6 diameters directly behind the the first one it is no more possible to calculate the velocity deficit assuming, as for the first turbine, the inflow as homogeneous but another reference profile needs to be defined.

Fig.7.39 shows the non-dimensional profiles of the U component measured at five diameters of distance from the first rotor. The profile was measured during the test of a single model, and also when the second model was installed. The good matching of the two curves indicates that the presence of the second wind turbine does not influence the wake of the first model as far as 1.6 rotor diameters of distance. Thus, the profile at $5D$ was taken as reference and used for the calculation of the velocity deficit.

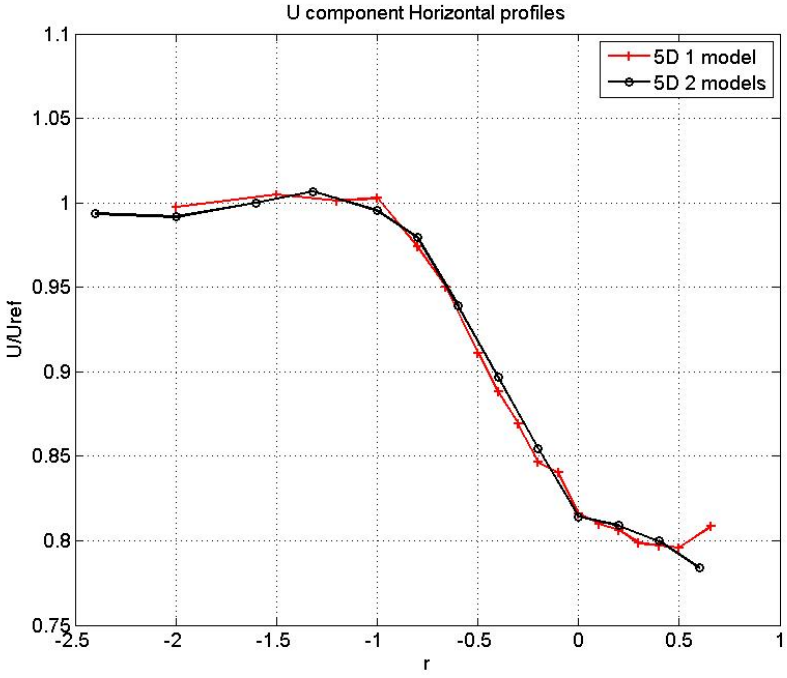

Figure 7.39.: Comparison of the mean non-dimensional velocity profile at 5 diameters downstream of the first turbine - U component - 1 and 2 wind turbines Free stream UW setup

Velocity deficit plots

Fig.7.40 shows the horizontal profiles of the velocity deficit of the U component. The second wind turbine obviously creates a deficit in the velocity reaching a value of 0.25: the second model is about 44% less effective than the first one in extracting momentum from the flow field. Particular attention must be paid to the profile at 12D which shows negative values. This feature indicates that the velocity recovers to a value higher than its inflow. As stated above, the inflow for the second model is the profile at $5D$, which already is in deficit with respect to the ambient flow.

The same feature is visible in the vertical profiles as well, see Fig.7.41.

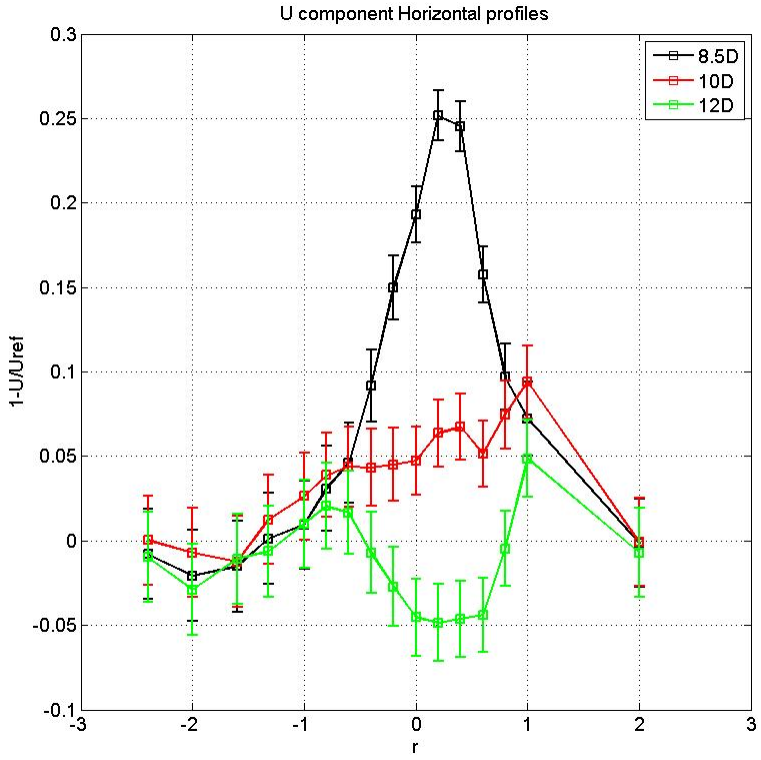

Figure 7.40.: Horizontal profiles velocity deficit - U component - 2 wind turbines Free stream UW setup

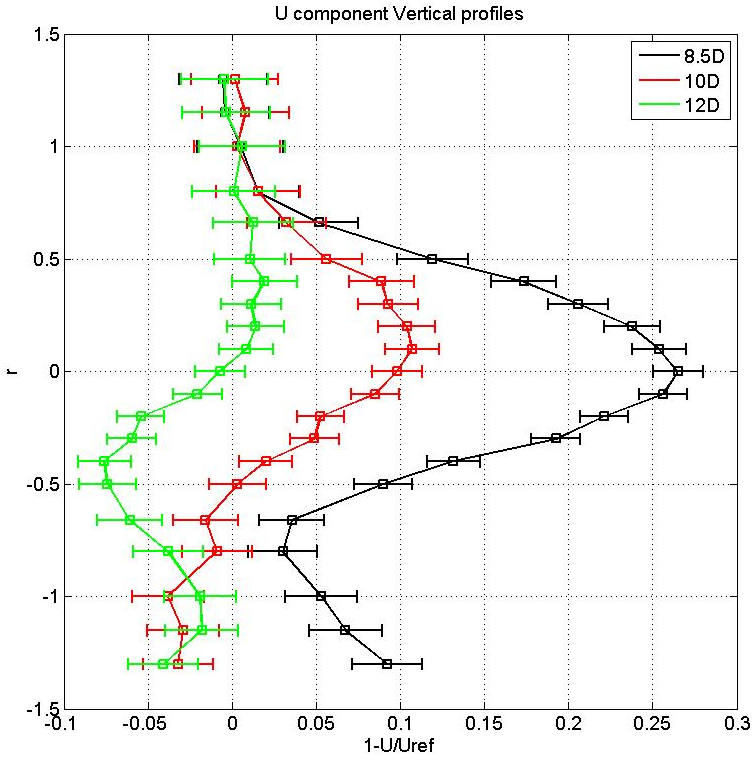

Figure 7.41.: Vertical profiles velocity deficit - U component - 2 wind turbines Free stream UW setup

Non-dimensional velocity plots

Non-dimensional velocity profiles of the W and V component of the velocity are presented in the following graphs.

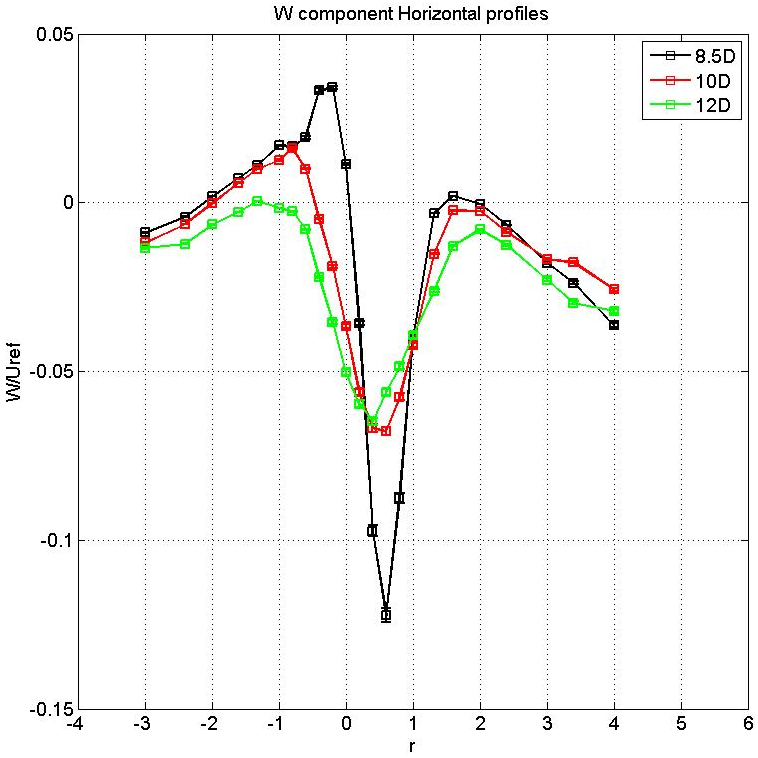

Figure 7.42.: Horizontal profiles non-dimensional velocity - W component - Free stream UW setup

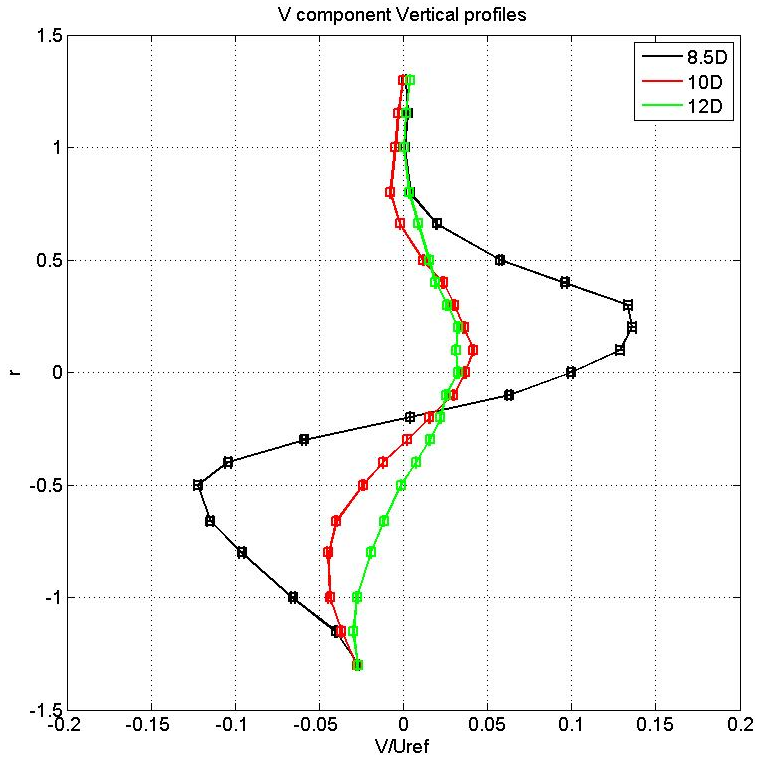

Figure 7.43.: Vertical profiles non-dimensional velocity - V component - Free stream UV setup

Turbulence intensity plots

Fig.7.44 shows turbulence intensity profiles behind the second model. In contrast to the case of one model, the increase in width of the wake is not clearly distinguishable. Fig.7.45 presents the turbulence intensity vertical profiles. In this case, the decrease of the turbulence level and the changes in the bottom part of the profiles are consistent with the case of sec.7.2.1.

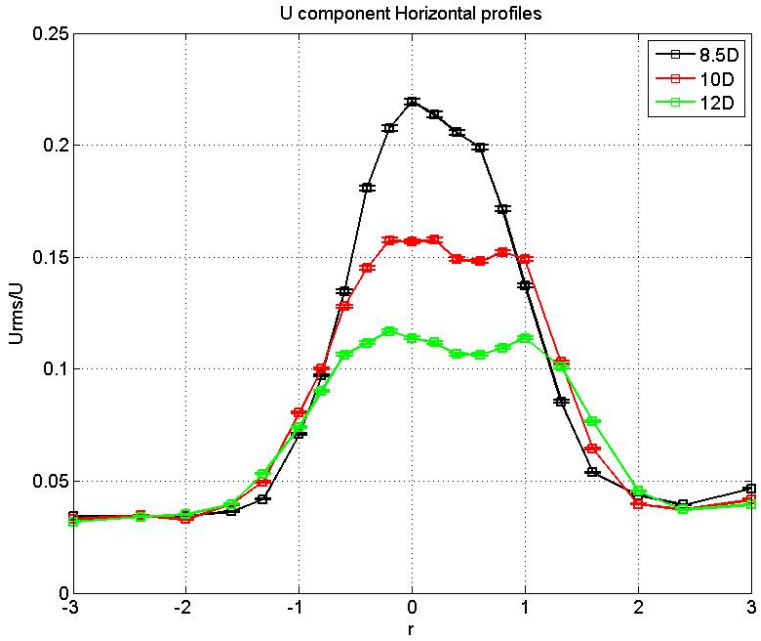

Figure 7.44.: Horizontal profiles turbulence intensity - U component - 2 wind turbines Free stream UW setup

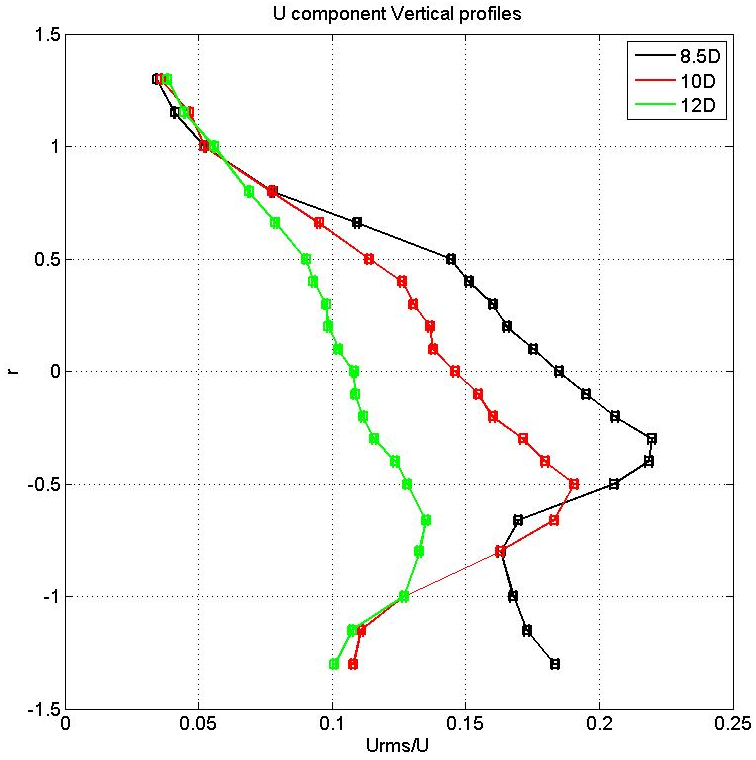

Figure 7.45.: Vertical profiles turbulence intensity - U component - 2 wind turbines Free stream UW setup

7.2.4. Results - 2 Wind Turbines - ABL flow

In this section results for the case of two models in ABL flow are presented. As in the previous section, the velocity deficit was calculated assuming as inflow the wake profile at five diameters of distance from the first rotor.

Velocity deficit plots

Although the overall behaviour is similar to the free stream case (recovery at 12D), the deficit plot is noticeably wider. The following Ch.8 shows direct comparisons.

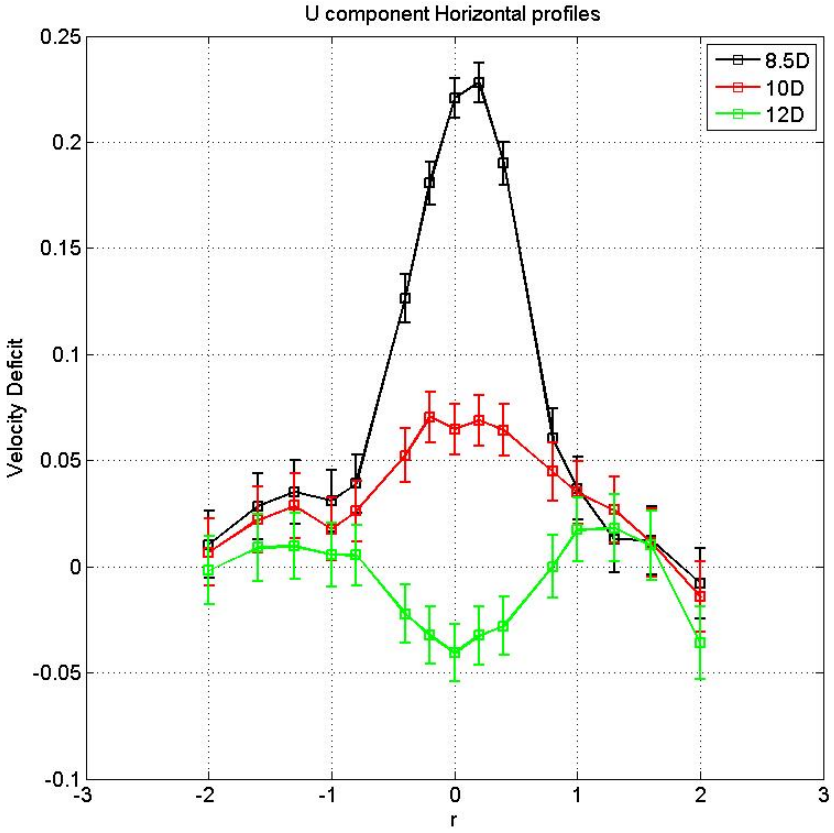

Figure 7.46.: Horizontal profiles velocity deficit - U component - 2 wind turbines ABL flow UW setup

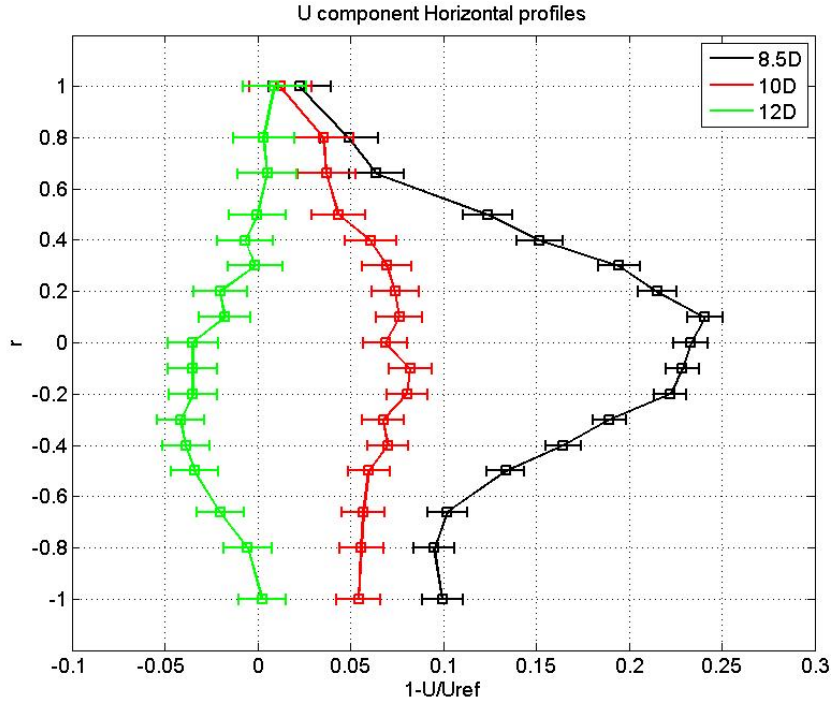

Figure 7.47.: Vertical profiles velocity deficit - U component - 2 wind turbines ABL flow UW setup

Non-dimensional velocity plots

Fig.7.48 and Fig.7.49 show the non-dimensional velocity profiles of the W and V component of the velocity respectively.

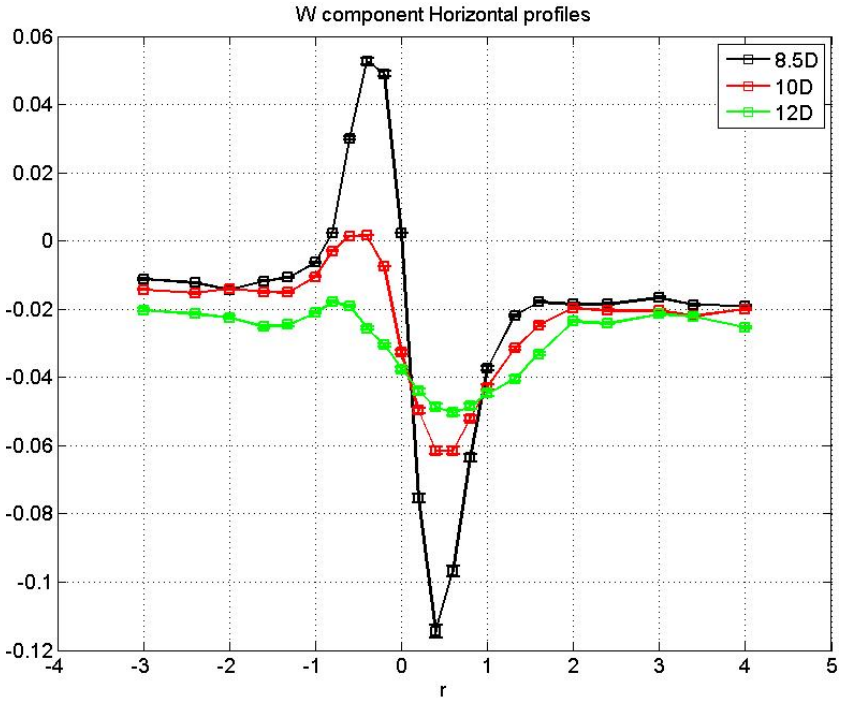

Figure 7.48.: Horizontal profiles non-dimensional velocity - W component - ABL flow UW setup

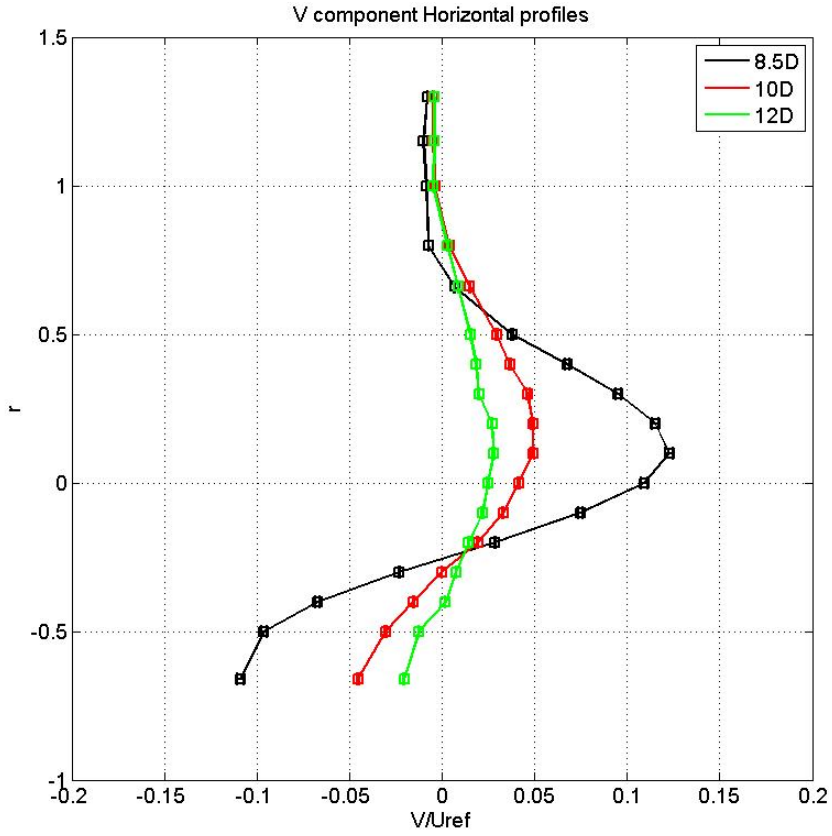

Figure 7.49.: Vertical profiles non-dimensional velocity - V component - ABL flow UV setup

Turbulence intensity plots

In contrast with the free stream case, Fig.7.50 shows that the highest peak in the turbulence intensity is located on the right side of the axis of rotation ($r = 0$). This might be related with a shifting of the wake. Being the measurement points geometrically defined, at certain locations this shifting might result in non-symmetrical plots. However, this feature might be assessed by carrying out on-purpose-designed experiments and numerical simulations. Also, the use of Particle Image Velocimetry (PIV) would be a great aid for mapping the wake flow.

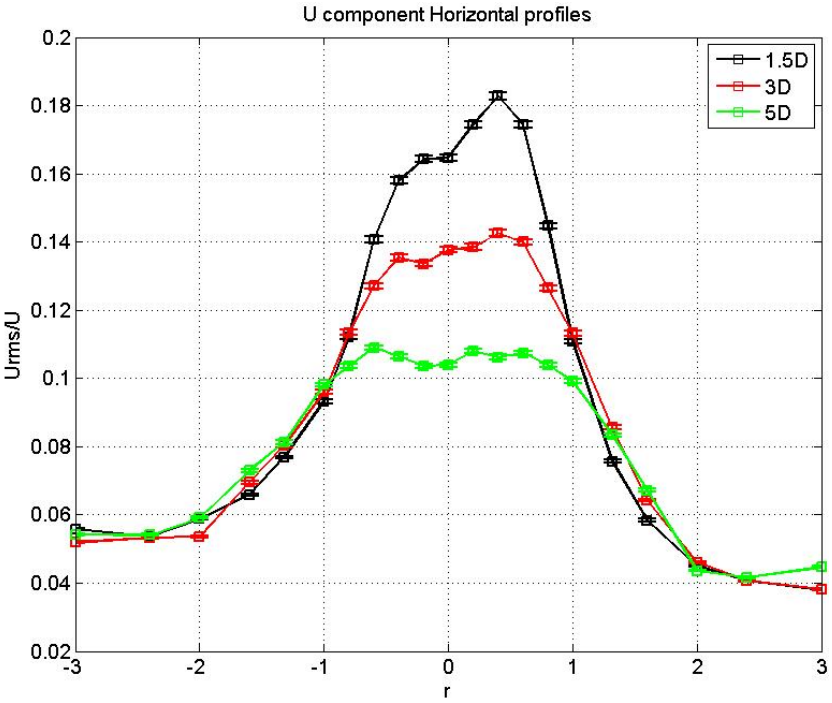

Figure 7.50.: Horizontal profiles turbulence intensity - U component - 2 wind turbines ABL flow UW setup

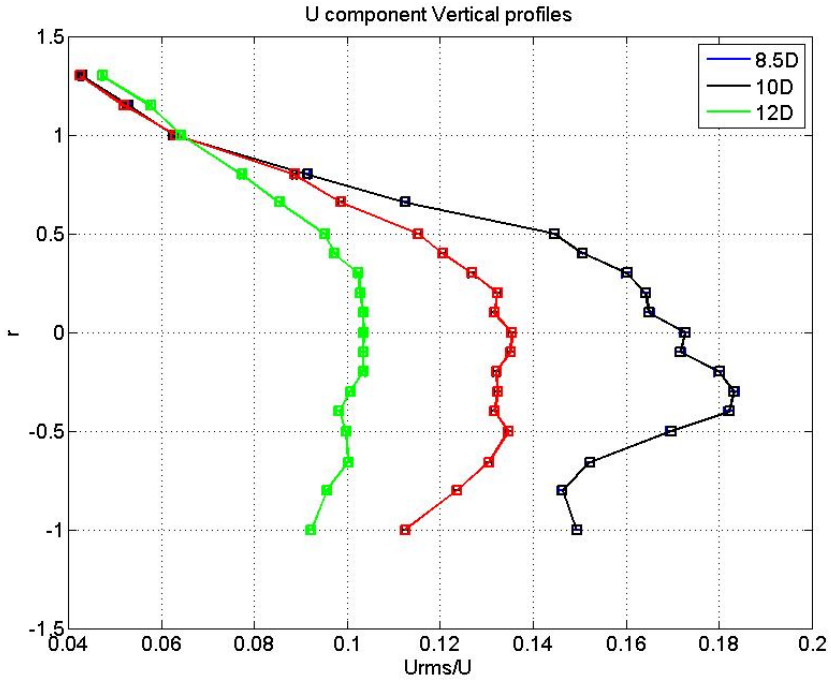

Figure 7.51.: Vertical profiles turbulence intensity - U component - 2 wind turbines ABL flow UW setup

8. Comparisons and interpretations of the results

8.1. Introduction

In order to highlight the differences between the test cases previously analysed, a number of comparisons between similar measurements is presented in this chapter.

First, in order to give a visual help to the reader, a reconstruction of the velocity field, based on the LDA measurements is shown. In addition two pictures from the visualization campaign are provided. Then, wake profiles comparisons between the cases of free stream and ABL flow are shown, as an assessment of the influence of the atmospheric boundary layer. Finally, differences between the wake of the first wind turbine model and the wake of the second one are illustrated.

8.2. Velocity field and flow visualizations

This section aims to give a visual help to the reader.

Fig.8.1 is a reconstruction of the velocity field behind the two wind turbine models in the case of ABL flow. The scale of the axes in the figures is tuned for easiness of visualization. In order to appreciate the different components, the top and the front views are shown in Fig.8.2 and Figs.8.3 and 8.4 respectively.

In detail:

- Fig.8.1 illustrates the velocity field. The scale of the arrow is not consistent for all measurement points. The rotation of the wake is visible up to three rotor diameters of distance downstream of the first model. The second model reintroduces it, but less effectively.
- Fig.8.2 highlights the introduction of a horizontal component by the wind turbine models. This component is present within $r = [-0.5, 0.5]$ only, a spatial range corresponding to the large-chord part of the blade. Also, this component becomes the less important the farer the wake is from the rotor. The second wind turbine reintroduces the horizontal component, only much less pronounced.
- Figs.8.3 and 8.4 illustrate the rotational component of the velocity and its evolution in the wake. After 5 diameters of distance from the first wind turbine, the wake shows almost no sign of rotation. The rotational component is then reintroduced by the second model but, at 10D (which is about 3.4 diameters downstream of the second rotor), it is again negligible.

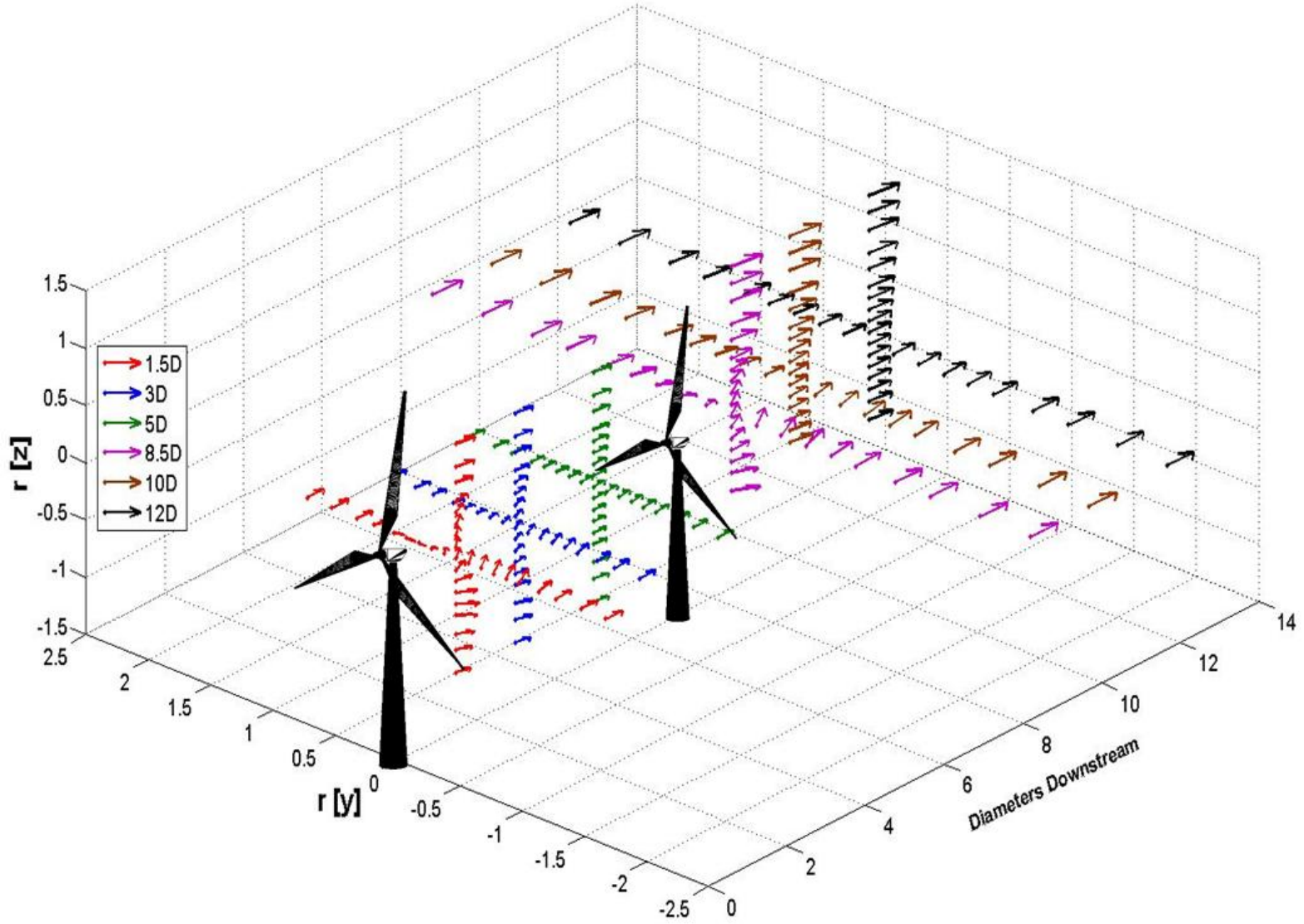

Figure 8.1.: Velocity field behind the two wind turbine models

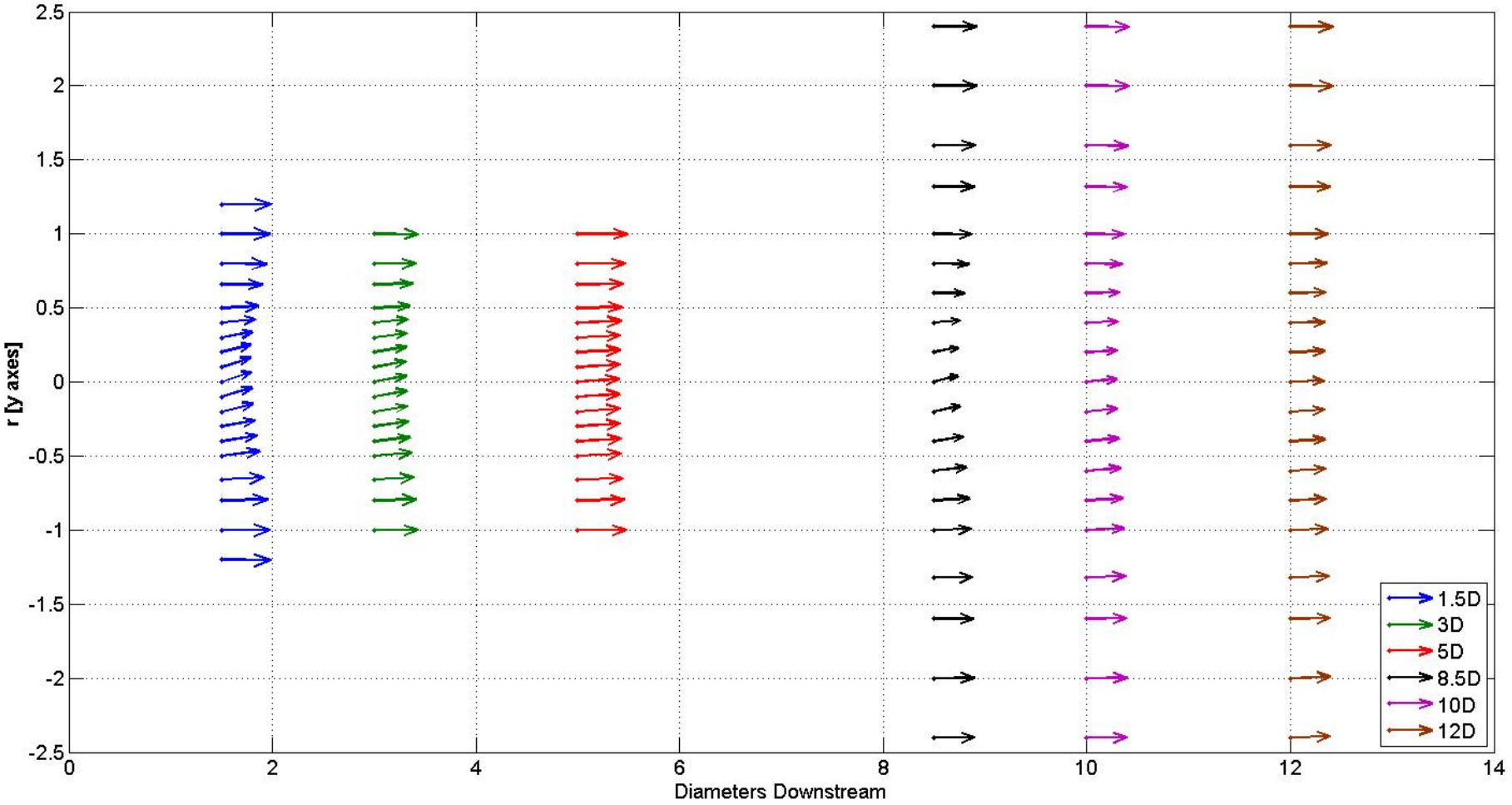

Figure 8.2.: Velocity field top view [x-y] - The presence of a horizontal component is noticeable

(a) plane at 1.5D

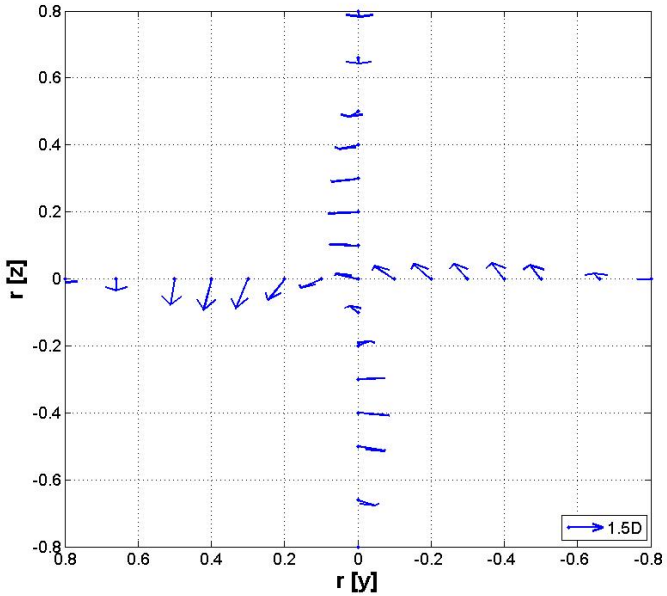

(b) plane at 5D

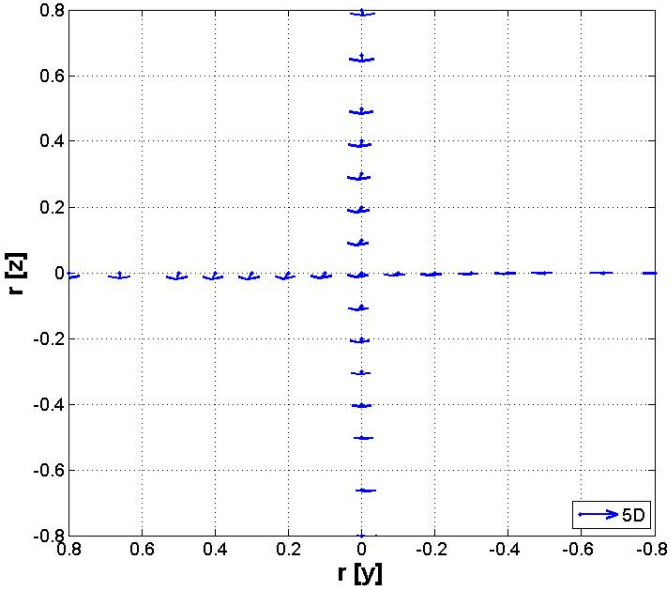

Figure 8.3.: Velocity field front view [y-z] after the first model

(a) plane at 8.5D

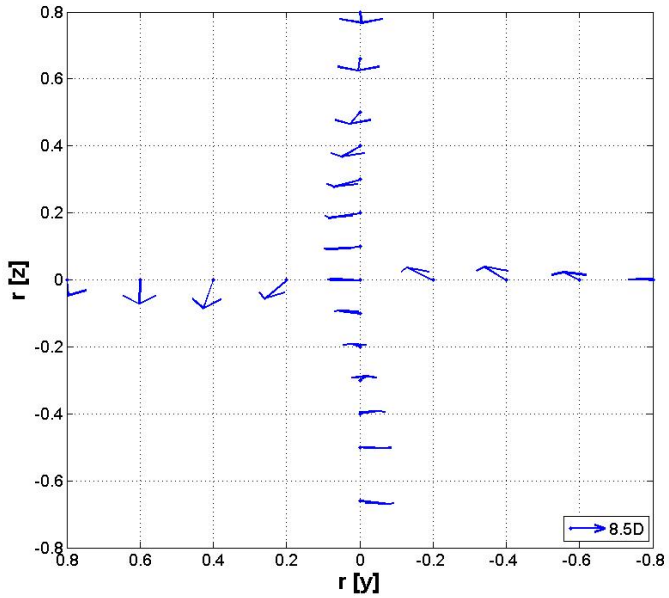

(b) plane at 10D

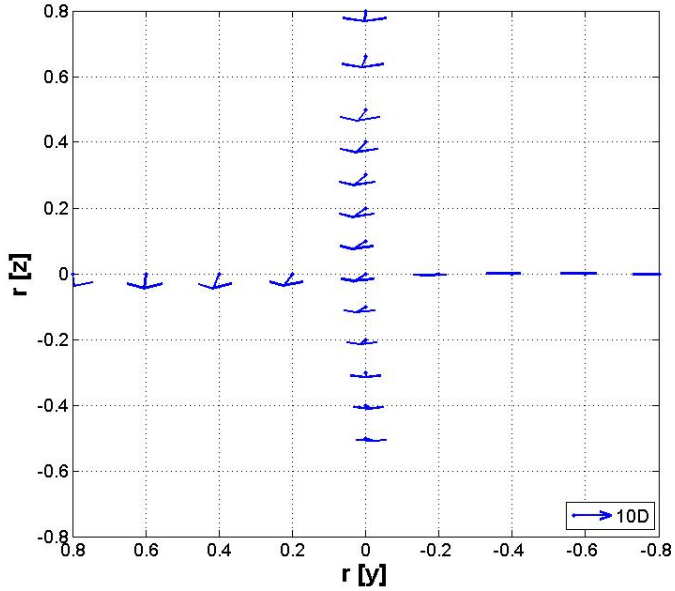

Figure 8.4.: Velocity field front view [y-z] after the second model

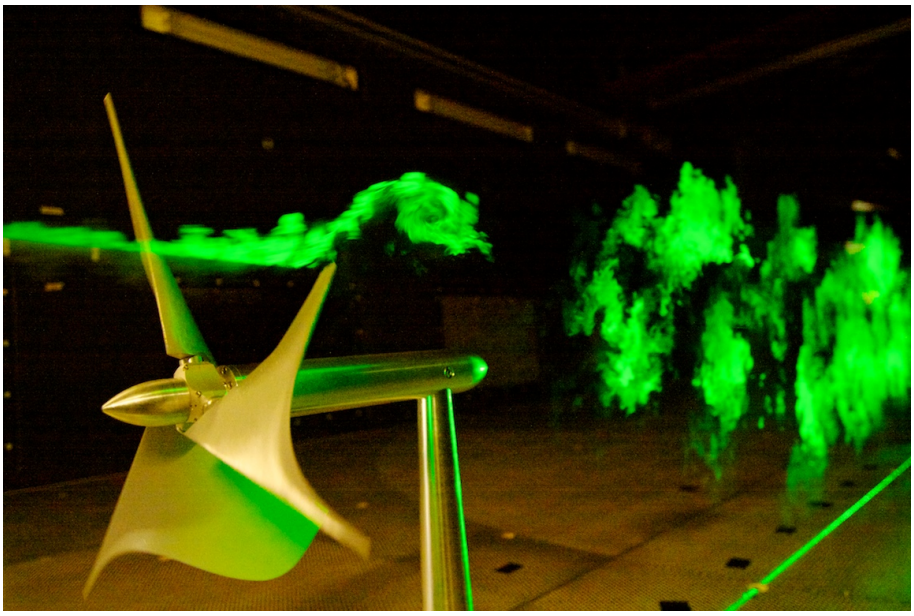

Figure 8.5.: Wake flow visualization - Tip vortex and near wake

Figure 8.6.: Wake flow visualization - helical structures and far wake

8.3. Influence of the Atmospheric Boundary Layer flow

8.3.1. One wind turbine model

In this section, comparisons of the wake of a single wind turbine in the two cases of free stream flow and ABL flow are presented. Fig.8.7 shows the horizontal profiles of the U component. The velocity deficit is higher in the case of ABL flow. In particular, focusing on Fig.8.8 which shows the profiles at $8D$, the ABL-flow case shows higher velocity deficit at each relative measurement point. Also, the ABL-flow case exhibits larger wake width.

The vertical profiles of the velocity deficit of the U component (Fig.8.9) clearly show how the downward motion of the point of maximum deficit $V_{D_{max}}$ follows the same trend for both cases. $V_{D_{max}}$ exhibits a shift, 0.5 rotor diameters large, between the profile at $1.5D$ and the one at $8D$.

Fig.8.10 and Fig.8.11 show respectively the horizontal profiles of the non dimensional W component of the velocity and the vertical ones of the V component. These components are responsible for the rotation of the wake. They decrease steadily in both cases, from values in the range of 20% of the reference velocity to less than 5%. The value of these components is higher in the free stream case.

Fig.8.12 and Fig.8.13 show the comparisons of the turbulence intensity plots. The highest values of the turbulence intensity are observed in the free stream flow case, however the ABL flow case exhibits a wider wake. Fig.8.14 highlights this feature for the profiles at 5 diameters of distance from the rotor.

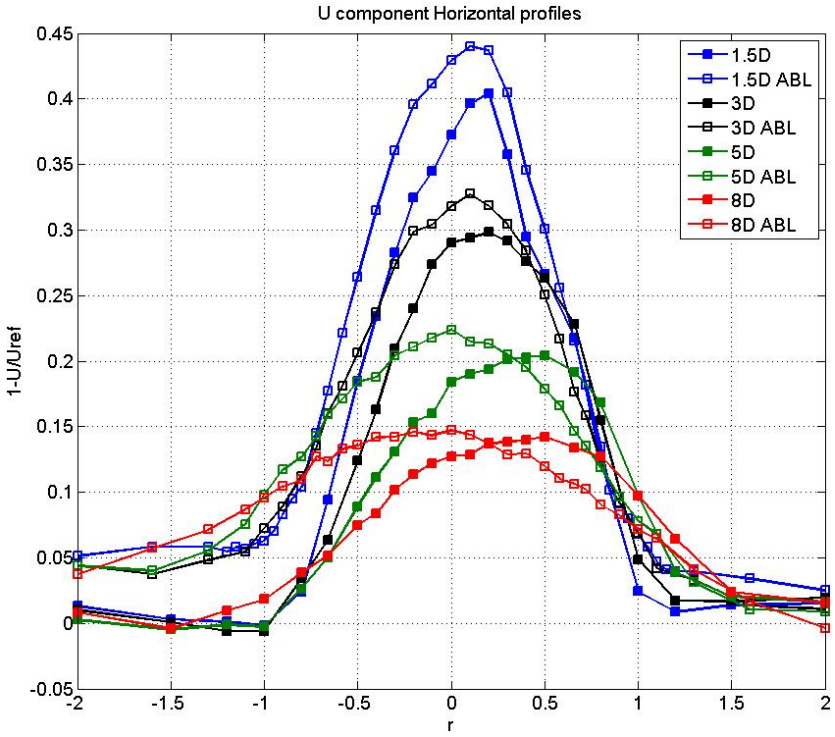

Figure 8.7.: Horizontal profiles - velocity deficit - U component - UW setup - comparison between free stream and ABL flow.

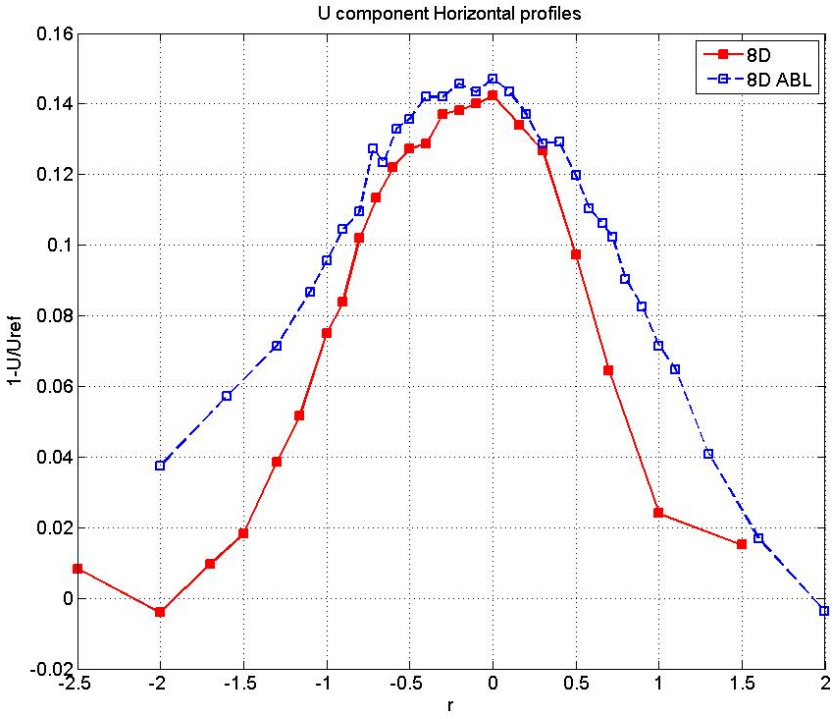

Figure 8.8.: Horizontal profiles - velocity deficit at 8D - U component - UW setup - comparison between free stream and ABL flow - free stream wake shifted for width comparison

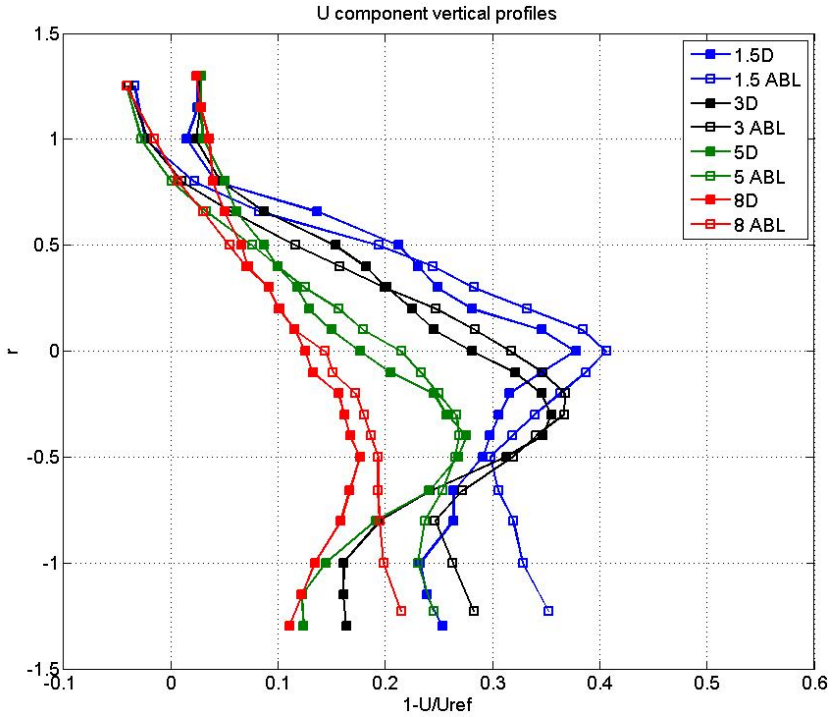

Figure 8.9.: Vertical profiles - velocity deficit - U component - UW setup - comparison between free stream and ABL flow.

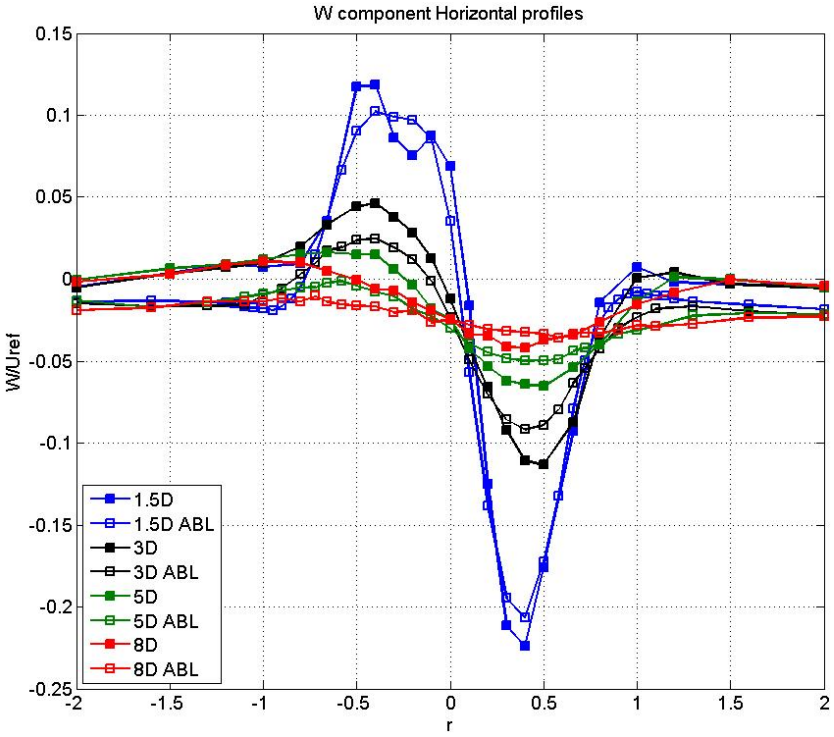

Figure 8.10.: Horizontal profiles - non-dimensional velocity - W component - UW setup - comparison between free stream and ABL flow.

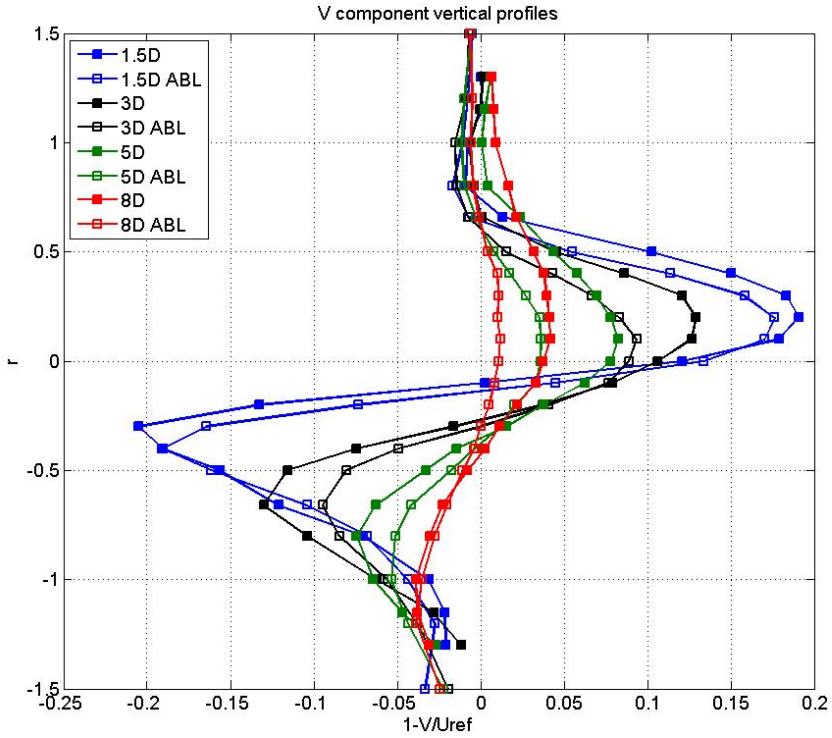

Figure 8.11.: Vertical profiles - non-dimensional velocity - V component - UV setup - comparison between free stream and ABL flow.

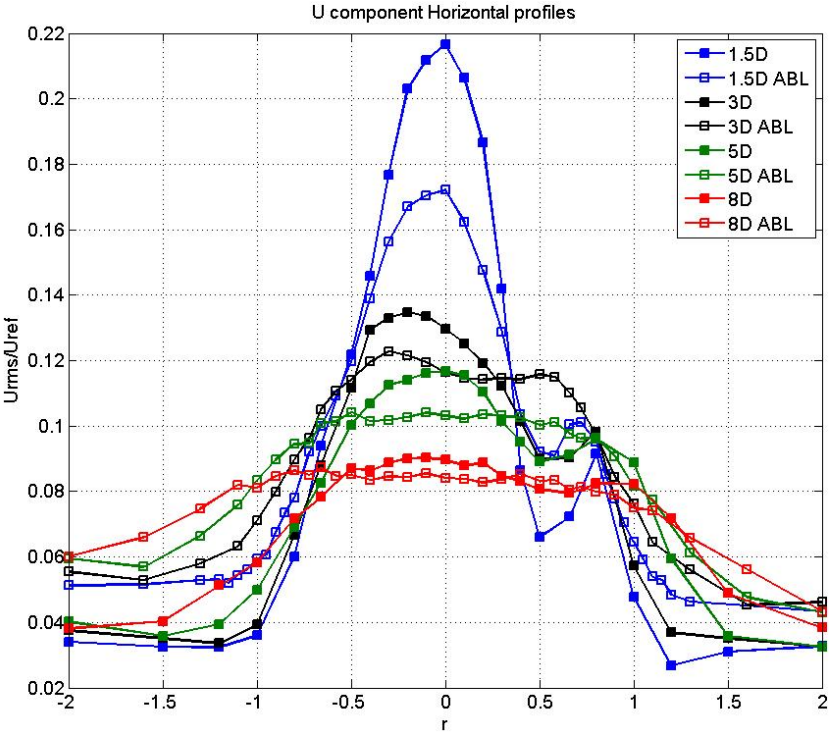

Figure 8.12.: Horizontal profiles - turbulence intensity - U component - UW setup - comparison between free stream and ABL flow.

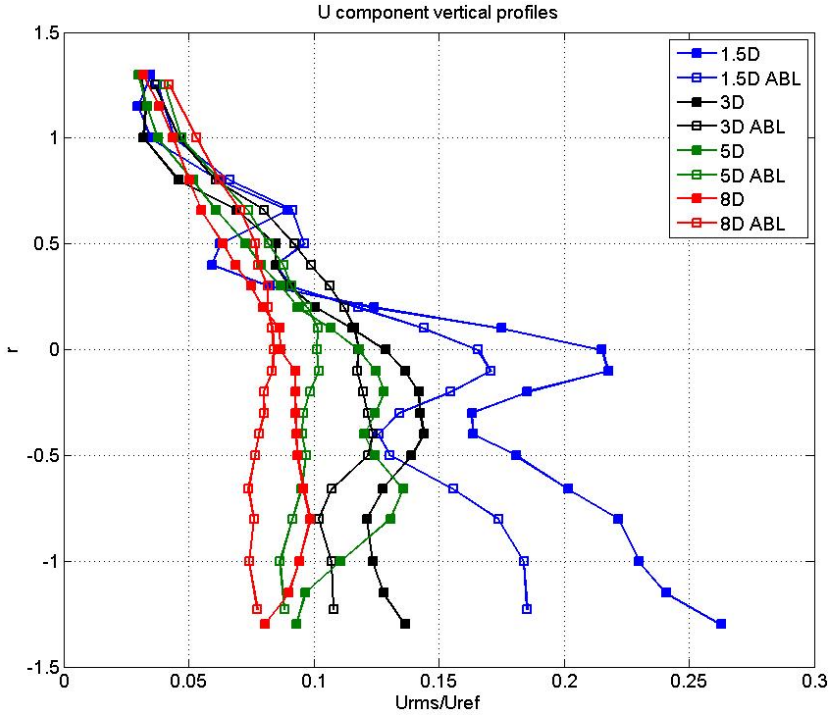

Figure 8.13.: Vertical profiles - turbulence intensity - U component - UW setup - comparison between free stream and ABL flow.

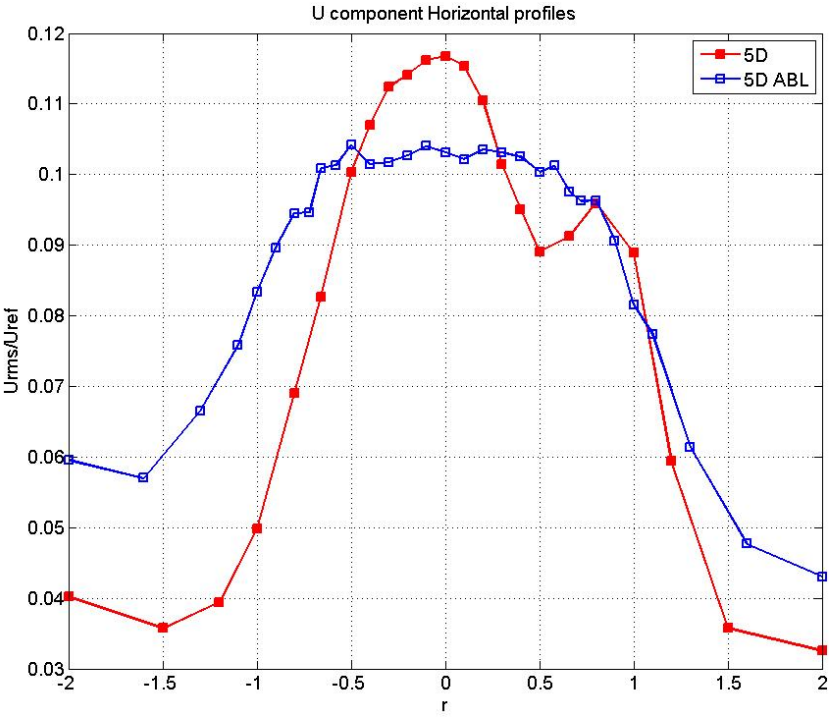

Figure 8.14.: Vertical profiles - turbulence intensity at 5D - U component - UW setup - comparison between free stream and ABL flow.

8.3.2. Two wind turbine models

Although the non dimensional velocity plot of Fig.8.16 shows that the U component is lower in the case of ABL flow than in the free stream one, the comparisons in Fig.8.15 illustrates a tendency of larger velocity deficit and a higher peak of turbulence intensity (in particular in Fig.8.21) for the free stream case. Nevertheless, the wake is wider in the ABL flow case, see Fig.8.16 and Fig.8.20.

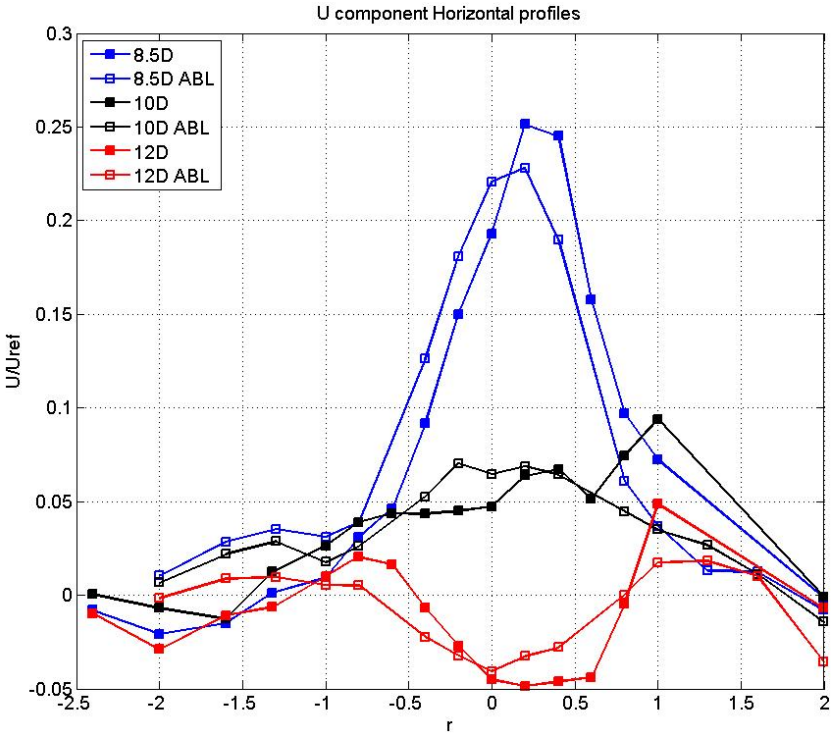

Figure 8.15.: Horizontal profiles - velocity deficit - U component - UW setup - comparison between free stream and ABL flow.

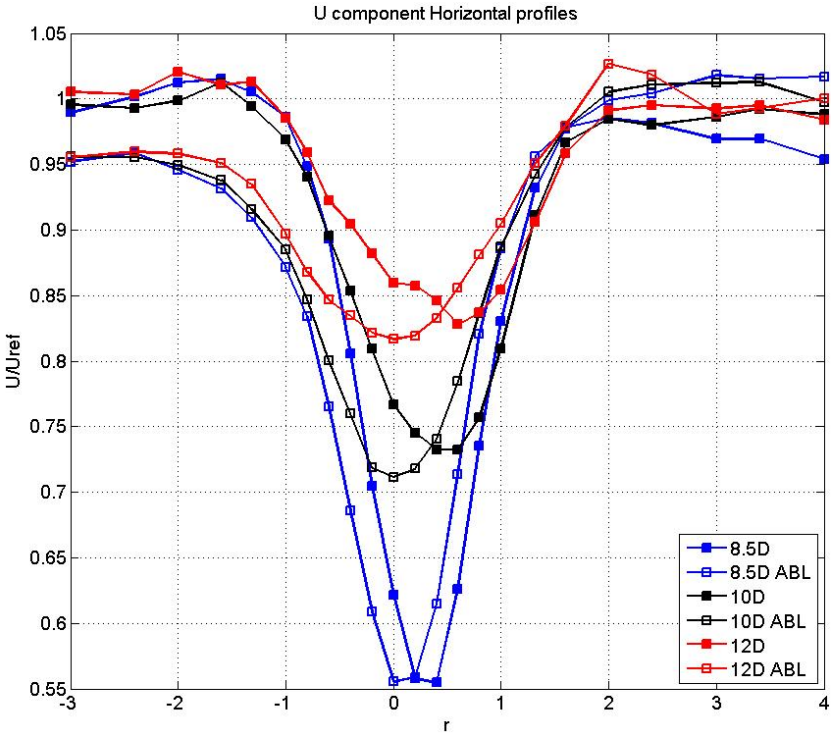

Figure 8.16.: Horizontal profiles non dimensional velocity - U component - UW setup - comparison between free stream and ABL flow.

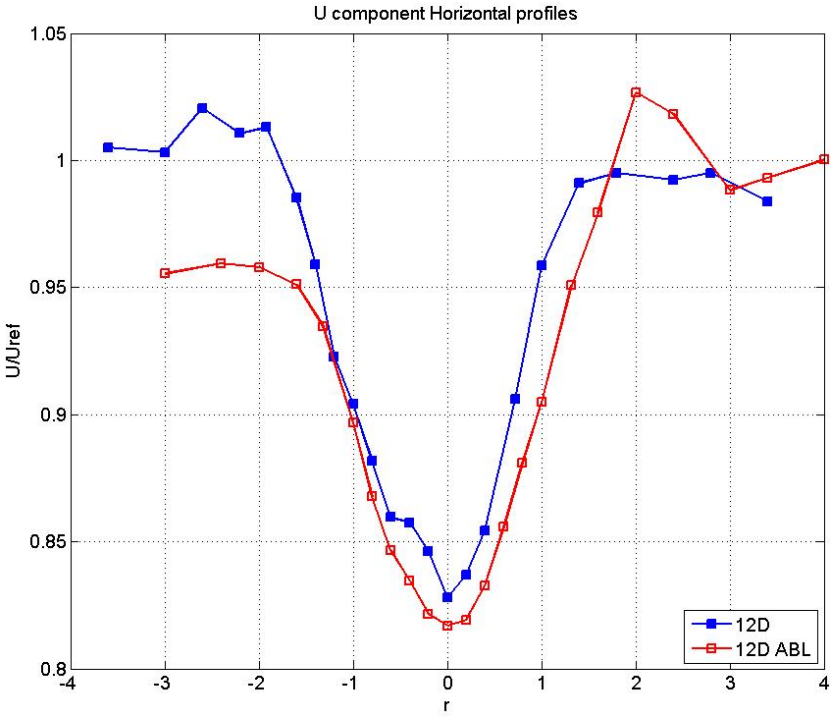

Figure 8.17.: Horizontal profiles non dimensional velocity at 12D - U component - UW setup - comparison between free stream and ABL flow - free stream wake shifted for width comparison

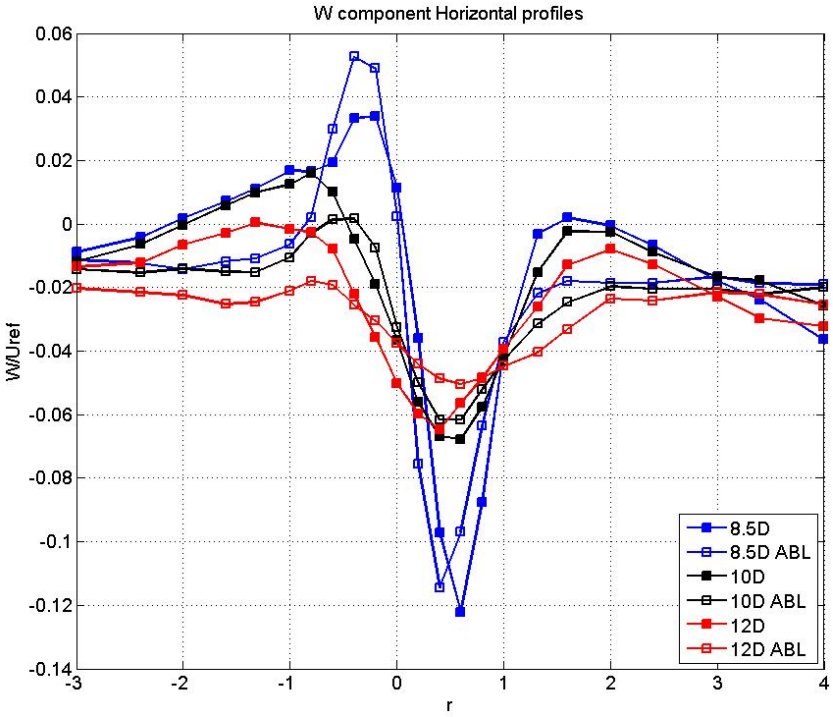

Figure 8.18.: Horizontal profiles - non-dimensional velocity - W component - UW setup - comparison between free stream and ABL flow.

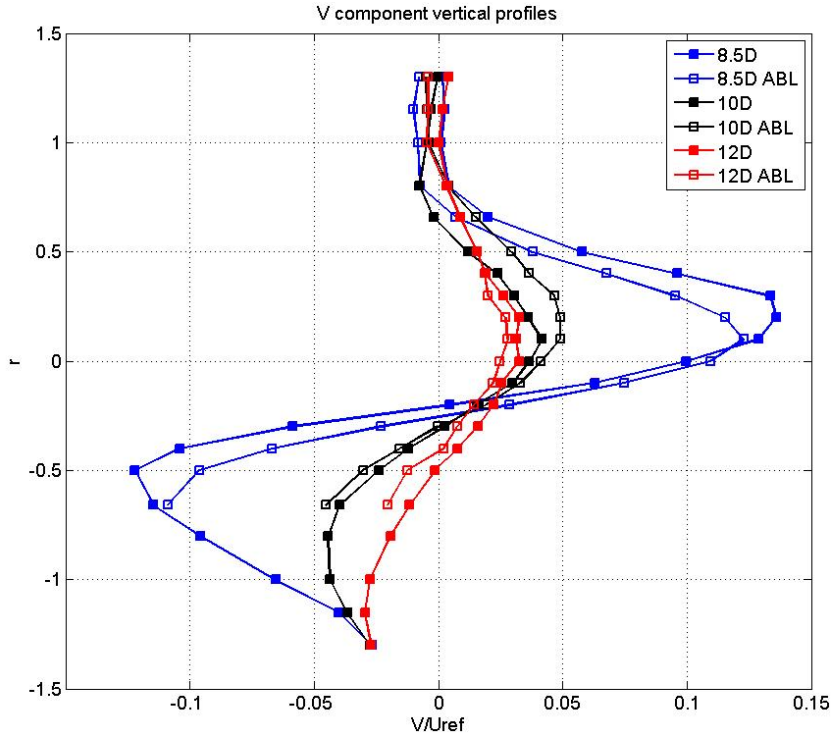

Figure 8.19.: Vertical profiles - non-dimensional velocity - V component - UV setup - comparison between free stream and ABL flow.

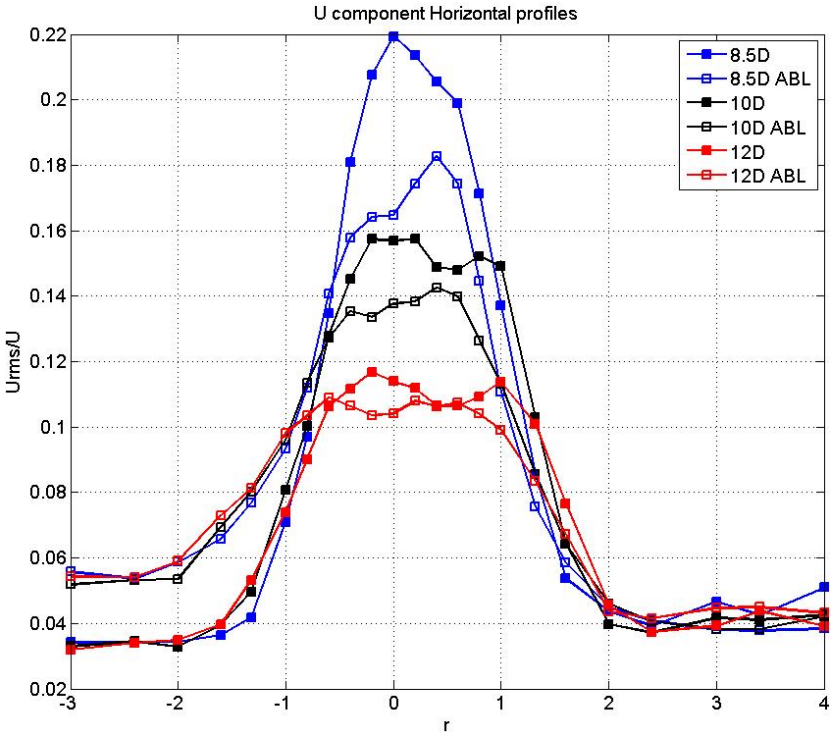

Figure 8.20.: Horizontal profiles - turbulence intensity - U component - UW setup - comparison between free stream and ABL flow.

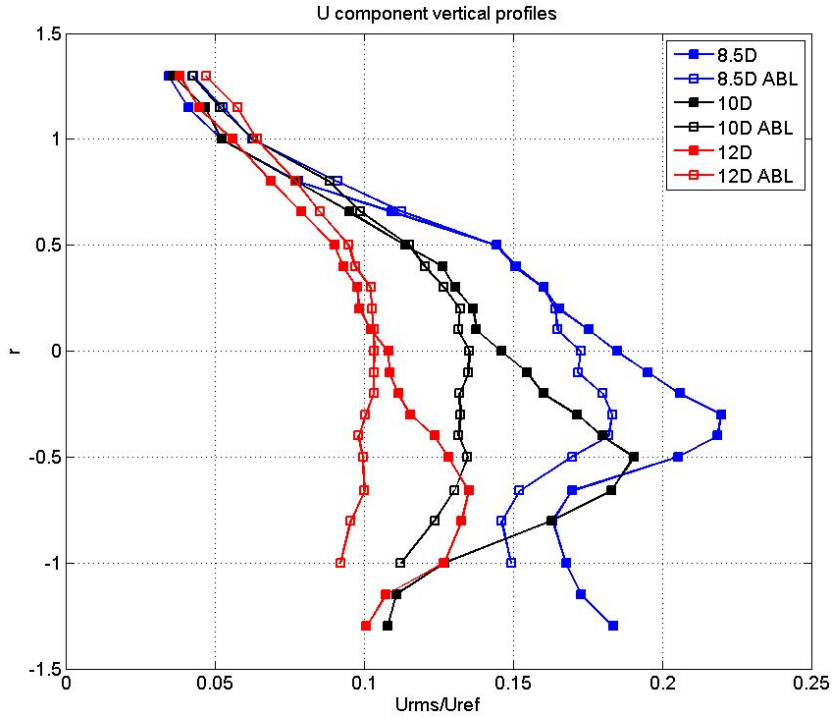

Figure 8.21.: Vertical profiles - turbulence intensity - U component - UW setup - comparison between free stream and ABL flow.

8.4. Influence of the aerodynamic shade of the wake

In this section wake profiles at the same relative position behind the first and the second model are shown. The aim of this section is to illustrate the differences in the flow when a wind turbine model is placed behind a first one. This information is very valuable as validation dataset of numerical models which focus on wind resource assessment or wind farm siting-optimization.

Fig.8.22 shows the velocity deficit profiles in the wake at 1.5D, 3D and 5D behind the respective rotor. Downstream of the second model, a drop of velocity deficit (less extraction of momentum) is clearly visible. In fact, at a distance of 1.5 rotor diameters from the rotor, the point of maximum deficit drops of about the 36%.

According to the calculation of the velocity deficit after the second model (see sec.7.2.3), it is important to point out that in the $5D$ profile behind the first model, the deficit is still more than the 20% of its inflow value (the unperturbed flow). At the same location after the second model, the flow has instead recovered to an higher value than its inflow (the $5D$ profile downstream of the first model). This suggests that the overall loss of momentum extraction, which exists between the first and the second row of wind turbines, might be higher than the drop between the second and an eventual third row.

The recovery of the turbulence intensity to the ambient level, see Fig.8.23, shows that the wake is about 50% wider after the second model. Also, as expected, the overall turbulence intensity and its peak are higher after the second model.

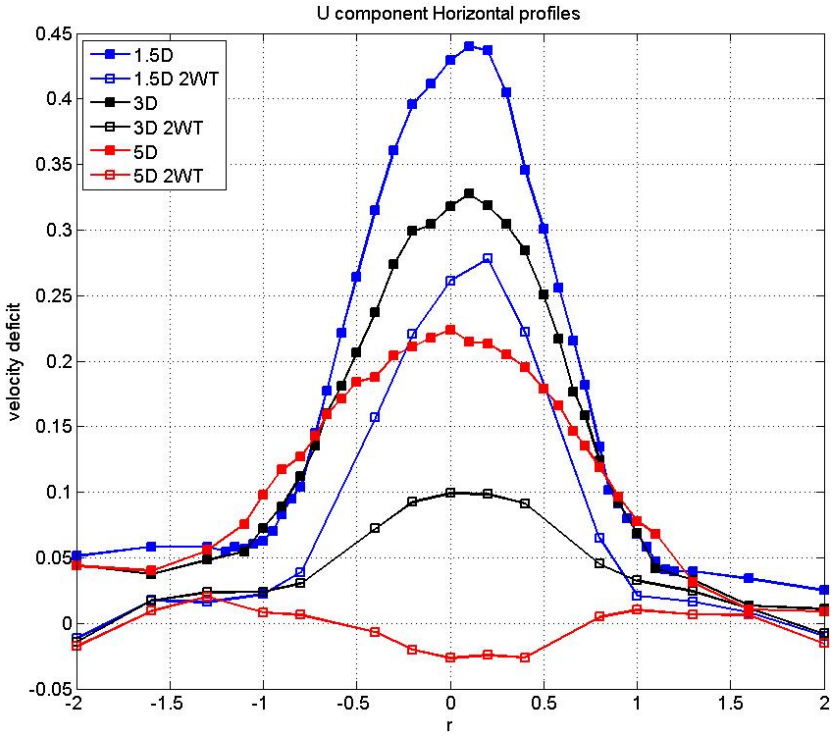

Figure 8.22.: Horizontal profiles - velocity deficit - U component - UW setup ABL flow- comparison between relative position behind the first and the second model.

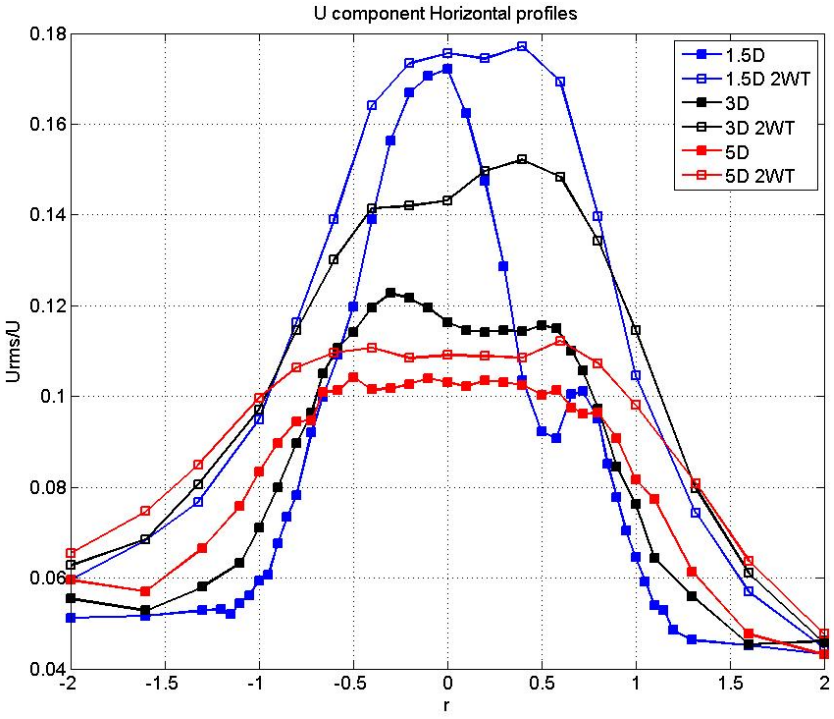

Figure 8.23.: Horizontal profiles - turbulence intensity - U component - UW setup ABL flow- comparison between relative position behind the first and the second model.

Part III.

Conclusions

9. Conclusions and further developments

9.1. A brief summary

This research project is part of a larger network, the WAUDIT project (see sec.2). In order to fit within the constraints of WAUDIT, a dataset of velocity measurements in the wake of wind turbine models had to be provided. This dataset not only can be used for validation of numerical models, but also it can be a basis for implementing the *quality assurance procedure for the evaluation of wind assessment models* also required by WAUDIT. In addition, data can be used for the evaluation of aerodynamic loads on wind turbine blades.

The physical modelling of wind turbine wakes in atmospheric boundary layer (ABL) flow is a very challenging task. In particular, four similarity parameters that describe the wake flow can be defined: Reynolds number Re, Tip Speed Ratio (TSR) λ, power coefficient C_P and thrust coefficient C_T. As pointed out in Ch.1, conditions of complete similarity for this case are not achievable in the laboratory, mainly due to the differences in scale.

Therefore, an appropriate strategy to experimentally investigate the wake of a wind turbine in ABL flow is to carry out a series of experiments. These tests must be designed for matching one by one all the similarity parameters. Hence, different similarity conditions can be achieved in each experiment. By varying systematically the parameters, it is possible to observe and monitor variations in the flow field. Then, dependencies of the flow on the parameters can be described. This procedure requires different rotors to be manufactured, each rotor specifically designed for matching one of the four similarity parameters.

The situation described above opens a scientific challenge that has to be addressed in order to meet the requirements of the WAUDIT project. The development of this methodology as a whole is a very complex and time demanding task. Moreover, results had to be provided in the strict time frame available of three years.

Being this project the first of its kind at the Meteorologisches Institut, I started this research from the very basis. Therefore, I designed my research with the intent to investigate one condition of partial similarity. In particular, following *Neff et al.* (1990), I investigated the test case of thrust coefficient (C_T) similarity. Thus, I designed a rotor that delivers a value of C_T comparable to full scale wind turbines.

My research consisted of three parts, which are reflected in the structure of this thesis:

1. Introduction
    - Identify the state of the art in wind turbine wake research;

- Definition of the experimental approach;

2. Development
    - Design of the wind turbine rotor model;
    - Preliminary testing to determine appropriate operative conditions;
    - Experimental campaign;
    - Data analysis and interpretation.

3. Conclusions
    - Conclusions and proposals for further developments.

A review of the existent literature showed that there have been many attempts to model experimentally wind turbine wakes, see Part I. A variety of approaches has been followed which address very particular cases only. Large models allow pressure measurements and near wake measurement only, moreover in free stream conditions. Wind turbine models based on the actuator disc concept do not introduce rotation in the wake and are not suitable for near wake studies. No design specifics are given for most of the rotor models used in previous studies. Also, a variety of different approaches has been followed for designing and operating rotor models. A belt-driven wind turbine was operated by *Adaramola and Krogstad* (2011), a geometrically scaled model was designed by *Campagnolo* (2013), rotors of small size were used by *Chamorro and Porté-Agel* (2009).

In my project, a BEM-based procedure for an aerodynamic design of the scaled rotor was applied.

The development part of the thesis describes the preparatory work carried out in order to start the scientific investigation. Although rather technical, this phase is of vital importance. In fact, scientific results are influenced by the quality of the technical work. Any imperfection in the design phase or in the manufacturing may cause a different behaviour of the model.

While the design procedure was implemented using Matlab, a number of constructive solutions have been examined with the technical workshop. Also, the choice of all the electric components was made. The definition of the operational conditions to be used for the main campaign was made, after performing a series of pre-tests with prototypes and after the sensitivity analysis of the wake on different rotors.

The availability of the atmospheric boundary layer wind tunnel Wotan allowed to investigate both near and far wake of the wind turbine model. Velocity profile measurements were carried out using a LDA system, recording the the three components of the velocity. Two different inflows were used: a free stream case and a typical offshore ABL. This allows not only to perform direct comparisons between the experimental results, also it gives the chance to test numerical models for the simplified case of the free stream.

In addition, a second model was placed in the wake of the first one and another dataset has been provided. This second experiment was carried out using the same inflow conditions of the first one and allows investigations on the wake of the second wind turbine model to be performed.

Finally, a number of Matlab scripts and functions were implemented for analysing the 154 velocity profiles measured, focusing mainly on mean values and on turbulence intensity.

The creation of this large dataset addresses the demand of validation data coming from the numerical modellers community. Also, it fulfilled the requirements of the WAUDIT project providing a high quality dataset suitable for wind resource assessment and for standardization procedures. The full potential of the dataset is yet to be exploited. Time series, which allow a statistical approach to the analysis, were also recorded and will be available for further investigations. Also, the provided data can be used for research in the field of blade design. In fact, the evaluation of loads on the blade due to introduced turbulence is very important in the design of blades and in the cost assessment of wind turbines.

The model was designed and structured to allow operational flexibility: it is possible to change the blades of the rotor, to vary their pitch angle, to substitute the motor/generator and eventually to use different towers and/or nacelles. After this first step, realized during this research project, the design of the model gives the chance to perform experiments with new rotors and to complete the methodology for the physical modelling of wind turbine wakes.

This research project realizes the assigned requirements of the WAUDIT project providing a dataset to be used for validation of numerical models. Also, it describes a methodology to be followed for the physical modelling of wind turbine wakes in ABL flow. In addition, after designing manufacturing and testing wind turbine models, it realizes one step of this methodology. This latter part generates a series of scientific questions that can be answered with further experiments and research. The following section describes some of these questions and it suggests solutions.

9.2. Concluding considerations and proposals of further developments

This project dealt with many challenges, some of them have already been tackled during the three years of the scholarship. In this section some of the open questions are discussed. Also, further developments and new investigation themes are proposed.

Comparisons with previous experiments

Before this research, a number of experimental investigations has been carried out. Unfortunately, direct comparisons are difficult to be performed. In fact, models differ in terms of rotor diameter: from the $150\mathrm{mm}$ rotor used by *Chamorro and Porté-Agel* (2009) to the large model ($2\mathrm{m}$) seen in *Campagnolo* (2013). Also, the model may be actively driven as in *Adaramola and Krogstad* (2011). In addition, operative conditions may be different. In the case of *Pascheke and Hancock* (2007), as an example, very low wind speed was used in order to investigate effects of thermal stratifications.

For this reason, direct comparisons are not performed in the present thesis. The creation of a

database containing an ensemble of the available experimental investigation might be considered as a future development.

Design procedure

The aerodynamic design procedure, based on the BEM theory, faces a few difficulties. The first one is the lack of aerodynamic data at low Reynolds number. Few airfoils, typically for aeronautic use, were tested in the range $Re < 2 \cdot 10^5$. For the EJ85 airfoil, the one used in this study, lift and drag coefficient data were available at one Reynolds number only. Thus, the variation of C_L and C_D due to the increasing Re along the span of the blade had to be neglected.

The iterative procedure was implemented following the code architecture illustrated in *Burton et al.* (2001), *Sanderse* (2009) and *Manwell et al.* (2009). This procedure at low Reynolds numbers (small rotor sizes) and at high values of the angle of attack (close to the root) might present convergence issues. These convergence issues led to neglect tip and root loss factors in the design procedure of the blade. The wind turbine design toolbox developed by UPM Madrid tackles this problem. App.B describes the contribution to the optimization procedure I gave during my WAUDIT secondment at UPM.

The design of a new, less solid blade, could be performed with this design toolbox. This new blade would allow experiments at higher tip speed ratio to be carried out. Also a second step in the development of the physical modelling methodology would be performed.

Velocity measurements

The locations of the measurement points that form a velocity profile have been geometrically defined with respect to the rotation axis of the wind turbine model. The wake might move out of this geometrical axis and it is unsure that the point of maximum velocity deficit was recorded at each plane. Therefore, a series of PIV measurements for mapping the wake flow should be considered.

Time series analysis

A thorough statistical analysis of all the time series recorded has not yet been performed. Spectral analysis is a powerful tool of investigation which might give a better insight on the turbulence characteristics of the wake. Also, it would provide additional data for validation and evaluation of numerical models. As an example, normalized spectral distributions of the turbulent kinetic energy are shown in App.C.

Tower effects

The wake of the tower of the wind turbine certainly has an influence on the flow behind the model. Geometrical scaling of a wind turbine tower is a challenging task. Vibrations might easily occur. An research project focusing on this topic should be sustained by an experimental and numerical

study. The influence of the tower wake could be described in detail, as well as the effects of the ground and of the low pressure area which surrounds the wake of the turbine.

Turbulence and power output

The models operated in this project allow also power output time series to be measured and synchronized with velocity measurement in the inflow. Turbulence is of great interest for the wind energy research community. In particular, turbulent structures influence both the power output and the aerodynamic loads on the rotor. Thus, an experimental campaign for the generation of this dataset is strongly suggested.

Part IV.

Appendices

Appendix A

Wind tunnels & measurement techniques

In this appendix the wind tunnels and the measurement techniques used are described.

Wind tunnels

Fig.A.1 shows the top view of the Göttingen-type wind tunnel at EWTL. The test section of tunnel is $1.75\mathrm{m}$ long, the jet of the tunnel is about $1\mathrm{m}$ in diameter.

The wind speed can be changed continuous from $0\mathrm{m\ s^{-1}}$ up to $20\mathrm{m\ s^{-1}}$ and the Reynolds number achievable, defined as $Re = v_c l_c/\nu$ where v_c is the flow speed and l_c is the diameter of the outlet of the free jet is in the range of $10^4 < Re < 4 \cdot 10^6$.

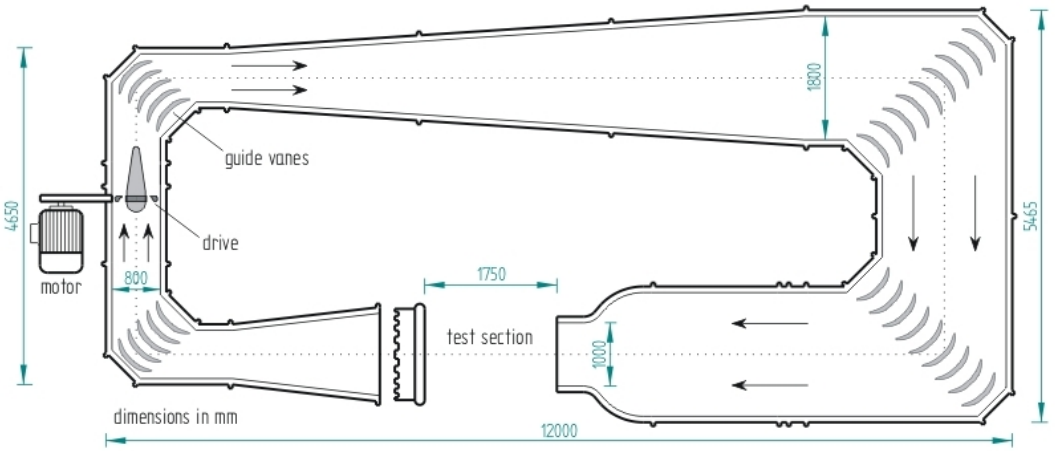

Figure A.1.: Top view of the Göttingen-type wind tunnel at EWTL, source:(*EWTL*, 2011)

The WOTAN wind tunnel in the Environmental Wind Tunnel Laboratory (**ETWL**) at the University of Hamburg, see Fig.A.2, is a large conventional type boundary layer wind tunnel with a wind speed range between $0\mathrm{m\ s^{-1}}$ and $20\mathrm{m\ s^{-1}}$. The tunnel has a test section $18\mathrm{m}$ long and it is equipped with two turntables and an adjustable ceiling. The cross section of the tunnel measures $4\mathrm{m}$ in width and, depending on the configuration of the ceiling, between $2.75\mathrm{m}$ and $3.25\mathrm{m}$ in height. In each of the different wind tunnel projects in WOTAN, model scale and meteorological characteristics of the inflow conditions are usually different. Hence, based on the meteorological and fluid dynamical target parameters, a project-specific set-up of spires and floor roughness is derived for each project individually. The test section of the tunnel is equipped with a computer-controlled traverse system with positioning accuracy below $0.1\mathrm{mm}$ on all three traverse directions. These information and more details on the wind tunnel facility are given in *Leitl et al.* (2009).

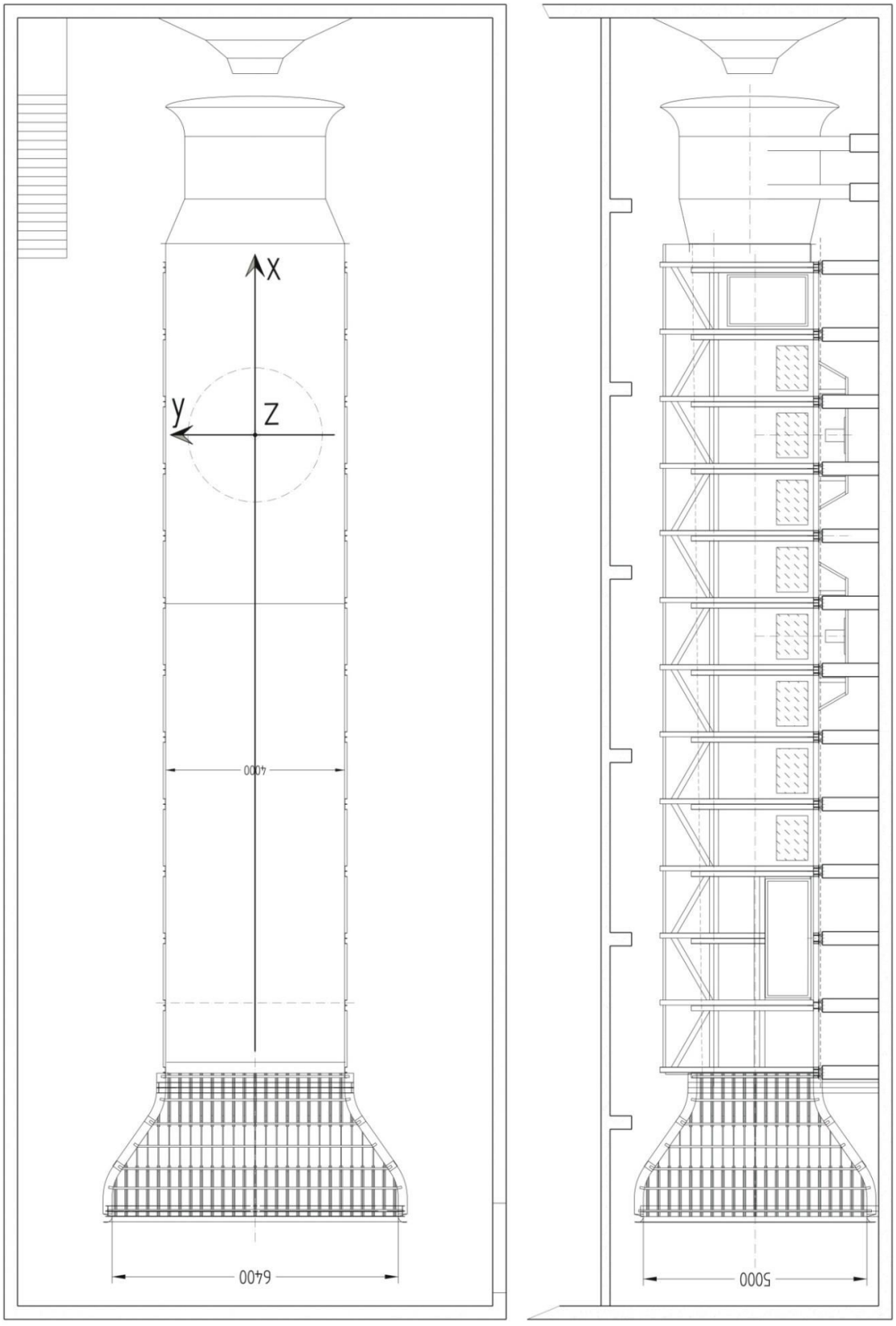

Figure A.2.: Technical drawing of the Wotan wind tunnel at EWTL. Left top view, right side view.

Fig.A.3 shows a diagram of the Malavard wind tunnel at Prisme laboratory. This facility is a closed circuit wind tunnel with two test sections $V1$ and $V2$. The first one is a conventional section $2\mathrm{m}$ high, $2\mathrm{m}$ wide and $5\mathrm{m}$ long. The wind speed can be varied between $10\mathrm{m\ s^{-1}}$ and $60\mathrm{m\ s^{-1}}$. The section is equipped with an external 6-components force balance.

The test section $V2$ is in the return part of the tunnel circuit, its dimensions are $[5\mathrm{m}x5\mathrm{m}x20\mathrm{m}]$ and it is used for ABL modelling.

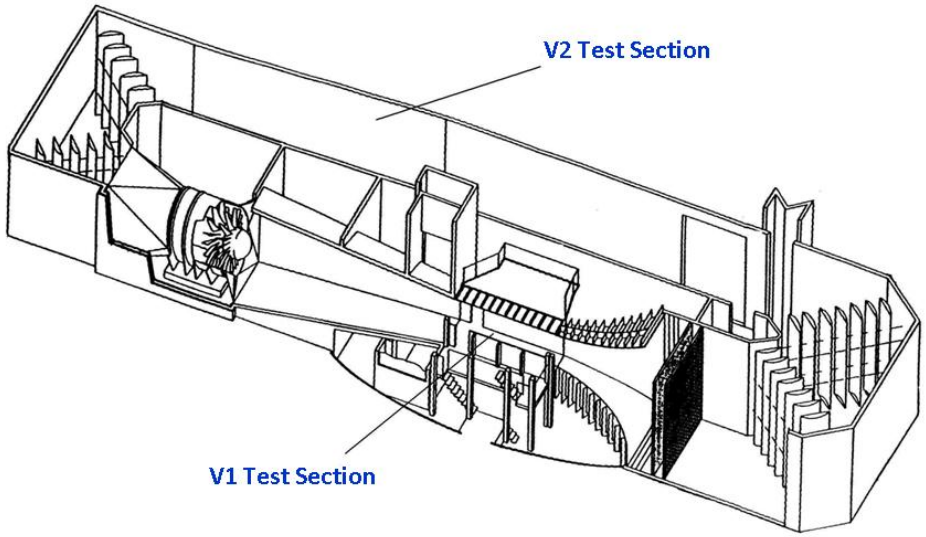

Figure A.3.: Schematic of the "Malavard" wind tunnel at Prisme laboratory, Orleans.

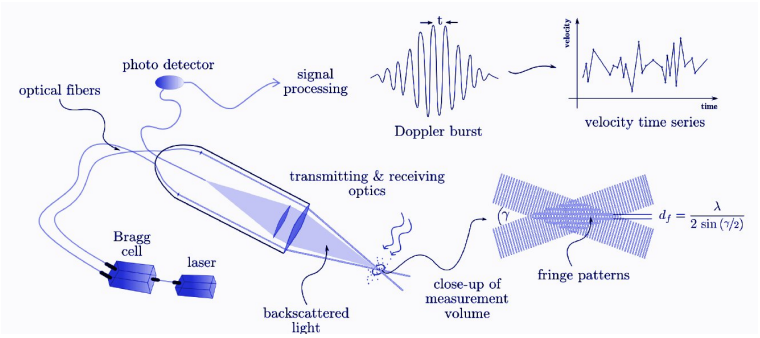

Figure A.4.: LDA-measurement principle, modified after *Hertwig* (2013)

Measurement techniques

Laser Doppler Anemometry (LDA) is a well known measure technique. This optical non-intrusive method is based on the Doppler effect caused by the particles that pass through the measurement volume. With this technique it is possible to achieve temporal resolution up to the order of the MHz.

Typically, most LDA system use the so-called *fringe mode*. The laser beam is split, creating two rays. These, after being emitted from the probe, intersect with the angle γ creating the measurement volume. In this volume, the interference between the two rays create a pattern of planes of laser light at high intensity (the fringes) alternated by dark planes. The fringes are orientated in order to be perpendicular to the direction of the velocity component intended to be measured. The distance between fringes δ_f is constant and it can be related to γ and to the wavelength of the laser light λ with the relation:

$$\delta_f = \frac{\lambda}{2sin(\gamma/2)}$$

When a particle passes through the measurement volume, the intensity of the scattered light fluctuates at the frequency f_D due to the interference pattern. The velocity component, e.g. U, can be calculated as:

$$U = \delta_f f_D = \frac{\lambda f_D}{2sin(\gamma/2)}$$

With this procedure it is not possible to distinguish between positive and negative values of the velocity, neither $U = 0$ can be measured. In order to overcome this ambiguities, other LDA systems, such as the one in use at EWTL Hamburg, a constant frequency shift f_0 is superposed to one of the beams. This shift is creating by the Bragg cell, which also splits the laser beam. In this case, the relation between the frequency f_D and the velocity U is the following:

$$\delta_f \simeq f_0 + \frac{2sin(\gamma/2)}{\lambda} U$$

Simultaneous 2-D measurements are carried out by using two laser beams of different wavelength, this is the case of the LDA system used for this study. Fig.A.4 illustrates the typical setup of a 1-D LDA system. Fig. A.5 shows the 2D LDA probe used in the experiment of sec.5.2.

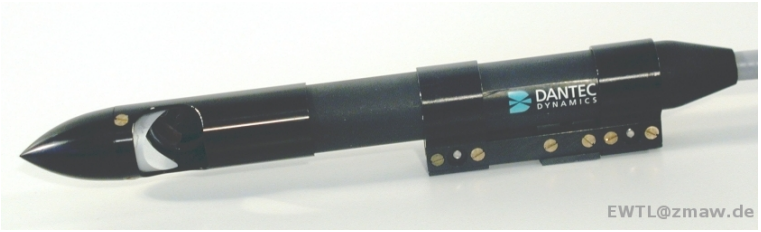

Figure A.5.: 2D Laser Doppler Anemometer probe by Dantec Dynamics

Probe setup. In order to measure the three components of the velocity, at each point measurements have to be repeated after turning the laser probe needs of $90\circ$. In particular, for measuring the U and the W components the probe needs to point sidewards while it points downwards when measuring U and V.

Hot Wire Anemometry (HWA) is a well established velocity measurement technique that achieves high frequency responses. The HWA functioning principle is shown on fig.A.6.

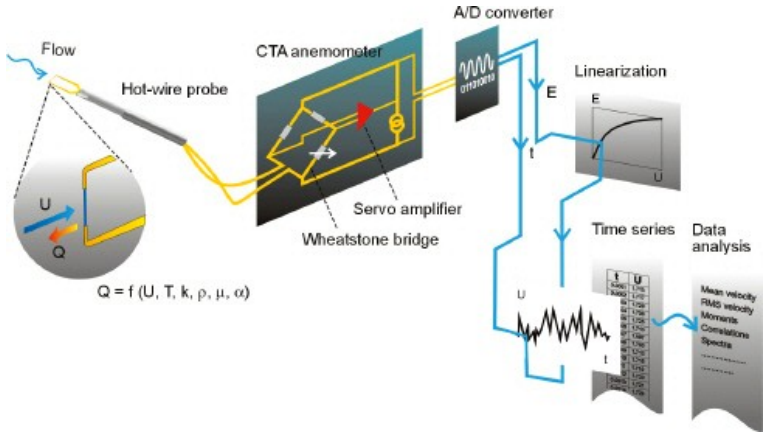

Figure A.6.: Schematic showing the HWA functioning. From *DantecDynamics* (2011)

HWA is based on the cooling effect of the flow on the heated wire, mainly due to the convection. This effect can be described as:

$$Nu = f(Re, Pr, Gr, l/d, (T_w - T_a)/T_a, \alpha) \tag{A.1}$$

where T_a and T_w are the ambient and wire temperature respectively, l and d are the length and the diameter of the wire, α is the angle between the wire and the velocity vector. Nu, Re, Pr, Gr are the Nusselt number, Reynolds number, Prandtl number and Grashof number respectively.

King (1914) proposed the expression:

$$Nu = A' + B' Re^{0.5} \tag{A.2}$$

where:

- $Nu = \frac{Q}{K\pi l(T_w - T_a)}$;
- $Re = \frac{\rho U d}{\mu}$;
- Q is the convective heat transfer (Joule effect);
- K is the thermal conductivity;
- ρ is the air density;
- U is the wind speed;
- μ is the dynamic viscosity.

Being $Q = \frac{E^2}{R}$, where E is the voltage and R is the wire resistance, the expression A.2 can be written as:

$$Q = A + BU^{0.5} \tag{A.3}$$

where A and B are constant defined after the calibration. Further details about HWA can be found in *Bruun* (1995).

In particular, at the Prisme laboratory a Dantec 55P91 probe is in use. This is a triple-sensor gold-plated wire probe, the sensor form a system with an acceptance cone of $70.4\circ$. The relative position between the prong ends and the sensors (perpendicular) increases the accuracy in decomposing the probe signals into velocity components.

Force balance are a tool of very common use in experimental aerodynamics. The first balance was developed by Otto von Lilienthal for lift measurements: the lift was counterbalanced by weights allowing the measurement of the force. Nowadays, instead of weights, load cells are used. The load cells typically consist in four strain gauges connected together forming a Wheatstone bridge. Strain gauges give an indirect measure of the force. They measure the change of electric resistance due to the deformation of the gauge. More details about the functioning of the strain gauges and about the calibration of a six-component balance are given in *Tropea et al.* (2007).

A schematic of a typical six-component external balance, similar to the one operating at the Prisme Laboratory (which is designed and manufactured in house), is shown in Fig.A.7. In particular, the vertical (f) and the horizontal (j) load cells are visible. The first ones measure the lift force and the pitching and rolling moment, the latter measure the horizontal force (side and drag) and the yawing moment.

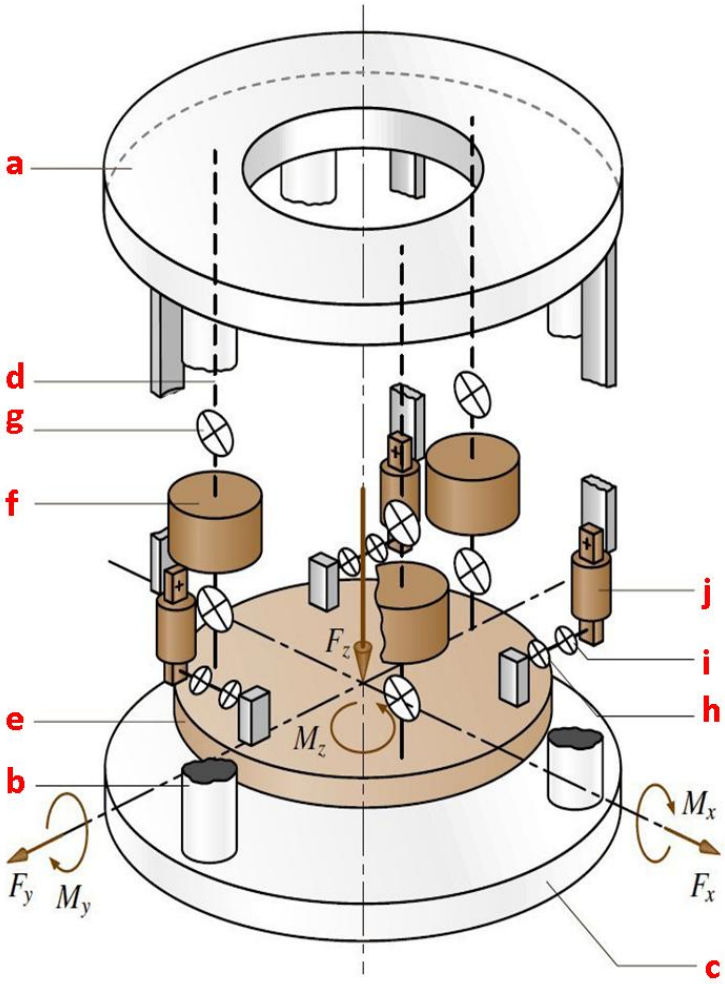

Figure A.7.: Typical external balance configuration. Modified after *Tropea et al.* (2007)

Appendix B

NACA 0012 lift and efficiency data preparation for low Reynolds number optimization procedures

The maximum value of the power coefficient of a wind turbine ($C_{P_{max}}$) depends on the Reynolds number (Re). The value of the tip speed ratio (TSR) which corresponds to $C_{P_{max}}$ (λ_{op}), also depends on Re.

Typically a *global* value of Re is considered, defined as $Re_g = U_\infty R/\nu$, where U_∞ is the wind speed, R is the rotor radius and ν is the kinematic viscosity. In the optimization of the blade geometry, the conclusions of the Glauert theory are generally accepted. Defining the blade solidity as $\sigma = \frac{Bc}{\pi r}$ (where B is the number of blades and c is the airfoil chord at the radius r, $2\pi r$ is the circumferential length at the same radius), the theory states that the radial distributions of σ (which defines the chord length) and of the pitch angle θ that correspond to $C_{P_{max}}$ are constant for all the wind speeds. Also λ_{op} is constant. Further details about this theory can be found in *Glauert* (1935) and *De Vries* (1983).

On the other hand, the aerodynamic characteristics of an airfoil (thus, of the blade) are dependent on the local Reynolds number Re_{loc}, see *Gad-el Hak* (1990). In the case of wind turbine blades, the local Reynolds number is defined as $Re_{loc} = \frac{U_{loc}c}{\nu}$, where U_{loc} is the wind speed at the blade section considered.

Cuerva (2009) demonstrates that the radial distributions of σ and θ and also λ_{op} that lead to $C_{P_{max}}$ are not constant for all wind speeds when this dependency is considered. In particular, Re_{loc} can be written as a function of the global Re as follows:

$$Re_{loc} = Re_g \pi b^{-1} \sigma [(1-a)^2 + \lambda^2 x^2 (1+a')^2]^{0.5} \tag{B.1}$$

Although less important at high values of $Re =\sim 10^6$, this conclusion plays an important role when designing wind turbine models, which generally operate at low Re. In this condition the aerodynamic characteristics of an airfoil, in terms of lift coefficient C_L and efficiency $K = \frac{C_L}{C_D}$ (C_D is the drag coefficient), are very Re-sensitive.

Unfortunately, lift and drag diagrams of airfoils commonly used for commercial wind turbines are not available at low Re. Therefore, the well-known $NACA0012$ airfoil was used. Many studies have been carried out about this airfoil. Results are available at different Re. Studies were carried out by different researchers and in different wind tunnels. In particular, data from *Laitone* (1997), *Sunada et al.* (1997), *Sheldahl and Klimas* (1981), *McCroskey* (1987), *Eppler* (1990), *Eastman and Sherman* (1937) were used. These data are not always consistent with each other. In order to assure the monotonic increase of the C_L with increasing Re a selection has to be

made. Also, the values of lift and drag coefficients are measured in a range of angle of attack α typical of aeronautical applications. In the case of the wind turbines, higher values of α have to be considered. In order to extend the C_L-α and K-α diagrams in the range $\alpha = [0° - 180°]$, the *Viterna-Corrigan* method has been used, following *Viterna and Corrigan* (1981). Fig.B.1 and Fig.B.2 show the C_L-α and K-α curve respectively.

Once the procedure is complete, it is possible to interpolate the curves and obtain the relations C_L-Re-α and K-Re-α. This relations provide all the interconnected values of angle of attack, Reynolds number and lift (drag) coefficient. The optimization procedure, based on the Lagrange multiplier method, can use a value of the C_L and of the E appropriate for every blade section. Fig.B.3 shows the C_L-Re-α diagram.

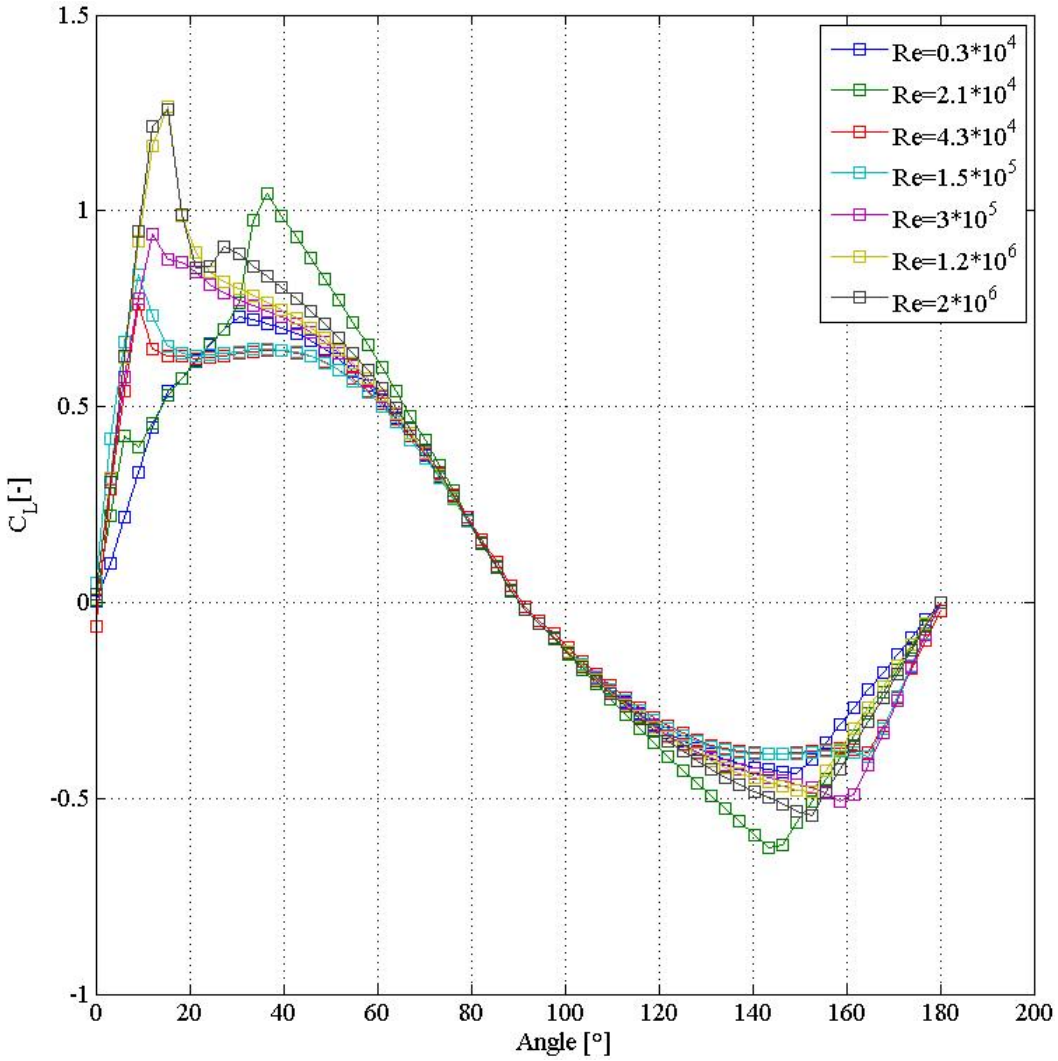

Figure B.1.: C_L-α curve of the NACA0012 airfoil, extended using Viterna-Corrigan method.

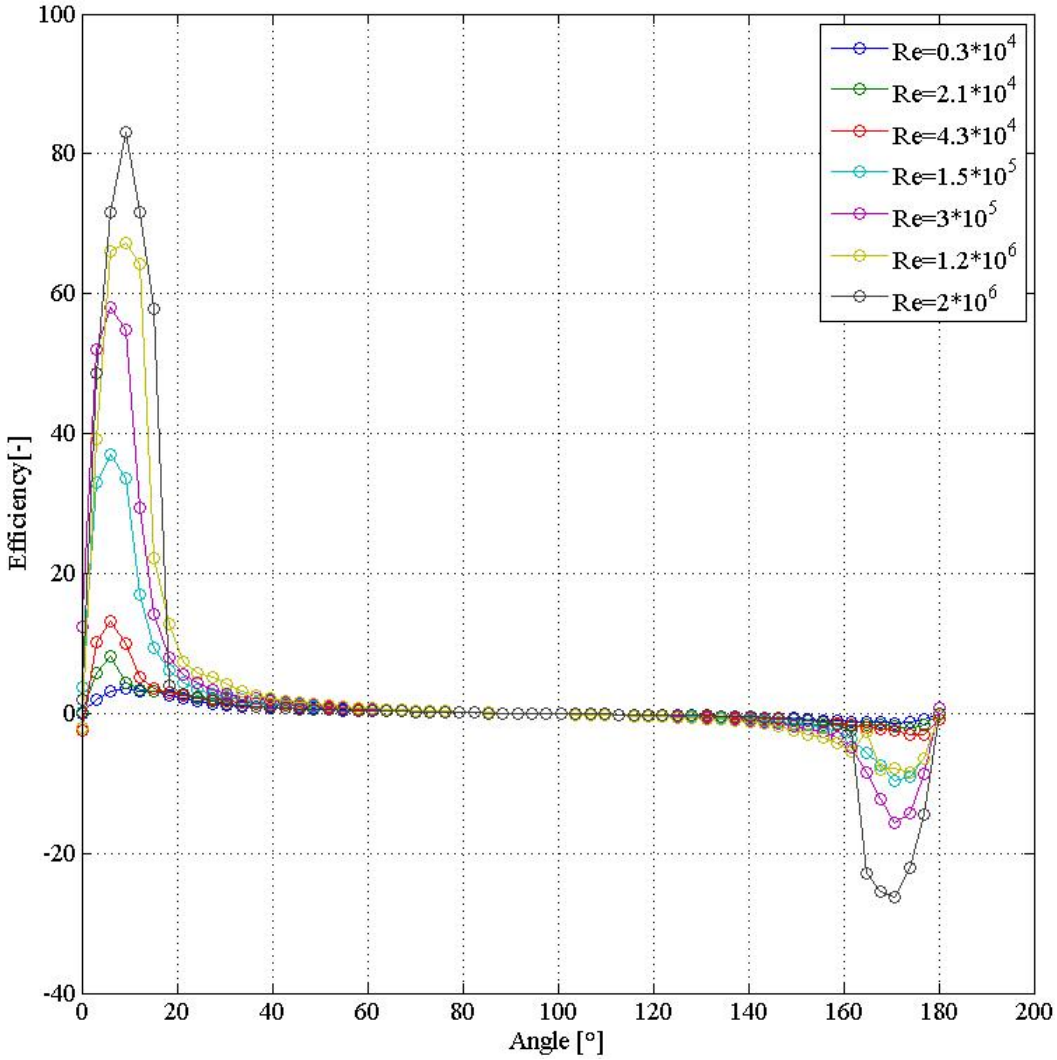

Figure B.2.: E-α curve of the NACA0012 airfoil, extended using Viterna-Corrigan method.

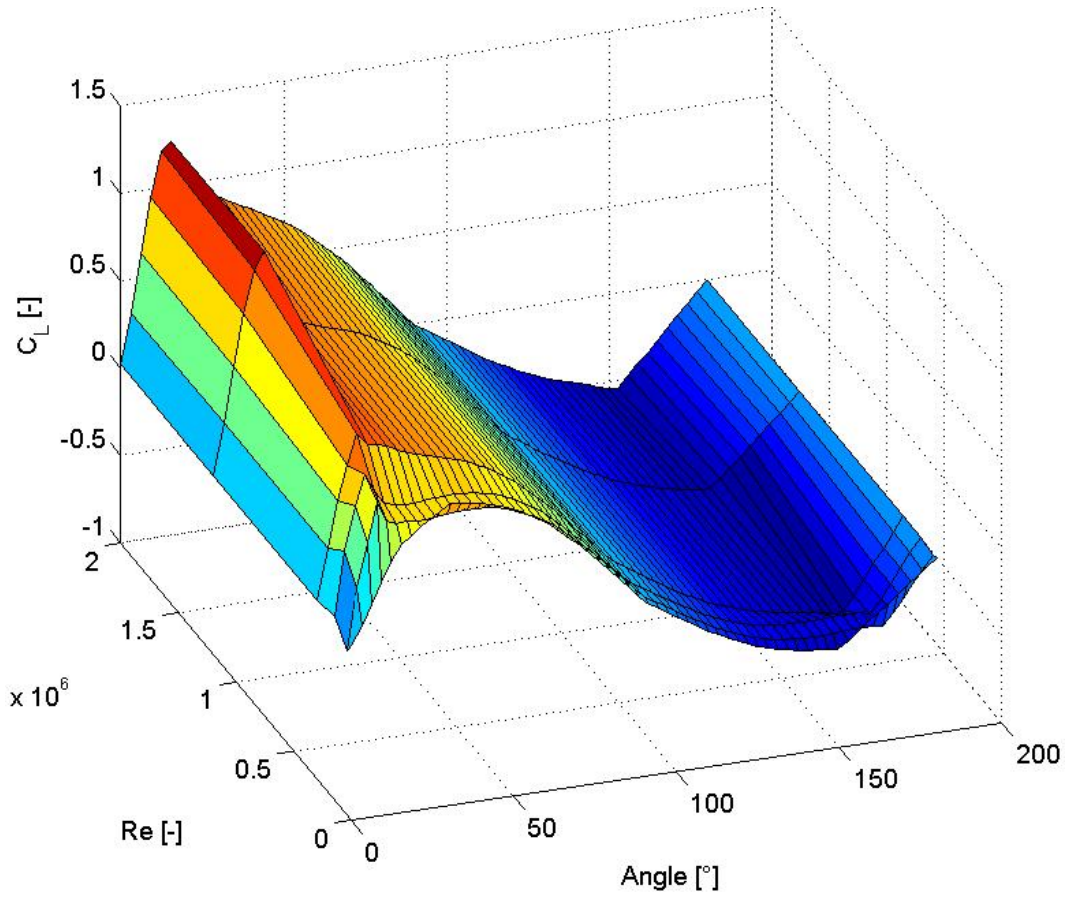

Figure B.3.: Lift coefficient variation with respect to the angle of attack and the Reynolds number

Appendix C

An example of spectral analysis

A statistical analysis of the full dataset has not be performed. This appendix gives an example of the results obtainable with this tool, by showing the normalized spectral distribution of the turbulent kinetic energy (TKE), for the U component of the velocity at different locations.

Time series were recorded measuring vertical profiles of the U and V component of the velocity at different cross-planes behind one wind turbine model in ABL flow.

Measurement locations are identified using the non-dimensional form $r = C/R$. Where C is the coordinate used for the particular profile and R is the rotor radius ($236\mathrm{mm}$). Spectra of the U component of the velocity at 1.5 diameters of distance from the rotor in the locations $r = 0$, $r = 0.4$ and $r = 1.2$ are shown. These locations are selected in order to represent two points in the wake of the turbine (at the rotational axis and at the 40% of the blade span), and one out of the wake flow (at the 120% of the blade span).

A peak at $32\mathrm{Hz}$ can be observed for the measurement locations within the wake flow, see Fig.C.1 and Fig.C.2. This value corresponds to the turbine rotational velocity of $640\mathrm{rpm}$. The peak is absent in the ambient flow region, as shown in Fig.C.3.

At a distance of three diameters downstream, in the measurement location $r = 0.4$, the turbulence in the ABL flow has already mixed the flow and the peak is absent, as shown in Fig.C.4.

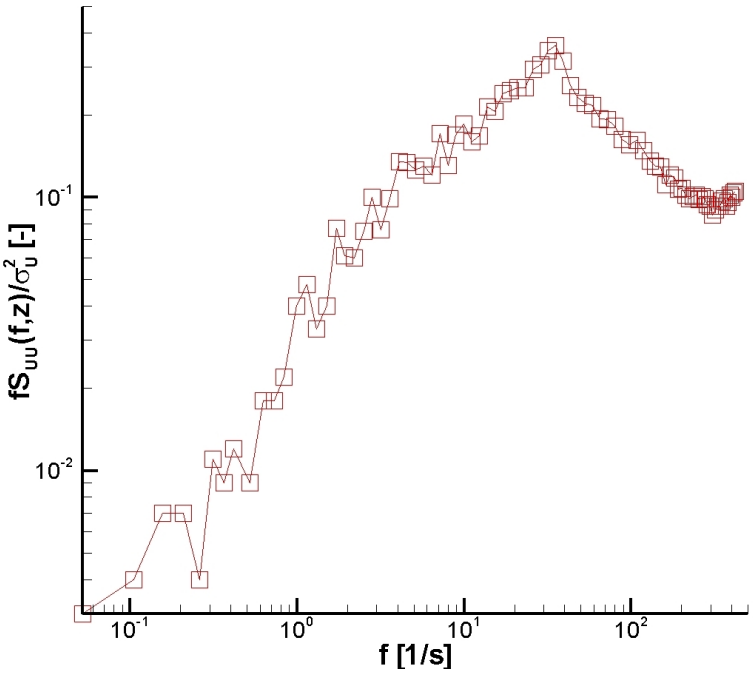

Figure C.1.: TKE normalized spectral distribution - 1.5 diameters downstream - r=0 - ABL flow - UV setup

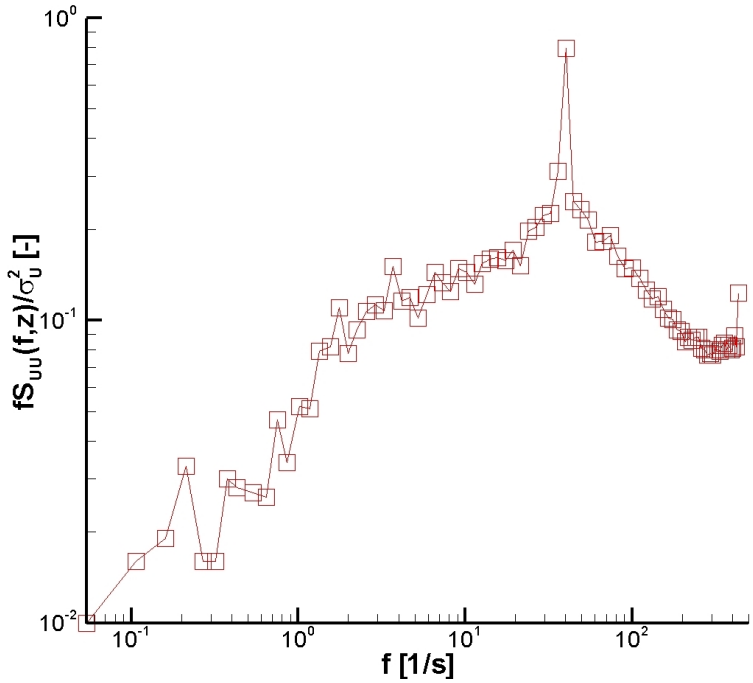

Figure C.2.: TKE normalized spectral distribution - 1.5 diameters downstream - r=0.4 - ABL flow - UV setup

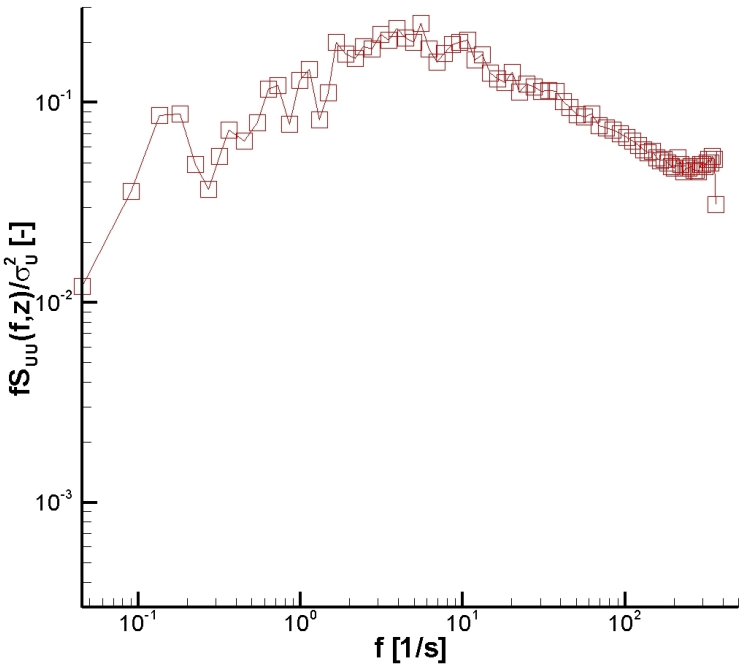

Figure C.3.: TKE normalized spectral distribution - 1.5 diameters downstream - r=1.2 - ABL flow - UV setup

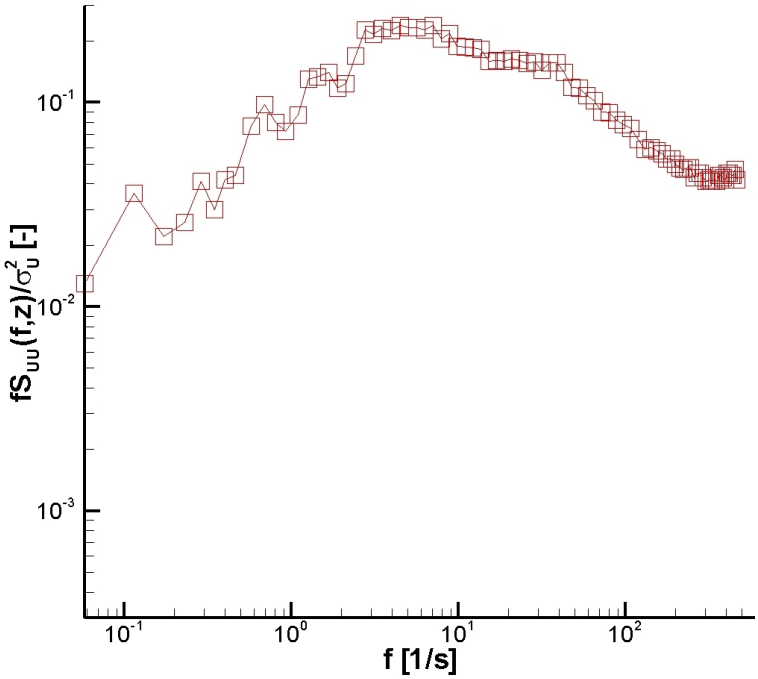

Figure C.4.: TKE normalized spectral distribution - 3 diameters downstream - r=0.4 - ABL flow - UV setup

Bibliography

Adaramola, M., and P. Krogstad (2011), Experimental investigation of wake effects on wind turbine performance, *Renewable Energy*, *36*, 2078–2086.

Ainslie, J. F. (1988), Calculating the flowfield in the wake of wind turbines, *Journal of Wind Engineering and Industrial Aerodynamics*, *27, Issues 1-3*, 213–224.

Alfredsson, P. H., and J. A. Dahlberg (1979), A preliminary wind tunnel study of windmill wake dispersion in various flow conditions, *FFA technical note AU-1499 part 7*, Aeronautical Research Institute of Sweden.

Aubrun, S. (2007), Modelling wind turbine wakes with a porosity concept, *Wind Energy*, pp. 265–269.

Aubrun, S., P. Devinant, and G. España (2007), Physical modelling of the far wake from wind turbines. application to wind turbine interactions, *European Wind Energy Conference*, pp. 1–8.

Bastigkeit, I. (2011), Erzeugung von validierungsdaten fuer wirbelaufloesende mikroskalige stroemungs- und ausbreitungsmodelle, Ph.D. thesis, Meteorologisches Istitut, Hamburg Universitaet.

Bendat, J. S., and A. G. Piersol (2011), *Random data: Analysis and measurement procedures*, vol. 729, Wiley.

Brigham, E. O., and R. E. Morrow (1967), The fast fourier transform, *Spectrum, IEEE*, *4*(12), 63–70.

Bruun, H. H. (1995), *Hot-wire anemometry: principles and signal analysis*, Oxford University Press.

Builtjes, P. J. H., and D. J. Millborrow (1980), Modelling of wind turbine arrays, in *3rd International Symposium on Wind Energy Systems*, TUD Lyngby.

Burton, T., D. Sharpe, N. Jenkins, and E. Bossanyi (2001), *Wind energy handbook*.

Campagnolo, F. (2013), Wind tunnel testing of scaled wind turbine models: Aerodynamics and beyond, Ph.D. thesis, Politecnico di Milano.

Chamorro, L. P., and F. Porté-Agel (2009), Wind tunnel investigation of wind turbine wakes: Boundary layer turbulence effects, *Boundary Layer Meteorology*, *132*, 129–149.

Chamorro, L. P., and F. Porté-Agel (2010), Flow characterization of wind-turbine wake (s) developed in a boundary layer flow with different thermal stratifications: A wind-tunnel study, in *The Fifth International Symposium on Computational Wind Engineering (CWE2010)*.

Corten, G. P., P. Schaak, and T. Hegberg (2004), Turbine interaction in large offshore wind farms - wind tunnel measurements, *Tech. Rep. ECN-C-04-048*, ECN, Energy Research Centre of the Netherlands.

Cuerva, A. (2009), Reynolds number implications on the determination of wind turbine optimum rotors, in *Proceedings of EWEC conference*, Marseille.

Cuzzola, F., S. Aubrun, and B. Leitl (2012), Characterization of a wind turbine model, in *EWEA Special Topic Conference The Science of Making Torque from Wind, Oldenburg, Germany.*

DantecDynamics (2011), Laser Doppler Anemometry - measurement principles, online: `http://www.dantecdynamics.com/Default.aspx?ID=1046` (visited: 2011-06-10).

De Vries, O. (1983), On the theory of the horizontal-axis wind turbine, *Annual review of fluid mechanics*, *15*(1), 77–96.

Doerenkaemper, M. (2011), Design, development and testing of a methodology to model wind turbines in boundary layer wind tunnels, Master's thesis.

Eastman, J., and A. N. Sherman (1937), Airfoil section characteristics as affected by variations of the reynolds number, *Tech. rep.*, NACA Report 586.

Eppler, R. (1990), *Airfoil Desing and Data*, Springer Verlag.

EWTL (2011), Environmental Wind Tunnel Laboratory - Website, online: `http://www.mi.uni-hamburg.de/ewtl` (visited: 2011-04-15).

Fischer, R. (2012), Entwicklung eines problemorientierten software-pakets zur automatisierten aufbereitung, analyse und dokumentation von im windkanal produzierten daten zur lesvalidierung, Ph.D. thesis, Meteorologisches Istitut, Hamburg Universitaet.

Gad-el Hak, M. (1990), Control of low-speed airfoil aerodynamics, *AIAA journal*, *28*(9), 1537–1552.

Giguere, P., and M. S. Selig (1999), Design of a tapered and twisted blade for the nrel combined experiment rotor, *Tech. Rep. SR-500-26173*, NREL.

Glauert, H. (1935), Windmills and fans, *Aerodynamic theory*, *14*, 324–340.

Heller, V. (2011), Scale effects in physical hydraulic engineering models, *Journal of Hydraulic Research*, *49, Issue 3*, 293–306.

Hertwig, D. (2009), Detection of coherent structures in atmospheric boundary layer flows: A comparative wind tunnel study using pod, lse, and wavelets, Master's thesis, Meteorologisches Institut, Hamburg Universitaet.

Hertwig, D. (2013), On aspects of large-eddy simulation validation for near-surface atmospheric flows, Ph.D. thesis, Meteorologisches Istitut, Hamburg Universitaet.

Khan, M. A., P. Pillay, and K. D. Visser (2005), On adapting a small pm wind generator for a multiblade, high solidity wind turbine, *IEEE Transactions on Energy Conversion*, *20*, 685–692.

King, L. V. (1914), On the convection of heat from small cylinders in a stream of fluid: determination of the convection constants of small platinum wires, with applications to hot-wire anemometry, *Proceedings of the Royal Society of London. Series A*, *90*(622), 563–570.

Laitone, E. V. (1997), Wind tunnel tests of wings at reynolds numbers below 70 000, *Experiment in Fluids*, *23(5)*, 405–409.

Leitl, B., M. Schatzmann, and F. Harms (2009), Benchmark for computational modeling of urban flows, final report., *Tech. rep.*, Meterological Institute, University of Hamburg.

Mann, J. (2010), Light detection and ranging measurements of wake dynamics part i: One dimensional scanning, *Wind Energy*, pp. 51–61.

Manwell, J. F., J. G. McGowan, and A. L. Rogers (2009), *Wind Energy Explained: Theory, Design and Application*.

McCroskey, W. J. (1987), A critical assessment of wind tunnel results fro naca 0012 airfoil, *Tech. rep.*, NASA.

Medici, D., and P. H. Alfredsson (2005), Measurements on a wind turbine wake: 3d effects and bluff body vortex shedding, *Wind Energy*, *9*(2006), 219–236.

Montgomerie, B., and J. A. Dahlberg (2003), Vortex system studies on small wind turbines, *FOI scientific report, ISRN FOI*, *9257*(September).

Neff, D., and R. N. Meroney (1995), Reynolds number independence of the wind-tunnel simulation of transport and dispersion about buildings, *Tech. rep.*, Fluid Mechanics and Wind Engineering Program, Colorado State University, Fort Collins, CA.

Neff, D., R. N. Meroney, E. McCarthy, and E. Davis (1990), Upstream and lateral wind turbine wake effects on nearby wind turbine performance, *Journal of Wind Engineering and Industrial Aerodynamics*, *36*, 1405–1414.

Pascheke, F., and P. E. Hancock (2007), Wake development and interactions within an array of large wind turbines, *Development*, pp. 1–9.

Petersen, G. (2013), Wind tunnel modelling of atmospheric boundary layer flow over hills, Ph.D. thesis, Meteorologisches Istitut, Hamburg Universitaet.

Rhethore, P.-E. (2009), Wind turbine wake in atmospheric turbulence, Ph.D. thesis, Risoe DTU.

Sanderse, B. (2009), Aerodynamics of wind turbine wakes, *ECN-e–09-016*.

Schepers, J. G., K. Boorsma, C. Kim, and T. Cho (2011), Analysis of detailed aerodynamic measurements on a 4.5m diameter rotor placed in the large german dutch wind tunnel dnw, EWEA Annual Event.

Sheldahl, R. E., and P. C. Klimas (1981), Aerodynamic characteristics of seven airfoil sections through 180 degrees angle of attack for use in aerodynamic analysis of vertical axis wind turbines, *Tech. rep.*, Sandia National Laboratories Report.

Simms, D. A., S. Schreck, M. Hand, and L. J. J. Fingersh (2001), Nrel unsteady aerodynamics experiment in the nasa-ames wind tunnel: a comparison of predictions to measurements, *Tech. Rep. June*, NREL.

Snel, H., and J. G. Schepers (2007), The mexico project (model experiments in controlled conditions): The database and first results of data processing and interpretation, *Journal of Physics:*, *012014*.

Snyder, W. H. (1972), Similarity criteria for the application of fluid models to the study of air pollution meteorology, *Boundary Layer Meteorology*, *3*, 113–134.

Sunada, S., A. Sakaguchi, and K. Kawachi (1997), Airfoil section characteristics at low reynolds number, *Journal of Fluid Engineering*, *119*, 129–135.

Townsend, A. A. (1956), *The Structure of Turbulent Shear Flow*, Cambridge.

Tropea, C., A. Yarin, and J. Foss (2007), *Springer handbook of experimental fluid mechanics*, vol. 1, Springer Verlag.

Vermeer, L., J. Sø rensen, and A. Crespo (2003), Wind turbine wake aerodynamics, *Progress in aerospace sciences*, *39*, 467–510.

Vermeulen, P. E. J. (1978), Mixing of simulated wind turbine wakes in turbulent shear flow, *Tech. Rep. 78-096/4*, MT-TNO.

Vermeulen, P. E. J., and P. J. H. Builtjes (1982), Turbulence measurements in simulated wind turbine clusters, *Tech. Rep. 82-03003*, TNO.

Viterna, L. A., and R. D. Corrigan (1981), Fixed pitch rotor performance of large horizontal axis wind turbines, in *DOE/NASA Workshop on Large Horizontal Axis Wind Turbines*.

List of Tables

List of Figures